ULTRAFAST, HIGHLY SENSITIVE OPTICAL FIBER RELATIVE HUMIDITY SENSOR EMPLOYING GRAPHENE-DERIVED NANOMATERIALS AND OTHER NOVEL MATERIALS FOR POTENTIAL APPLICATIONS IN HUMAN BREATH MONITORING AND VOICE-PRINT RECOGNITION

A Thesis Submitted in Partial Fulfillment of the Requirements for the

Award of the Degree

of

DOCTOR OF PHILOSOPHY

by

Sunil Mohan

(Roll No.: 156121019)

DEPARTMENT OF PHYSICS

INDIAN INSTITUTE OF TECHNOLOGY GUWAHATI

GUWAHATI-781039, INDIA

May 2024

The present thesis dedicated to

my parents!

STATEMENT

I hereby declare that the research work presented in this thesis entitled, "**ULTRAFAST, HIGHLY SENSITIVE OPTICAL FIBER RELATIVE HUMIDITY SENSOR EMPLOYING GRAPHENE-DERIVED NANOMATERIALS AND OTHER NOVEL MATERIALS FOR POTENTIAL APPLICATIONS IN HUMAN BREATH MONITORING AND VOICE-PRINT RECOGNITION"**, is carried out by me under the supervision of **Prof. Sunil K. Khijwania**, Professor, Department of Physics, Indian Institute of Technology-Guwahati. The contents of this thesis have not been submitted to any other Institute or University for the award of any degree.

Date ……..

Sunil Mohan
(156121019)

Research student
Department of Physics
Indian Institute of Technology-Guwahati
Assam-781039
India

CERTIFICATE

This is to certify that work contained in the thesis entitled, "**ULTRAFAST, HIGHLY SENSITIVE OPTICAL FIBER RELATIVE HUMIDITY SENSOR EMPLOYING GRAPHENE-DERIVED NANOMATERIALS AND OTHER NOVEL MATERIALS FOR POTENTIAL APPLICATIONS IN HUMAN BREATH MONITORING AND VOICE-PRINT RECOGNITION**" by Mr. Sunil Mohan (Roll No. 156121019), a student of Department of Physics, Indian Institute of Technology-Guwahati, for the award of degree of Doctor of Philosophy, has been carried out under my supervision. The contents of this thesis have not been submitted to any other Institute or University for the award of any degree.

Date ……..

Prof Sunil K. Khijwania

Professor, Department of Physics
Indian Institute of Technology Guwahati
Assam-781039 India

ACKNOWLEDGEMENTS

First and foremost, I would like to express my deepest gratitude to my respected guide **Prof. Sunil K. Khijwania** for granting me the invaluable opportunity to work under his guidance. He has supported me throughout my thesis with his knowledge, ideas and patience which gave me right path in all the time of research for and writing of this thesis. His stimulating suggestions, encouragement and training have made him a source of inspiration throughout my life. I am also thankful for the excellent example he has provided as a successful physicist and professor.

I would like to express my sincere thanks my doctoral committee members, **Prof. Girish S. Setlur, Prof. Perumal Alagarsamy and Dr. Gaurav Trivedi** for reviewing my research work regularly and for all valuable suggestions.

I am profoundly grateful to the members of the Fiber Optics lab, Mr. Debabrata Paul, Mr. Manish Shing Negi, Ms. Fatima Banoo and Mr. Subham Koley for their continuous support and invaluable contributions.

My special thanks to the staffs of Department of Physics, Mr. Basab Purkhastya, Dr. Sidananda Sarma, and Mr. Atul Chandra Deka, for their support and timely assistance.

I am grateful to my friends, Rishav, Nagendra, Sumit, Suresh, Manvendra, Manisha, Nitu, Rohit, Rahul, Pushpesh, Debraj, Ankan, Samten, Lwithwsa, Madhav, Roli and all others who helped me at various levels during my stay at IIT Guwahati.

Finally, I am forever grateful to my parents and sister for their understanding, endless patience, and encouragement when it was most required.

Guwahati

Sunil Mohan

April 2024

ABSTRACT

This thesis aims to develop an optical fiber relative humidity sensor that exhibits a linear response across a wide dynamic range, with optimum sensitivity, ultrafast response, high resolution, and a high degree of repeatability. This is to be achieved by employing the simplest possible optical fiber configuration. Finally, the objective is to explore the feasibility of the developed optical fiber RH sensors for successful application in human breath monitoring and voice print recognition. Intensity modulation through evanescent-wave absorption is exploited to develop optical fiber RH sensors employing novel sensing configurations. Comprehensive experimental investigations are conducted to optimize sensor performance by effectively controlling all possible parameters, such as chemical composition, reaction parameters, film thickness, and other relevant factors. Throughout linear response over a wide dynamic range of 15.0−95.3%RH, with sensitivity of 0.1036 dB/%RH is observed for the sensor having GO-doped silica sol-gel film thickness. To enhance the sensitivity further, another optical fiber RH is developed employing reduced graphene oxide (rGO) in sol-gel silica nanostructured film over the same fiber configuration. An optimized sensing cladding configuration shows an enhanced sensitivity of 56.3mV/%RH (0.1262dB/%RH). Additionally, response and recovery times of 0.18s are observed in this case. The quest for achieving higher sensitivity over the wider dynamic range and better response/recovery time continued in the present research, which led to the development of another optical fiber sensor by exploiting graphene oxide quantum dots (GQDs), keeping the same sensor configuration and the same sensing scheme. Enhanced sensitivity of 0.2437 dB/%RH, over the linear dynamic range of 3% to 70%RH, with average response/recovery times of 0.025s is achieved. Though the sensitivity, dynamic range, and response/recovery times all improved, the scope for further improvement of sensor's response is still wide open. Hence, another sensor has been developed that employs GO-ZnO nanocomposite-based sensing cladding. A linear response over the RH range of 17−91%RH with a sensitivity of 33.6mV/%RH and response and recovery time of 0.33s and 0.45s are observed for the developed sensor. To further improve the response characteristics, another optical fiber sensor is developed employing GO-ZnO-Fe nanocomposite-based sensing cladding. A sensitivity of 60.6mV/%RH over the dynamic range of 17−80% RH and response/recovery times of 0.031s are observed for this sensor. Though the sensitivity and dynamic range improved, it is felt that the scope for improving response/recovery times is still there. Keeping this point, another sensor that employs rGO-TiO_2 nanocomposite-based sensing

cladding is explored. A sensitivity as high as 103.5mV/%RH over a dynamic range of 3−70%RH and recovery/response times of 0.025s are observed for this sensor. In order to further improve response/recovery times, research is further extended. Another sensor is developed by employing GO-coated reduced-to-few-micron core-diameter (RFMCD) PCS multimode optical fiber. Experimental results demonstrate that the proposed sensor exhibits the widest linear dynamic range of 3−94%RH with a sensitivity of 0.0115%RH^{-1}. Importantly, an ultrafast response time of 50ms is achieved. Such ultrafast response is achieved for the first time to the best of the author's knowledge. Though this sensor is well suited for real-time breath monitoring and voice print recognition, fixing it inside the testing wearable mask that covers both the nose and mouth requires special and delicate packaging of the sensor. Hence, research is further extended by incorporating biodegradable polymer polyhydroxybutyrate (PHB) immobilized PVA sensing cladding over the centrally decladded fiber. A sensitivity of 66mV/%RH over a dynamic range of 58−98% RH and response/recovery times of 0.0125s are observed for the sensor. This biodegradable polymer-based optical fiber RH sensor is successfully employed for real-time breath monitoring and voice print recognition. In the final part of the research, biowaste (ash from a mentha oil boiling plant) is used to develop an optical fiber RH sensor. The proposed sensor exhibits linear response across a wide dynamic range of 4−90%RH with an optimal sensitivity of 9.7mV/%RH and response/recovery times of 0.013s and 0.014s, respectively. All the sensors developed in the research presented here exhibit a high degree of reversibility, repeatability, stability, and extraordinarily good resolution.

List of Contents

List of Figure

List of tables

List of Abbreviations

Term	Abbreviation
AZO	Aluminium-doped zinc oxide
BPQDs	Black phosphorus quantum dots
CA	Critical angle
DAQ	Data acquisition
DWDM	Dense wavelength-division-multiplexing
EDX	Energy dispersive X-ray
ESA	Electrostatic self-assembly
ESMF	Etched single-mode fiber
EW	Evanescent wave
FBG	Fiber bragg grating
FESEM	Field emission electron microscope
FPI	Fabry–Perot interferometer
GO	Graphene oxide
rGO	Reduced graphene oxide
GQDs	Graphene quantum dots
HAP	Hydroxyapatite
HCF	Hollow core fiber
HMT	Hexamethylenetetramine
HVAC	Air-conditioning and heating, ventilation, and air conditioning
LPG	Long period grating
MFBG	Micro FBG
MI	Michelson interferometer
MOF	metal–organic framework

MMF	Multimode fiber
MZI	Mach-Zehnder interferometer
NCF	No-core fiber
OFS	Optical fiber sensor
PCF	Photonic Crystal Fiber
PCS	Plastic cladding silica
PI	Polyimide
PHB	Polyhydroxybutyrate
PMMA	Poly (methyl methacrylate)
PM-PCF	Polarization Maintaining Photonic Crystal Fiber
PVA	poly-vinyl-alcohol
RFMCD	Reduced-to-few-micron core-diameter
RH	Relative Humidity
SHM	Structural health monitoring
SI	Sagnac interferometer
SMF	Single mode fiber
SP SMF	Side polished single mode fiber
TEOS	Tetra ethyl orthosilicate
TDM	Time division-multiplexing
TFBG	Tilted fiber Bragg grating
TMOS	Tetra Methyl orthosilicate
VOC	volatile organic compounds
XRD	X ray diffraction

Chapter 1 : Introduction

1.1 Introduction

Accurate control and monitoring of relative humidity (RH) is critically important in structural health monitoring (SHM), chemical/biochemical, food processing, air-conditioning, electronic processing applications, agriculture and medical/pharmaceutical industries [1]. In SHM, regulating RH is crucial for safeguarding infrastructure integrity by preventing moisture-induced deterioration. In other areas, such as food processing industry, RH plays a critical role in preserving the quality, safety, and shelf-life of perishable food products. High humidity can accelerate microbial growth, promote spoilage, and compromise food safety standards. Furthermore, accurate RH control is essential for maintaining indoor air quality, occupant comfort, and equipment performance in air-conditioning, heating ventilation, and air conditioning (HVAC) systems. In electronic processing applications, RH control is critical for preventing moisture damage to sensitive electronic components and assemblies. Excessive moisture can lead to corrosion, electrical short circuits, and performance degradation in electronic devices. In agriculture, humidity sensors are helpful for green-house air-conditioning, plantation protection, soil moisture monitoring and cereal storage. The medical and pharmaceutical industries rely heavily on RH control to preserve the efficacy and stability of medications, vaccines, and biological materials. High humidity can degrade the active ingredient in drugs or alter the molecular structure of sensitive compounds, rendering them ineffective or harmful. Humidity sensors are also used in respiratory equipment, sterilizers and incubators. Additionally, the humidity present in exhaled breath holds significant potential for offering insights into human health conditions. Monitoring human breathing patterns through the humidity content in exhaled air can provide vital data on health concerns related to heart attacks, asphyxia, anxiety, sleep apnea, and epilepsy. Furthermore, humidity information from exhaled air during human speech has the potential to reduce intrusions into authentication systems [2].

Humidity is a general term for the amount of water vapour present in gaseous state in the atmosphere. It is expressed in two different ways; absolute humidity and relative humidity. Absolute humidity is the mass of water vapour contained in unit volume of air. The most common term used for expressing humidity is relative humidity (RH). Relative humidity is the ratio of actual vapour content of the air to the saturated vapour content of the air at the same temperature. This can be expressed as the ratio of the actual water vapour pressure to the saturation water vapour pressure at a specific temperature. When air is fully saturated with water, the pressure exerted by the water vapour present is defined as the saturation water vapour pressure which is a function of temperature. The saturation point also increases rapidly as the temperature of the air rises. This is because the kinetic energy of water molecules is higher at higher temperature. At higher temperature, more water molecules can escape from the liquid water surface into air and this will result higher saturation vapour pressure. In percentage form, RH is expressed as [3]:

$$\%RH = \left(\frac{P_w}{P_{ws}}\right) \times 100$$

where P_w is the partial pressure of water vapour and P_{ws} is the saturation water vapour pressure.

Depending on the need for humidity monitoring, many efforts have been made over the years, employing different schemes to obtain meaningful humidity measurements. The various schemes employed in conventional humidity sensors relate the fundamental properties of water vapour to different transduction schemes that relay on mechanical and electrical approaches to provide humidity induced measurements. These include mechanical hygrometer, which monitors humidity from the expansion and contraction of materials as a result of surrounding humidity. The commonly used humidity sensing materials include synthetic fibers and human hair. Another device used for humidity measurement is wet and dry psychrometer. It is made of two thermometers (glass or electric) one of which has a wet cotton or linen wick around its bulb to determine the wet bulb temperature and the other to measure the temperature of the sample gas (dry bulb temperature). Evaporation of water from the wick absorbs heat from the thermometer bulb, causing the thermometer reading to drop. The dry bulb temperature simply monitors the temperature of the air. Relative humidity is calculated by comparing the readings using a calculation table that compares the ambient temperature (monitored by the dry bulb) to the difference in temperatures between the two thermometers [3]. However, performance of these sensors is limited by slow response and large size. The demand for low cost, reliable, fast and compact sensor has led to the development of electronic humidity sensor. These are mainly

resistive and capacitive types. A resistive humidity sensor converts surrounding humidity variation to impedance change [4]. This can be measured by a current, a voltage or a resistance. Commonly used humidity sensing materials are ceramics, polymer and electrolytes. It is simple and has a fast response, but it is easily contaminated by water soluble salts. Capacitive humidity sensor is most popular among commercial humidity sensors. This sensor determines humidity variation through dielectric constant change of a thin hygroscopic film upon exposure to moisture [5]. The change in dielectric constant is nearly directly proportional to the relative humidity of the surrounding environment. Thus, by monitoring the change in capacitance, relative humidity can be determined. All the techniques discussed so far have their own particular advantages. However, performance of these sensors is limited owing to their inability towards remote and distributed sensing, multiplexing, deployment in harsh environments and their susceptibility to electromagnetic and radio frequency interference Switching sensing to optical domain is the only possible way to overcome these shortcomings, and hence worldwide research shifted to exploiting various optical techniques for the development of humidity sensor. A major thrust in this direction was observed by the inclusion of optical fiber.

1.2 Optical fiber sensor

The discovery of optical fiber was a major breakthrough in the communication engineering. During the early seventies, when the optical fiber technology was evolving to realize world-wide telecommunication system with high information carrying capacity (ICC) it was observed that the sensitivity of fiber to bend, microband, and pressure posed a challenge to realize reliable signal transmission in optical fiber communication networks. Initially, extensive effort was dedicated in mitigating the sensitivity of optical fiber to external perturbations. However, soon it was realized that the exceptional sensitivity of optical fibers to external perturbations can be exploited for sensing various parameters of interest. Thus, the field of optical fiber sensor was born. The phenomenal advancements in the field of optical fiber technology and optoelectronics including the availability of low-loss optical fiber and advanced optical sources/interrogators, have made great impact and accelerated the design and development of optical fiber-based sensors for various science and engineering applications that include civil, mechanical, aeronautical, chemical, electrical, automotive, biomedical, environmental sciences, and homeland security to a name of few.

Distinct inherent and unmatchable advantages offered by optical fiber sensors over the conventional sensors drive global interest and investment in the research and development of

optical fiber sensors. These remarkable advantages, integrated to the optical fiber sensing technology are as following:

1. Optical fiber sensors offer very high sensitivity compared to traditional conventional sensors.
2. Ease of miniaturization enables the potential development of extremely small, lightweight, and flexible optical fiber sensors.
3. Low-loss optical fibers in conjugation with fiber amplifiers facilitate the transmission of light-wave signals across long distances. Additionally, they enable the implementation of dense wavelength-division-multiplexing (DWDM) technology, to realize optical fibre communication systems with the capability of data transmission rate as high as ~1.06Pb/s-km [6]. Such extensive information-carrying capacity across long distances enables remote sensing, facilitating real-time reception, monitoring, and analysis of sensor data in distant ultraclean control stations. This is especially beneficial for samples located in challenging or hazardous environments.
4. Largest bandwidth of 100THz (as against other electrical channels) and hence the massive information carrying capacity offered by optical fiber enable: (a) achieving high sensing information density through a single optical channel where each optical characteristic (such as wavelength, phase, intensity, etc.) could be independently and simultaneously encoded through external perturbations of interest. By employing various modulation schemes for this optical channel against different and independent external perturbations, multiplexing all such sensors and simultaneous multi-parameter sensing become a possibility, (b) multiplexing large number of sensors, each characterized at a particular optical channel over a single optical fiber transmission line, (c) distributed sensing, i.e. continues sensing along the entire fiber transmission line.
5. As optical fibers are made of dielectric materials, optical fiber sensors are naturally electrically isolated from interrogating electronics.
6. As a point sensor, they can be deployed to sense a given measured at normally inaccessible regions without perturbation of the transmitted signals.
7. As the information carrying signal is in optical domain, it is immune to electromagnetic interference and carries zero risk against fire/sparks. This leads to the highly reliable nature of optical fiber sensor.
8. Excellent stability, even when; in permanent contact with electrolyte solutions enables optical fiber sensors to be readily deployed in chemical processes and

biomedical instrumentation. Further low volume and weight enables them to be embedded in a desired structure without affecting the structure itself (example, civil engineering applications).

Owing these illustrious advantages, which triggered intensive research and development efforts worldwide, numerous fiber optic sensors have been developed for monitoring a wide variety of physical, chemical, and biological parameters. Today, almost all parameters of the practical and engineering interests such as pressure, temperature, liquid level, refractive index, pH, antibodies, electric current, voltage, rotation, displacement, acceleration, acoustic, electric and magnetic field measurements, tilt, torsion, strain are accurately and successfully monitored in real-field environment.

Optical fiber sensors may be broadly classified as extrinsic sensors and intrinsic sensors. These two categories represent separate and independent methodologies for utilizing optical fibers for sensing applications. In extrinsic sensors, the sensing process happens outside of the fiber. In this scenario, the fiber functions just as a channel to transmit light signals to and from the sensor head. Imprinting of environmental/external perturbations on the optical signal via modulation takes place outside the fiber. Whereas in intrinsic sensors, the measuring parameter directly interacts with the guided light. As a result, one of the fundamental characteristics of the guided optical, signal such as, intensity, wavelength, polarization or phase gets modulated within the fiber and fiber itself act as a sensor. Therefore, the intrinsic optical fiber sensor can be further classified on the basis of the modulation techniques, such as, intensity modulation-based optical fiber sensors, wavelength modulation-based optical fiber sensors, phase modulation-based optical fiber sensors and polarization modulation based optical fiber sensors.

1.2.1 Intensity modulation-based optical fiber sensors

Intensity modulation-based sensors have additional advantages of simplicity in fabrication and compatibility with multi-mode optical fiber. Intensity modulation in optical fiber can be realized through various techniques. Among these techniques, evanescent wave (EW)-based intensity modulation has attracted a lot of attention from researchers and has been used extensively. When a light beam associated with a plane wave travelling in the medium of high refractive index is incident on the interface between two optically transparent media of high and low refractive indices, and if the angle of incidence exceeds the critical angle, the light beam undergoes total internal reflection (TIR). Applying wave optics by solving Maxwell's equations and carefully introducing appropriate boundary conditions across the interface

reveals the existence of plane wave in the lower refractive index medium, which is known as the evanescent wave (EW). This is a very special progressive wave which travels along the interface whereas, its amplitude of the EW decreases exponentially with the distance from the interface. Owing to the cylindrical symmetry of optical fiber, a light beam associated with the (plane wave) in meridional plane that enters the fiber core at a given guided angle θ and strikes the core-clad (high index-low index) interface at an angle greater than the critical angle of the fiber undergoes total internal reflections at upper as well as lower core clad interface. Such light beams are guided by the optical fiber through the successive TIR. Also, there exists a corresponding light beam traveling at an angle $-\theta$ within the fiber. The mode of the fiber arises from the superposition of these two guided beams. There exists a set of discrete values of angle θ so that, if light beams are traveling at these angles, they will be guided by the optical fiber, giving the rise to various modes of an optical

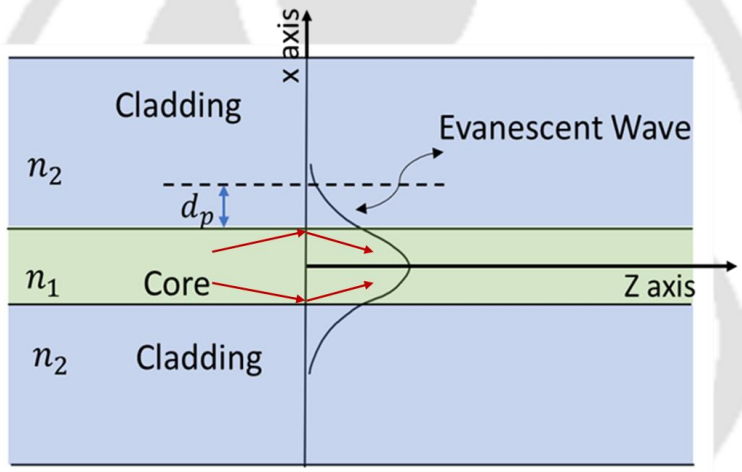

Fig 1.1 : *Total internal reflection and evanescent wave in an optical fiber.*

fiber. Fig 1.1 illustrates the intensity variation of one such mode (the fundamental mode). The intensity variation extends beyond the core (high index medium) and into the clading (low index medium) due to of the evanescent wave associated with the phenomena of total internal reflection. As the distance from the core-cladding interface increases, the energy carried by the evanescent tail of the mode decreases exponentially in the cladding. A key characteristic parameter of the evanescent wave is the penetration depth d_p, defining the distance from the core-cladding interface at which the amplitude of the evanescent wave decreases to $1/e$ of its value at the interface [7]:

$$d_p = \frac{\lambda}{2\pi n_1 (cos^2\theta_{cs} - cos^2\theta sin^2\theta_\phi)^{1/2}} \qquad 1.1$$

where λ represents the free-space wavelength of the light launched into the fiber, n_1 is the core refractive index of the fiber. θ is the angle of the guided lightwave with respect to the normal at the core-cladding interface.

When the cladding is removed in the middle and over a very short length of the fiber core is directly exposed to the analyte/ measurand that occupies the decladded region this short decladded region defines the sensing region of the optical fiber sensor in this regime. θ_{cs} is the critical angle at the sensing region. θ_ϕ is the skewness angle, which is equal to $\pi/2$ for meridional rays. As evident form the Eq 1.1, d_p, usually smaller than the operating wavelength (λ), defines a short range of sensing volume wherein, evanescent wave interacts with the measurand and carried by it gets attenuated via absorption, scattering, or refractive index changes. Since an optical fiber can support large number of guided modes, effective evanescent wave field around the fiber core is the superposition of the field distribution of all the guided mode. However, the amount of energy available to interact with the measurand within the limited range of the evanescent wave is described by the fraction of the total guided power (r) that is present in the cladding region. This is defined as [7]:

$$r = \frac{P_{clad}}{P_{total}} \qquad 1.2$$

where P_{clad} is the power in the cladding region and P_{Total} is the total guided power. This fraction is typically less than 1% for weakly guiding multimode fiber (MMF) [7]. However, d_p, as well as r, both, rises sharply as the guided ray angle approaches to the critical angle of the sensing region. This elevation is crucial for attaining greater sensitivity and can be accomplished through techniques such as tapering, bending the optical fiber within the sensing region or masking to eliminate low-order modes at the launch optics. Importantly the value of d_p as well as r are significantly very high in the case of single mode fiber (SMF) in comparison to the multimode fiber (MMF). Hence, SMF is to be preferred for designing and developing EW based optical fiber sensor.

The first step towards developing an optical fiber sensor (OFS) based on intensity modulation through the EW involves the access of the EW. However, it is difficult to remove the hard silica cladding of single-mode fiber. One way to access the evanescent wave in a SMF

is to prepare side-polished half-block [8]. In this technique, a single-mode optical fiber is fixed within a curved groove carved into a fused silica/quartz block. The entire structure is subsequently mounted onto a polishing machine and polished until it reaches the desired proximity to the core-cladding interface, facilitating access to the evanescent field. Precise alignment and pressure control are crucial throughout this process. An alternative method to access the evanescent field in SMF involves etching the cladding using Hydrofluoric acid (HF) [9]. However, extreme caution is imperative while handling HF due to its hazardous nature. Additionally, due to the small core diameter, aligning and efficiently coupling optical power into a SMF is quite challenging. On other hand, getting an access to the EW is quite easy for specifically fabricated MMF having polymer/plastic cladding and a silica core. The polymer/plastic cladding can be easily removed using a normal razor blade. Furthermore, large throughput power and ease of power coupling to MMF make them more popular in designing and development of evanescent wave modulation-based sensors.

There are two ways to exploit such fibers for the development of the desired sensors. In the scenario where the wavelength of the propagating light falls within the absorption band of the analyte, direct absorption the of power carried in the evanescent wave takes place in the decladded sensing region. This approach is termed as direct sensing. Conversely, for a given source, if the wavelength of the light propagating through the fiber doesn't fall within the absorption band of the analyte, it becomes necessary to switch to a different source with a compatible wavelength. Still, it might not be possible to find a suitable source where output wavelength falls in the absorption band. Even it one finds an appropriate source, it might be very expensive. In that case, an indirect sensing approach is employed in the decladded sensing region is chemically synthesized using suitable chemical and optimum configuration needs to react when exposed to the external perturbations with a compatibility to alter chemical and physical properties in a way that modulation of EW occurs at that the wavelength of the employed simple source. An example of direct sensing is reported by Tai *et al*., [10] where an optical fiber methane gas sensor that was based on EW absorption is developed employing He-Ne laser. Prasanth *et al*., [11] reported an optical fiber sensor to monitor the concentration of volatile organic compound utilizing indirect sensing mechanism. In this study Zinc oxide (ZnO), aluminium-doped zinc oxide (AZO), and tin oxide (SnO_2) were utilized as a sensing reagent that were deposited onto the decladded sensing region.

1.2.2 Wavelength modulation-based optical fiber sensor

Wavelength modulation is another important and very popular technique to realize optical fiber sensors for many scientific/industrial and specially in engineering applications. In wavelength-modulated optical fiber sensors, changes in the wavelength of light are exploited to detect different/monitor various parameters of interest. There are various ways to employ wavelength-modulation scheme. Some of these are wavelength-dependent absorption, dispersion, interference [12], and scattering. However, since its invention and successive advancements, in fiber devices, such as in-fiber gratings {fiber Bragg grating (FBG) and long period grating (LPG)} have become synonyms to optical sensing technology as for as real-field applications are concerned [13], [14]. The reason is, apart from inheriting the advantages of fiber optics, FBG sensors are characterized with additional advantages, such as, (1) inherently self-referencing, (2) ease of designing spectral and phase response of FBG as per the requirement, (3) capability of multiplexing a large number of FBGs on a single fiber channel, (4) ease of employing DWDM, spatial-division-multiplexing, time-division multiplexing (TDM) and quasi-distributed sensing, (5) insensitive to the fluctuations in the irradiance of the illuminating source to name a few. Owing to these enormous merits of FBG sensor, they have emerged as a most viable and integral solution for almost all of the engineering/industrial applications, such as, structural-health-monitoring (SHM), mechanical engineering, aeronautical engineering, communication engineering, biomedical/micro-fluidics to name a few. FBG is inherently sensitive to the temperature and strain perturbations. Hence, the inherent strain and temperature cross sensitivity remains a major issue along with the need very costly and bulky integrative device.

1.2.3 Phase modulation-based optical fiber sensor

Phase modulation-based optical fiber sensor is also a popular technique to realize optical fiber sensors for many applications. The phase change that occurs in an optical fiber due to environmental perturbation is detected using optical fiber interferometric techniques, converting phase modulation into intensity modulation. The most commonly used interferometers are Sagnac interferometer, Mach-Zehnder interferometer (MZI), Michelson interferometer (MI), Febry-Perot interferometer (FPI) [15], [16]. The optical fiber Sagnac interferometer is a specialized interferometer where light is launched in two opposite directions around a fiber loop. When the loop rotates, the light traveling towards the directional coupler reaches it a bit earlier than the light traveling in the opposite direction. The time differences directly correlate with the rotation rate and can be precisely measured as phase fluctuations,

providing remarkable sensitivity and precision. Optical fiber Mach-Zehnder interferometers (MZIs) are a type of interferometer commonly used in various applications, including sensing. The basic principle involves splitting a beam of light into two separate paths (the reference arm and the sensing arm), recombining them, and observing the interference pattern. When there's a change in the length of one of the arms, such as due to mechanical or thermal strain in the sensing arm, it leads to a phase shift between the two beams when they are recombined. This phase shift alters the interference pattern observed at the detector, allowing the precise measurement of the strain or other parameters affecting the arm length. In Optical fiber Michelson interferometers, a single-directional coupler splits and recombines light, initially dividing it into sensing and reference arms. After traversing these arms and reflecting back, the light is recombined at the initial splitter. Michelson and Mach–Zehnder interferometers share similarities as folded versions of each other, yielding comparable optical loss budgets and Mach–Zehnder-like outputs. However, Michelson employs just one optical fiber coupler, doubling the optical phase shift per unit length as light passes through both arms twice [15].

1.2.4 Polarization modulation based optical fiber sensor

Polarization modulation-based sensors take advantage of the birefringence phenomenon in optical fibers. Birefringence refers to the property of certain materials to have two different refractive indices depending on the polarization of light traveling through them. There are specially designed fiber to realise polarization modulation. Such fibers are known as polarization maintaining fiber (PMF). When strain is applied to these optical fibers, it can cause a change in the birefringence, resulting in a measurable phase difference between the two polarization states of light. This phase difference can then be detected and correlated with the amount of strain or stress applied to the fiber. By monitoring these changes in the polarization state of light, polarization-based sensors can accurately measure various physical quantities such as strain, pressure, temperature, magnetic field and even biochemical parameters in certain cases. In the last few decades, polarization maintaining photonic crystal fiber (PM-PCF) based sagnac interferometer is used vastly to realize polarization modulation-based optical fiber sensors [17]–[19]. PM-PCF provides several advantages over conventional optical fiber, such as endless single mode guidance, less temperature sensitivity compared to conventional fiber, large mode area and high birefringence. PM-PCF possesses very low bending loss due to the large numerical aperture and small core diameter. In the case of PM-PCF, significant birefringence can be introduced with the help of the glass-air index difference. Here, the core can be easily distorted by introducing capillaries of different wall thicknesses above and below

the core which leads to an extremely high value of birefringence or polarisation maintaining capacity. PM-PCF based sensors are widely used in aerospace, civil engineering, telecommunications, and healthcare industries for precise and reliable measurements in challenging environments.

1.3 Optical fiber humidity sensing

Optical fiber sensors have become an integral part of the monitoring and sensing systems for almost all the engineering/industrial applications. Some of the most important fields of application that have witnessed tremendous rise recently and have attracted lots of interest as far as human security is concerned are structural health monitoring (SHM) and homeland security. Today, approximately all parameters such as temperature, pressure, refractive index, RH, voltage, electric current, rotation, displacement, acceleration, acoustic signal, electric field, magnetic field, tilt, and strain are measured more easily and accurately with the help of optical fiber sensors. As already mentioned, RH is a critical parameter for various industrial applications. Consequently, various sensing schemes in conjunction with fiber optics have been exploited over the years to develop an optical fiber humidity sensor. For example, Ballantine *et al.,* [20] proposed a humidity sensor that utilized a 9cm long glass capillary waveguide coated with a film of $CoCl_2$/poly (vinylpyrrolidone) (PVP). The sensor demonstrated good sensitivity within the relative humidity (RH) range of 60-85%RH. Zhou *et al.*, [21] utilized the same calorimetric reagent along with a porous optical fiber to monitor humidity in the low range. Bowness *et al.,* [22] proposed a humidity sensor using a single-mode fiber. Here, the sensing principle was based on the refractive index change in an organic film coated on the cladding of a bent fiber. This sensor was capable to monitor humidity variations within a broad range of 62-80%RH. Bariáin *et al.*, [23] reported an RH sensor that utilized a tapered fiber coated with agarose gel. The sensor demonstrated a dynamic range of 30-80%RH. Gaston *et al.* [24] proposed RH sensor that relied on the interaction of the evanescent wave within a side-polished single-mode fiber with a poly-vinyl-alcohol (PVA) overlay. The sensor exhibited a linear response over the 70-90%RH range only. Herrero *et al.,*[25] demonstrated TiO_2 overlayed side-polished single-mode fiber to realize an RH sensor. The sensor responded linearly over the dynamic range of 0-15%RH. In an another article, an RH sensor based on nano magnesium oxide(MgO) film deposited onto a U-shaped glass rod was reported by Shukla *et al.*, [26]. The proposed sensor responded nonlinearly over a wide dynamic range of ~5-80%RH. Khijwania *et al.,* [7] reported a RH sensor employing U shaped optical fiber probe which was coated with anhydrous $CoCl_2$ doped PVA film. The sensor responded nonlinearly

over a wide dynamic range of ~1.6-91%RH with a rapid response of less than 1s. Corres *et al.,* [27] presented tapered SMF based humidity sensor employing nanostructured [PDDA/Poly R-478] sensitive film. A variation of 16dB in optical power was achieved with a response time of 300 ms for changes in relative humidity from 75% to 100%RH. Matias *et al.*, [28] reported an optical fiber humidity sensor that utilized nano-coating, developed through the electrostatic self-assembly (ESA) technique. The dynamic range of the sensor was observed to be 75-100%RH with a response time of 300ms. Vijayan *et al.*, [29] proposed an evanescent wave fiber optic humidity sensor, which was developed by depositing Co nanoparticles dispersed in polyaniline onto an exposed core region of a multimode fiber. The sensor demonstrated a dynamic range from 20-95%RH, with response and recovery times of 8s and 60s, respectively. Aneesh *et al.,* [30] reported an optical fiber RH sensor where ZnO nanoparticles immobilised porous silica matrix was deposited onto a centrally de-cladded plastic-clad silica (PCS) fiber. The sensor displayed a linear dynamic range from 4% to 96% RH with sensitivity of 0.0012 RH^{-1}. In another article, Aneesh *et al.,*[31] demonstrated a highly sensitive optical fiber RH sensor employing TiO_2 nanoparticle immobilised porous silica matrix as a sensing cladding over the centrally decladed fiber. The sensor achieved a linear dynamic range of 24-95%RH with a remarkable sensitivity of 27.1 mV/%RH. Mathew *et al.,* [32] proposed an ultrafast optical fiber sensor based on agarose-coated U-bend probe. A nonlinear response over the dynamic range of 25-90%RH was observed. Xiao *et al*. [33] reported a side-polished SMF (SP-SMF) based RH sensor that employed humidity-sensitive reduced graphene oxide (rGO) film. The sensor exhibited a linear response within 75–95%RH, with a sensitivity of 0.31dB/%RH, response times of 5s during humidification and a recovery time of 15s during dehumidification. Du *et al.*, [34] employed etched single-mode fiber (ESMF) coated with MoS_2 in order to develop a RH sensor. The sensor exhibited a nonlinear response within the dynamic range of 20-80% RH, with rapid response and recovery times of 0.066s and 2.395s, respectively. Azad *et al.*, [35] proposed ZnO nanorods coated etched optical fiber as the RH sensor. The sensor response was observed to be piecewise linear with a good linear sensitivity only in 30–55%RH range. Whereas in an another article, Gomez *et al*., [36] utilized hydrophilic bilayers of poly(allylamine hydrochloride) and SiO_2 nanoparticles on POF for humidity measurement. The proposed sensor demonstrated a linear response (10-75%RH) with sensitivity of $0.0038RH^{-1}$. Zhang *et al.*, [37] employed niobium disulfide-coated tapered SMF for relative humidity (RH) sensing. A liner sensitivity of 1.05 dB/%RH within the dynamic range of 72–97% RH was achieved. The sensor also demonstrates very fast response and recovery times of 0.015s and 0.065s, respectively. Zhong *et al.*, [38] presented a relative humidity (RH) sensor utilizing

polyimide and graphene oxide (GO) coating on a U-shaped plastic optical fiber (POF). A linear sensitivity of 0.0017 RH^{-1} across a dynamic range of 10–90%RH was observed for the developed sensor. The observed response and recovery times were 145s and 155s, respectively. Huang *et al*. [39] proposed an optical fiber RH sensor utilizing a GO-coated side-polished single-mode fiber. The observed dynamic range for the proposed sensor was 58.5–92.5%RH with a linear sensitivity of 0.427 dB/%RH. The response and recovery times of sensors were 2.73 s and 7.27s, respectively. Harith *et al.*,[40] employed tapered POF and ZnO nanorods to develop RH sensor. The sensor response was linear over a dynamic range of 50–80%RH with a sensitivity of 0.0295 mV/%RH. Owji *et al*. [41] employed graphene and GO coating composition onto an etched single-mode fiber (SMF) to develop an RH sensor. Piece-wise and non-linear response was observed over the dynamic range of 40-80%RH. Huang *et al.*, [42] employed SiO_2/TiO_2-coated straight fiber for the development of optical fiber RH sensor. Sensor exhibited piecewise linear response in the 15-95% RH range with response and recovery times of 25s and 50s, respectively. Liu *et al*., [43] introduced an evanescent wave modulation scheme-based RH sensor that utilized a GO-coated micro-capillary. The sensor exhibited a dynamic range of 30-70%RH, with a linear sensitivity of 0.211 nm/%RH. Guo *et al.*, [44] reported an optical fiber sensor for RH measurement utilizing a carbomer-coated taper single-mode fiber (SMF). The experimental response of the sensor was nonlinear for 68% to 90% RH with fast response and recovery time of 0.46s and 0.32s, respectively. Zhao *et al*., [45] reported an RH sensor using a multimode fiber where the sensing region was coated with PVA doped Tween-20. The logarithm of the output light intensity displayed a linear response within the dynamic range of 22–82% RH and response and recovery time of 11s and 9s, respectively. Afsharipour *et al.*, [46] reported ZnO-np-coated U-shaped optical fiber RH sensor with a sensitivity of 0.143mV/%RH over the dynamic range of 10–80% RH. The response and recovery time of the developed sensor were 3s and 4s, respectively.

With the considerable advancement and invention of mature optical fiber-based devices, alternative schemes have also been exploited for the development of all-optical humidity sensors to achieve large dynamic range, linear response, and improved sensitivity. For example, Alwis *et al.*, [47] reported a polyimide-coated Long Period Grating (LPG) for humidity detection. This sensor response was observed to be linear for the range of 20-80%RH with a sensitivity of ~0.1nm/%RH. Wang *et al.* [48] proposed a tilted fiber Bragg grating (TFBG)-based sensor for measuring RH. The experimental response of the sensor was observed to be linear from 10% to 50%RH with a sensitivity of 0.085dB/%RH. In an another study, Wang *et al*., [49] proposed FBG based optical fiber relative humidity sensor where FBG was coated

with various pore-foaming agent-doped polyimide (PI). Among these sensing probes, the highest sensitivity of 1.71 pm/%RH over the RH range of 20-85%RH was observed for the sensing probe (FBG) coated with lithium chloride-doped PI. Zhang *et al*., [50] developed RH sensor using a thermoplastic polyimide (PI) coated FBG. The sensor exploits PI's expansion upon water absorption, demonstrating a linear response from 10% to 85% RH, with a sensitivity of 2 pm/%RH. Li *et al*. [51] proposed FBG based humidity sensor where FBG was coated with polyimide and graphene films. This sensor exhibited a linear response from 30% to 70% RH with a sensitivity of 19.8 pm/%RH. Swanson *et al*., [52] presented an RH sensor employing P84 polyimide coated FBG. A linear sensitivity of 5.29 pm/%RH across the dynamic range of 20-85%RH was achieved. Tian *et al*. [53] proposed a high-performance relative humidity (RH) sensor utilizing a micro-nano fiber Bragg grating (MFBG) coated with a GO film. A high sensitivity of 17.62pm/%RH for 20% to 80%RH was observed for the proposed sensor. Additionally, the sensor demonstrated average response and recovery times of 3.2 s and 8.3s, respectively. Riza *et al*. [54] reported another sensor that employed etched FBG with ZnO nanostructure reinforced with hexamethylenetetramine (HTM) additives for humidity detection. A linear sensitivity of 0.0004 nm/%RH over the dynamic range of 40-80%RH was observed for the developed RH sensor. Dissanayake *et al*., [55] employed graphene- oxide-coated long-period grating for the RH sensing. The proposed sensor responded linearly for the RH range 60-95%RH with a sensitivity of 0.15dB/%RH. Hou *et al*., [56] reported FBG based RH sensor where a thin sensing film of PI doped with graphene quantum dots (GQDs) was coated on the sensing region (FBG). The sensor demonstrated a linear sensitivity of 3.26 pm/%RH over the humidity range of 10–90%RH. As mentioned earlier, the major limitation of grating-based optical fiber sensors are temperature and strain cross sensitivities. Furthermore, grating-based sensors require sophisticated manufacturing techniques and bulky and expensive interrogation devices.

Furthermore, several interferometric sensors such as Mach–Zehnder interferometers (MZIs), Michelson interferometers, Sagnac interferometers, and Fabry–Perot interferometers (FPIs) are also extensively used to develop all-optical fiber RH sensors. For example, Wang *et al*., [57] proposed an optical fiber RH sensor that utilized an in-fiber Mach-Zehnder interferometer (MZI) coated with a GO/PVA composite film. The developed sensor exhibited a linear dynamic range of 30-75%RH, with a sensitivity of 0.193 dB/%RH. In an another research, Liu *et al*., [58] utilized GO-coated core-offset fiber Mach-Zehnder interferometer (MZI) for humidity sensing. Experimental response was observed to be linear in 30-60%RH range with a sensitivity of 0.104 dB/%RH. Bian *et al*., [59] proposed a RH sensor based on two

single-mode fibers spliced on the two sides of a no-core fiber (NCF). NCF was coated with a calcium alginate (CaAlg) hydrogel film. A linear sensitivity of 0.38dB/%RH over the dynamic range of 30-80%RH was observed. The response and recovery time of the proposed sensor were 3s and 4 s, respectively. Fan *et al*., [60] proposed an RH sensor based on a graphene oxide-coated few-mode fiber MZI. The MZI configuration was prepared by splicing a few-mode fiber (FMF) segment between the two segments of NCF. This NCF-FMF -NCF configuration was spliced between the two segments of SMF to realize the sensor. An overall nonlinear response with intermediate piecewise linear sensitivities of 0.191 and 0.061 nm/%RH were observed for the RH range of 30%-55%RH and 55%-95%RH, respectively. In an another research, Peng *et al*., [61] reported a Fabry–Perot (F-P) interferometer based RH sensor that was designed by depositing three layers $ZrO_2/SiO_2/ZrO_2$ thin film of thicknesses 60nm/5000nm/60nm onto one of the fiber end face. The sensor responded nonlinearly over the dynamic range of 0.06-70% RH, with a response and recovery times of 4s. Zhang *et al*., [62] proposed an optical fiber RH sensor where Fabry-Perot (F-P) interferometer was designed by fixing SMF into an appropriate length of capillary tube, with distal end of the tube being coated with a composite film of hyaluronic acid (HA) and polyvinyl alcohol (PVA). The response of the proposed sensor was observed to be linear over the humidity range of 35-85%RH with sensitivity of 0.233nm/%RH. Additionally, the response and recovery time of the proposed sensor are 3 s and 4s, respectively. Liang *et al*., [63] reported RH sensor based on cascaded FBG and FPI an F-P interferometer prepared where thin layer of PI film was coated on the end face of single-mode fiber that carried the FBG. The sensor could detect the humidity in the range of 35-65%RH with a very high linear sensitivity of 986.25 pm/%RH. Response and recovery times were observed to be 400ms and 5 s, respectively. Liu *et al*., [64] proposed a humidity sensor utilizing a nafion film-based F-P interferometer, demonstrating a linear sensitivity of 3.78 nm/%RH across the 30-85%RH range. Li *et al*., [65] employed GO diaphragm suspended onto the end face of capillary tube where other end was spliced with SMF to realize F-P interferometer for the RH sensor. The sensor exhibited a piecewise linear response with a sensitivity of 0.082 nm/%RH for 10-70%RH range and 0.63 nm/%RH for 70-90%RH range. An ultrafast response of 60ms was observed for the proposed sensor. In an another article Liu *et al*., [66] demonstrated F-P interferometer-based RH sensor utilizing the metal–organic framework (MOF) crystal. The dynamic range of the developed sensor was observed to be 10–90% RH with a linear sensitivity of 315 pm/%RH. The response and recovery times of the proposed sensor as high as 323s and 326s, respectively. Shao *et al*., [67] reported an optical fiber humidity sensor based on an F-P interferometer developed by utilizing black phosphorus quantum dots-polyvinyl alcohol

(BPQDs-PVA) gel sandwiched between two SMFs. The sensor's response was observed to be piece-wise linear over the dynamic range of 42-60%RH with a sensitivity of 12.43nm/%RH. Zhao *et al*., [68] reported another F-P interferometer based optical fiber relative humidity sensor. The F-P interferometer comprises a photonic crystal fiber (PCF), single-mode fiber, and partially filled hollow core fiber (HCF) with GQD and PVA. A linear response over the dynamic range of 19.63-78.86%RH with sensitivity of 0.456nm/%RH was observed for the developed sensor. Gao *et al*., [69] employed rGO coated F-P resonator for RH detection. The F-P resonator was prepared by splicing an rGO-coated hollow core fiber between two SMF. The sensor demonstrated a linear sensitivity of 0.229 dB/% RH within 60-90% RH range, with response and recovery times of 5.2s and 8.1s respectively. Xu *et al*.,[70] proposed a tip Michelson interferometer (MI) for RH sensing, employing a capillary tube spliced to a single-mode fiber and coated with agarose gel. The sensor achieved a linear response across the dynamic range of 25- 90% RH, with a sensitivity of 0.752 nm/%RH, along with response and recovery times of 97 ms and 1000 ms, respectively. Shao *et al*., [71] proposed MI interferometer based optical fiber RH sensor that was fabricated by sandwiching a taper between a PCF and a standard SMF. The proposed sensor was observed to be linear over the dynamic range of 30- 90%RH with a sensitivity of 0.166dB/%RH and a response/recovery time of 200ms/300ms. Li *et al*., [72] employed PCF based Sagnac interferometer (SI) where the PCF and the coupling zone were coated with graphene to fabricate a sensor for RH detection. The proposed sensor was able to monitor RH in the range of 36-75.3% RH, with a sensitivity of 324.11 pm/%RH. Wang *et al*., [73] proposed a RH sensor based on Loop-Fiber that incorporates a FBG. A uniform waist area of the tapered area was coated with GO for RH measurement. The sensor demonstrated a linear sensitivity of 141.7 pm/%RH across the RH range of 37.7% to 65.5%, with response and recovery times of 10.53s and 12.27s, respectively. Even though the interferometric-based RH sensors demonstrate very high sensitivity over the wide dynamic range, these sensors are complicated in the sense that they require very complex and sophisticated manufacturing processes along with costly interrogation devices. A simpler, cost-effective alternative is desirable, prioritizing ease of manufacturing, use and affordability while maintaining reliability and accuracy.

As can be observed from the above discussion, most of the sensors employ indirect sensing methods for measuring relative humidity (RH), in the sense that a suitable material is required to facilitate the interaction of the optical signal (usually at wavelengths of 632.8 nm or 1550 nm) with the RH variations applied to the fiber sensor. A range of humidity-sensitive hygroscopic materials, such as polyamide, poly (ethylene oxide)/cobalt chloride, agarose

chitosan, polyvinyl alcohol (PVA), PI, metal oxides, MOF etc. are utilized not only for this function but also to amplify the sensitivity of the RH measurement. It is important to mantion that, recently, graphene and graphene-derived materials have attracted significant research interests in the field of sensing because of their unique and excellent properties over other materials. Graphene oxide (GO), a two-dimensional nanomaterial, is one of the most important derivatives of graphene. The monolayer of GO contains sp2 and sp3 hybridized carbon atoms along with oxygen-rich functional groups such as hydroxyl and epoxide groups on the basal plane, whereas carbonyl and carboxyl groups at the edge [74]. The structure of graphene oxide (GO), along with its oxygen functional groups and high surface area to volume ratio make GO film exceptionally permeable and adsorptive to water molecules. These characteristic result in outstanding dispersibility, hygroscopicity, and unique hydrophilicity making GO an exceptional choice for relative humidity (RH) sensing. Naturally and as evident from the previous discussion, researchers utilized GO as the RH sensing medium in conjunction with various fiber geometries/configurations e.g., interferometry, side-polished SMF/tapered SMF/grating structures, or specialized fibers like microcapillary/hollow-core fiber/PCF to develop an effective RH sensor [38], [41], [51], [53], [55], [57], [58], [60]. On the other hand, reduced graphene oxide (rGO) is another important derivative of graphene oxide, which has a less number of oxygen functional groups. It retains graphene's hexagonal carbon lattice structure but with reduced electrical conductivity. Due to its unique properties, rGO is utilized in various applications, including sensors, super-capacitors, and composites. rGO is also used to develop optical fiber RH sensors [33], [69]. Further, graphene quantum dots (GQDs) are zero-dimensional graphene oxide derivatives with a lateral size less than 10 nm. GQDs consist of a graphene oxide structure and many oxygens functional groups on the edge (hydroxyl, carbonyl, carboxyl, and epoxy). Due to several unique and exciting (luminance, electrical, chemical, and optical) properties of GQDs, they offer great potential for application in RH sensing. GQDs are also used for the development of optical fiber RH sensor [56], [68].

Metal oxide such as ZnO and TiO_2 have been extensively used independently for the development of humidity sensors [25], [30], [31], [35], [40], [42], [46], [54]. However, the introduction of ZnO in GO to realize a nanocomposite, leads to the exfoliation and improved dispersion of GO nanosheets. This enhances the extent of interfacial polarization and hydrophilic functional groups. Furthermore, the introduction of Fe in GO-ZnO nanocomposites further amplifies the polar nature of the material [75]. Consequently, GO-ZnO-Fe is expected to exhibit greater polarity compared to pristine GO, ZnO nanoparticles, and GO-ZnO nanocomposite. Therefore, both GO-ZnO and GO-ZnO-Fe nanocomposites are expected to

enhance the sensitivity of relative humidity (RH) measurements. Recently, GO-ZnO composites is employed for the development of conventional resistance-based RH sensors [76]. A significant observation in all these sensors is that those with a large dynamic range often exhibit nonlinear responses, while those with linear responses have a limited dynamic range. While sone sensors exhibit a linear response over a wide dynamic range, but their sensitivity is relatively low. Furthermore, the response and recovery times of these sensors are also considerably high. This leads to a large scope of research for realizing optical fiber sensors with the widest possible linear dynamic range as well as an optimum sensitivity with ultrafast response and recovery time.

1.4 Objective of the work

The main objective of the thesis is to develop an optical fiber RH sensor with optimum sensitivity over the widest possible dynamic range having linear response, high resolution, ultrafast response time, and a very high degree of repeatability and reliability. This is to be achieved by employing the simplest possible optical fiber configuration. Finally, the objective is to explore the feasibility of the developed optical fiber RH sensors for successful application in human breath monitoring and voice print recognition. For precise breath monitoring and effective voice recognition, it is crucial for the developed humidity sensors to exhibit exceptionally high sensitivity and extremely fast response and recovery time, especially within the high humidity range (around 90%RH and above). In recent times, there have been remarkable advancements in nano-scaling, not only within the field of material science but also in the domains of optical fiber technology and photonics as a whole. When the dimensions of the sensing material are reduced to the nano-scale, it results in a significantly higher surface-to-volume ratio. This increased ratio offers a larger surface area for the sensing material to interact with the measurand, thereby enhancing its sensing capabilities. Hence, fiber optics is integrated with nanotechnology in order to accomplish the objectives of the present research. Intensity modulation through evanescent-wave absorption is exploited for the development of optical fiber RH sensors employing novel sensing configurations and the design of fiber cladding in a very short sensing region. In the first part of the research, simplest optical fiber sensing configuration is employed. In this configuration, GO doped nanostructured (sol-gel) silica film of appropriate thickness and composition is synthesized over the centrally decladded region of straight and uniform plastic-clad silica (PCS) multimode optical fiber. Throughout linear response over a dynamic range as wide as 15.0−95.3%RH, and optimum sensitivity of 0.1036 dB/%RH is observed for the sensor. The developed sensor is observed to be highly

reversible, stable, with average response and recovery times of 0.1436s and 0.1547s, respectively. In order to enhance the sensitivity further, another optical fiber RH is developed employing reduced graphene oxide (rGO) in sol-gel silica nanostructured film over the same fiber configuration. With an optimized sensing cladding configuration, an enhanced sensitivity of 56.3mV/%RH (0.1262dB/%RH) is observed. Additionally, slightly improved response and recovery time of 0.18s is observed in this case. However, the dynamic range of the linear response is observed to be 5−57%RH. Sensor response is again observed to be highly reversible, and repeatable. Quest for achieving higher sensitivity over the wider dynamic range and better response/recovery time continued in the present research, which led to the development of another optical fiber sensor by exploiting graphene oxide quantum dots (GQDs) keeping the same sensor configuration and the sensing scheme. GQD based sensor not only improves the sensitivity, but also improves the range of linear operation and the response/recovery times. A sensitivity of 0.2437 dB/%RH over the dynamic range of 4−70%RH and the response/recovery times of 0.025s are observed. Though the sensitivity, dynamic range and response/recovery times all improved, but the scope for further improvement of sensor's response is observed to be still wide open. Hence, another sensor is developed employing GO-ZnO nanocomposite-based sensing cladding. A sensitivity of 33.6mV/%RH over of 17−91%RH range of linear response and response/recovery times of 0.33s and 0.45s are observed. To further improve the response characteristics, another optical fiber sensor is developed employing GO-ZnO-Fe nanocomposite-based sensing cladding. A sensitivity of 62mV/%RH over the dynamic range of 3−80% RH and the response/recovery times of 0.031s are observed for this sensor. Though the sensitivity and dynamic range got improved, it is felt that the scope for improving response/recovery times is still there. Keeping this point, another sensor that employs rGO-TiO_2 nanocomposite-based sensing cladding is explored. A sensitivity as high as 103.5mV/%RH over 3−70%RH dynamic range of linear response and the recovery/response times of 0.025s are observed for this sensor. Quest of improving response/recovery times led to extend the research further. Hence, another sensor is developed by employing GO coated reduced-to-few-micron core-diameter (RFMCD) PCS multimode optical fiber. Experimental results demonstrate that the proposed sensor exhibits widest linear dynamic range of 3−94%RH with a sensitivity of 0.0115%RH^{-1}. Importantly, an ultrafast response time of 0.64ms is achieved. Such ultrafast response is achieved for the first time in the best of author's knowledge. Though, this sensor is well suited for real-time breath monitoring and voice print recognition, however fixing it inside the testing wearable mask that covers nose and mouth both, requires special and delicate packaging of the sensor. Hence,

research is further extended by incorporating biodegradable polymer polyhydroxybutyrate (PHB) immobilized PVA sensing cladding over the centrally decladded fiber. A sensitivity of 66mV/%RH (0.0236%RH^{-1}) over 58−98% RH dynamic range and the response/recovery times of 0.0125s are observed for the sensor. This biodegradable polymer based optical fiber RH sensor is successfully employed for the real-time breath monitoring and voice print recognition. In the final part of research, biowaste (ash from a Menthol boiling plant) is used for the development of an optical fiber RH sensor. The proposed sensor exhibits linear response across a wide dynamic range of 4−90%RH with an optimal sensitivity of 9.7mV/%RH and response/recovery times of 0.013s and 0.017s, respectively. It is worth mentioning that all the novel sensors developed in the research presented here exhibit high degree of reversibility, repeatability, stability and extraordinarily good resolution.

1.5 Organization of thesis

- **Chapter 2:** This Chapter of the thesis focuses on the development of an optical fiber RH sensor with a high sensitivity, linear response across a wide dynamic range and superfast response and recovery times by employing simplest optical fiber sensing configuration. To fulfil the objective, a suitable chemically synthesized GO doped nanostructure and superfast response and recovery time by employing simplest optical fiber sensing configuration. (sol-gel) silica film was coated onto the decladded portion of straight and uniform multimode plastic cladding silica (PCS) fiber. For the development of the sensor, GO was synthesized by modified Hummer's method [77]. Then the GO diffused silica nanostructure film was fabricated over the centrally decladded PCS fiber having a length and core diameter of 60cm and 125µm, respectively. In the process of optimizing sensor's response, the effects of composition as well as thickness of the sensing film were investigated. The composition of the sensing film was varied by varying amount of water dispersed GO in the sol (in the order of 0.005g/ml, 0.010g/ml, 0.015g/ml) and thickness of the film was varied by employing successive dip-coating (1-dip, 2-dip, 3-dip and 4-dip) for each composition. After preparing the sensing probes, all sensing probes were dried for 48hrs at room temperature and further annealed for 2 hrs at 150°C in order to remove the water and ethanol from the sensing probe. To examine the developed sensors having different GO concentrations and different sensing film thicknesses, they were individually characterized by fixing inside a humidity chamber (dimension: 11 cm× 9cm× 7 cm) in such a way that the sensing portion of the sensor remained in the middle of the chamber.

A commercial sensor having operational range of 0%RH to 100%RH with a sensitivity of 0.01 v/%RH was fixed inside the chamber in order to monitor temperature as well as RH inside the chamber. Humidity level within the chamber was controlled by properly mixing dry and humid air through two very sophisticated flow meters. Light from the He-Ne laser (632.8 nm) source was coupled from one end of the fiber whereas the distal end of the fiber was connected to a photodiode. Photodiode and the commercial sensor were interfaced with a computer through the data acquisition (DAQ) card and MATLAB program for real-time monitoring of the outputs of both the sensors. During the experimental investigations, RH was first reduced to the minimum level by passing dry air within the chamber. Afterward, RH was slowly increased in suitable steps to the maximum possible level by mixing controlled amount of humid air. Outputs from the fiber sensor and the commercial sensor were recorded as a function of time with a resolution of 1s. The temperature inside the chamber remains 24°C throughout the experiment. The experimental study shows that the intensity of fiber output decreases as the humidity inside the chamber increases. From the analysis of experimental data, it is observed that 3-dip coated probe of having 0.015g/ml water dispersed GO concentration in the sol shows the optimum performance. Notably, sensor shows a liner response from 15.0% to 95.3%RH with a sensitivity 0.1036dB/%RH. Further, the dynamic performance and repeatability characteristics of the proposed sensor were investigated by exposing the sensor to the quick and cyclic RH step changes between minimum (~4%RH) and maximum (~88%RH) humidity values. From the results, it is observed that fiber sensor output almost instantly and smoothly changes during the humidification (4%RH to 88%RH) and the desiccation (88%RH to 4%RH). An average response and recovery times of 0.1436s and 0.1547s, were observed for humidification and desiccation respectively. Finally, rigorous analysis was carried out to examine long term performance (repeatability and reliability) of proposed sensor. To do so, optimized optical fiber RH sensing probe was tested in the span of 15 days. At an interval of 4 days, three experiments were carried out. Fiber output corresponding to three different humidity levels (27%, 51% and 69% RH) on three different days. Experimental study shows the maximum variation in output of the optimized fiber sensor 0.1% compared to the first day.

- **Chapter 3:** In order to increase the sensitivity and to achieve better time response, another novel sensor was developed employing reduced graphene oxide (rGO)

immobilized nanostructured (sol-gel) silica sensing film on the centrally decladded straight and uniform multimode PCS optical fiber. For the development of the sensor, rGO was synthesized by chemical reduction of GO [78]. Afterwards, rGO diffused silica matrix was synthesized over the fiber core using sol-gel method. In order to examine the effect rGO concentration and the thickness of silica film on the sensor performance, multiple sensing probes were prepared by varying the rGO concentration in silica film and the film thickness. All developed sensing probes were characterized in a humidity chamber as discussed in Chapter 2. The sensing probe having rGO concentration of 0.1g in 25ml silica sol with film thickness corresponding to 1 dip coating shows the optimum response. The optimized sensing probe shows linear dynamic range of 5−58%RH with a sensitivity of 56.3mV/%RH (0.1262dB/%RH or $0.0104RH^{-1}$).). Afterwards, sensor was exposed to the repeated and quick RH step changes between the 5%RH and 45%RH to investigate the dynamic performance and repeatability characteristics. Slightly improved response and recovery time of 0.18s is observed in this case. In order to ensure the reliability and repeatability of the sensing probe, a series of experiments were conducted. In these experiments, optimized sensing probe was tested in the span of 15 days at an interval of 4 days. The tests were conducted for three different humidity levels (12%, 30%, and 48% RH). It was observed that the maximum variation in the output of the proposed optical fiber sensor in comparison to the day one was only 0.4% across all three humidity levels. As can be observed, though the sensitivity increases and time response improves for the present sensor in compression to the sensor developed and reported in Chapter 2, linear dynamic range was limited. This observation laid the foundation of the research work discussed in the next chapter.

- **Chapter 4:** Quest for achieving higher sensitivity over the wider dynamic range and better response/recovery time continued in the present research, which led to the development of another novel optical fiber sensor by exploiting graphene oxide quantum dots (GQDs) keeping the same sensor configuration and the sensing scheme. For this sensor, graphene oxide quantum dots (GQDs) (zero-dimensional graphene oxide derivative) doped (sol-gel) silica nanostructure thin film was deposited onto the centrally decladded PCS optical fiber. To do so, first, GQDs was prepared using the hydrothermal method [79]. PCS fiber with a length of 60 cm and a core diameter of 125 µm was used to develop an optical fiber RH sensor. A similar method as described in

Chapter 2 was used to develop GQDs doped nanostructured silica sensing film over the centrally decladded PCS optical fiber. Multiple sensing probes were prepared by varying amounts of GQDs in silica sol to examine the effect of GQDs concentration on sensor's performance. For every composition, the film thickness was again varied using multiple dip coating. After preparation, all the developed sensing probes were dried for 48 hrs at room temperature and then annealed for 2 hrs at 120°C to remove the trace of alcohol and water from sensing film. Similar procedures, as explained in Chapter 2, were followed in order to characterize the sensing probes. Experimental investigation establishes that the sensor comprising of film composition of 100mg in 20ml silica sol with the film thickness corresponding to 3 dip coating exibits optimum performance. Linear response over a dynamic range of 4−70%RH with optimum sensitivity of 0.2437dB/%RH are observed for the sensor. Further, in order to investigate the dynamic performance (time-response) of the sensor, it was exposed to the cyclic RH variations between 4%RH and 83%RH. From the result, it is observed that the fiber sensor output almost instantly and smoothly changes during the forward (4%RH to 83%RH) as well as the reverse (83%RH to 4%RH) cycle of the humidity variations. The average response and recovery times are observed to be 0.025s. Stability, repeatability and reliability are other critical parameters for RH detection. Rigorous analysis was carried out to examine short-term and long-term stability performance of the proposed sensor. For analysing the short-term stability test, the sensor was exposed for about 30 minutes at RH levels, once stabilized at three typical values. The maximum standard deviation of intensity is observed to be ±0.016dB. Hence, the maximum resolution of the sensor for RH detection is observed to be ±0.069%RH, which validates the excellent stability and accuracy of RH detection. Finally, to analyze the long-term response (repeatability and reliability) of the proposed sensor. The optimized optical fiber humidity sensing probe was tested in the span of 15 days. The experiments were repeated on four different days with an interval of 5 days at three different RH levels (10%, 39%, and 66%RH). It was observed from the experimental study that the maximum variation in output of the optimized fiber sensor is ±0.73% compared to the first day. As can be observed the sensitivity increases up to 0.2436dB/%RH with a wide dynamic range from 4% to 70%RH and a fast response time of 0.025s. Though the sensitivity, dynamic range and response/recovery times all improved, but the scope for further improvement of sensor's response is observed to be still wide open, which led the foundation of the development of another sensor discussed in the next Chapter.

- **Chapter 5:** As highlighted in the previous chapter, an increase in sensitivity across a wide dynamic range while maintaining a fast response time was successfully achieved, but the scope for the improvement of the response characteristics of sensor still remains to be exploited. Thus, another novel sensor is developed by employing GO-ZnO nanocomposite. The motivation behind utilizing this nanocomposite is the fact that GO is a 2D nanomaterial that exhibits exceptional super-permeability and super-adsorptive capabilities towards water molecules, resulting in excellent dispersibility, hygroscopicity and unique hydrophilicity. On the other hand, ZnO also exhibits humidity sensitive hydroscopic nature [30]. Hence, GO-ZnO nanocomposite is expected to enhance the sensitivity of RH measurement. To do so, GO-ZnO nanocomposite-doped nanostructured (sol-gel) silica film is synthesized onto the centrally decladded PCS fiber to develop the sensor. It is important to mention that GO-ZnO nanocomposite is used for the first time to the best of author's knowledge. For the development of the sensor, GO-ZnO nanocomposites was first prepared by chemical method [77]. PCS fiber with a length of 60 cm and a core diameter of 200μm was used to develop an optical fiber RH sensor. A similar method as described in Chapter-2 was used to develop GO-ZnO doped nanostructured silica sensing film over the centrally decladded PCS optical fiber. A similar methodology as discussed in Chapter 2, was used for the characterization of sensor. Detailed experimental investigations were carried out. Experimental results show that the optimized sensing probe demonstrate a linear response over a dynamic range of 17%-91%RH, with sensitivity of 33.6 mV/%RH. Further, the fiber sensors were exposed to repeated, quick RH step changes between the minimum (5%RH) and maximum (80%RH) values to investigate the dynamic performance of the developed sensor. For the GO-ZnO nanocomposite-based sensor, the average response time and recovery time are observed to be 0.33s and 0.45s, respectively. Finally, rigorous experimental investigation was carried out for long-term stability test. For this, experiments were repeated on three different days with an interval of 4 days at three different humidity levels (21%, 43%, and 71%RH). Maximum variation in the proposed optical fiber sensor's output, compared to day one at all three RH levels, is observed to be as low as ±0.79%.

  Even though the GO-ZnO nanocomposite-based sensing probe shows a wide dynamic range with good sensitivity, the response time still needs to be improved. Hence, another sensing probe based on novel GO-ZnO-Fe nanocomposite doped silica

was developed. The GO-ZnO-Fe nanocomposite-based sensing probe shows a linear response over 17-80%RH, with a sensitivity of 60.6 mV/%RH. The average response and recovery time of the GO-ZnO-Fe nanocomposite-based sensor is observed to be 0.031s. Hence the incorporation of Fe in GO-ZnO nanocomposite enhanced the sensitivity with approximately 10 times faster response time. For analyzing short-term response, the sensor was exposed for about 60 minutes at three RH levels. The maximum standard deviation of intensity is ±4.9mV. Hence, the maximum resolution of the sensor for RH detection is observed to be ±0.079%RH. Further in the long-term stability test, the maximum variation in the proposed optical fiber sensor's output, compared to day one at all three RH levels, is observed to be ±0.37%. Though the sensitivity, dynamic range as well as response time all got improved, it is felt that the scope of improving response/recovery times is still there, which led the foundation of the development of another sensor reported in Chapter 6.

- **Chapter 6:** In the previous Chapter, a wider dynamic range with optimum sensitivity is achieved. However, there is considerable scope for further enhancement in the sensor's response. To, achieve this objective, another novel sensor is developed using rGO-TiO2 nanocomposite doped nanostructured (sol-gel) silica film on the centrally decladded PCS optical fiber. For the development of the sensor, first rGO-TiO2 nanocomposite was prepared by ultrasonication method [80]. Plastic-clad silica fiber with a length of 60 cm and a core diameter of 200µm was used to develop an optical fiber RH sensor. A similar method, as described in Chapter-2, was used to develop rGO-TiO2 doped nanostructured (sol-gel) silica sensing film over the centrally decladded PCS optical fiber. Multiple sensing probes were prepared by varying amounts of rGO-TiO_2 in silica sol to examine the effect of nanocomposite concentration on sensor's performance. Similar procedure, as explained in Chapter-2 was followed in order to characterize the sensing probes. Experimental investigation established that the film composition 100mg in 20ml silica sol shows optimum response. The proposed sensor exhibits a linear response over 3%-70%RH with a very high sensitivity of 103.5 mV/%RH (0.0145RH-1). In the next step, the dynamic performance of the optimized probe was investigated following similar procedures as explained in Chapter 4. The recovery and response times for the rGO-TiO2 nanocomposite-based sensor is observed to be 0.025s. Further, the optimized sensing probe was tested for short-term and long-term stability performance. For analyzing short-term stability performance, the sensor was exposed for about 60 minutes at three different RH levels. The maximum standard deviation of

intensity is ±10.3mV. Hence, the maximum resolution of the sensor for RH detection is observed to be ±0.101%RH. Finally, a rigorous experimental investigation was carried out for a long-term stability test. For this, experiments with the same sensing optical fiber probe were repeated at an interval of 4, 5 and 5 days. A total of 4 such repeat experiments on three different days were carried out in a span of 15 days. The maximum variation in the optical fiber sensor output, compared to day 1, at the three different humidity values of 10%RH, 36%RH and 66%RH is observed to be of the order of ±0.4%. As can be observed, enormously high sensitivity is observed for the sensor reported in this chapter. However, the response and recovery times remain the same as observed for the GO-ZnO-Fe nanocomposite based optical fiber sensor reported in Chapter 5. Quest of improving response/recovery times led to extend the research further.

- **Chapter 7:** As discussed in the previous chapter, a very high sensitivity for RH detection is achieved employing rGO-TiO_2 nanocomposite-based sensing cladding over the decladded optical fiber. At the same time, the dynamic range was observed to be only 3−70%RH. It is important to mention that a sensor that exhibits high linear sensitivity in higher RH range with fast response time is the requirement for human breath monitoring and voice-print recognition. In order to fulfil the objective, a novel optical fiber humidity sensor is developed by depositing 675nm thick sensing film of graphene oxide (GO) onto the reduced-to-few-micron core-diameter (RFMCD) straight and uniform sensing region of a PCS multimode optical fiber. For this, graphene oxide (GO) was synthesized using a modified Hummer's method. Then, approximately 2.5 cm from the central portion of the fiber, having a total length of 50 cm was centrally decladed and etched. Etching of the fiber was done using hydrofluoric acid (HF). After that, etched portion of the fiber was coated by a thick layer of pure GO. For the synthesis of GO film on the centrally etched portion of the fiber first, GO was dispersed in alcohol (0.5g in 80ml ethanol). Then the fiber was dipped in the mixed solution and kept in the oven at a temperature 65°C, so that the ethanol gets evaporated, leaving the decladded central part of the fiber coated with GO. Investigation of response characteristics of the sensor was carried out as discussed in the previous chapter. However, in this case one end of the fiber was connected to the broadband hyalogen lamp, and the other end was connected to a spectrometer (ocean optics RH4000). Fiber sensor output spectra corresponding to different values of applied humidity were recorded using the spectrometer. Linear response over a dynamic range of 3-94%RH with an optimum

sensitivity of $0.0115RH^{-1}$ was observed for this sensor. After that, the sensor was exposed to repeated, quick RH step changes between the 5% and 83% RH values to investigate the dynamic performance and repeatability characteristics. An ultrafast averege response and recovery times are observed to be 0.64ms. Rigorous analysis was carried out to examine short-term and long-term stability performance of the proposed sensor. For analysing short-term stability performance, sensor was exposed for about 30 minutes at RH levels, once stabilized at three humidity values. The maximum standard deviation of normalized intensity is observed to be $\pm 5.57\times10^{-4}$. Hence, the maximum resolution of the sensor for RH detection is ±0.049%RH. For analyzing the long-term stability test, experiments were repeated on four different days with an interval of 3, 5 and 4 days, thus spanning a total of 16 days. These experiments were performed at three different RH levels (18%, 55% and 80%RH). Compared to day one, the maximum variation in the normalized output of the proposed sensor is observed to be less than 0.8% at all three RH levels. The sensor shows a linear response over the widest dynamic range with ultrafast response in comparison to previously reported sensors. Though, this sensor is well suited for real-time breath monitoring and voice print recognition, however fixing it inside the testing wearable mask that covers nose and mouth both, requires special and delicate packaging of the sensor. Hence, research is further extended to develop another optical fiber sensor as discussed in Chapter 8.

- **Chapter 8:** The sensor reported in the previous chapter shows an ultrafast response over a wide dynamic range with optimum sensitivity, and hence, is highly advantageous for real-time humidity detection in diverse applications. Though, this sensor is well suited for real-time breath monitoring and voice print recognition, however fixing it inside the testing wearable mask that covers nose and mouth both, requires special and delicate packaging of the sensor. Hence, research is further extended to development another novel optical fiber RH sensor, which is done by incorporating biodegradable polymer polyhydroxybutyrate (PHB) immobilized PVA sensing cladding over the centrally decladded fiber. To the best of the author's knowledge, PHB-doped PVA is used for the first time in the development of an optical fiber humidity sensor. For the development of the sensor, first, PHB was extracted from cyanobacteria algae. Subsequently, PHB-doped PVA was coated over the centrally decladded optical fiber via the dip coating method. Similar procedure, as discussed in Chapter 2, was followed in order to characterize each sensing probe. The sensing probe having 6-dip film

thickness with film composition 10ml 0.25%PVA+10mg PHB shows the optimum response. A sensitivity of 66mV/%RH ($0.0236RH^{-1}$) over the dynamic range of 58-98%RH is observed in the sensor. For the dynamic performance, the optimized sensing probe was subjected to quick cyclic relative humidity (RH) change from 55% RH to 98% RH. An average response time of 0.0125s is observed during humidification and dehumidification. Further, the sensor was tested for short-term and long-term stability performances. For the short-term stability performance, the sensor was exposed for about 30 minutes at three different RH levels. The maximum standard deviation in intensity ±5.4mV is observed. Thus, the maximum resolution of the sensor for RH detection is observed to be ± 0.0818%RH. For long-time stability of the optimized sensing probe was tested at three different humidity levels at four different days in the span of 15 days. The maximum intensity fluctuation was observed to be 0.5%. The PHB-based optical fiber sensor demonstrates very-fast response and recovery characteristics, along with excellent long-term stability when operating within a high humidity range of 58–98% RH. Consequently, the PHB-based optical fiber sensor proves to be highly advantageous for real-time humidity detection in diverse applications, including breath monitoring and voiceprint recognition. For the breath monitoring and voiceprint recognition, a new sensing probe having a sensing length of 2.5cm was developed and fixed in a nebulizer mask. Light from He-Ne laser was launched from one end of the sensor and another end of the sensor was connected to the photodetector. Sensor's output intensity was continuously measured throughout the breath cycle at intervals of 10ms. Experiments were performed for diverse breathing patterns across various age groups. Experimental results show that the proposed sensor is able to monitor humidity variation for various breath conditions. Further, the sensing probe was also tested for voice print recognition. The experimental result shows that the sensor responds exceptionally well when words such as “hi”, “fiber”, and “optics” are spoken by a volunteer (a 31-year-old man).

- **Chapter 9:** In this chapter, out of box idea of using ash to develop optical RH sensor is exploited. For this, a biowaste (ash from Mentha boiling plant) is used for the development of optical fiber RH sensor for the first time to the best of author’s knowledge. In order to prepare the sensing probe, ash collected from the menthol boiling plant was initially filtered using a fine mesh and then subjected to 40 hours of sonication in deionized water. After sonication, the solution was filtered and dried to

get fine Ash powder. Then the ash was coated over the centrally decladded PCS fiber. For this, a suitable amount of ash is dispersed in acetone. Fiber is then dipped in the mixed solution and kept in the oven at a temperature 65°C, so that acetone gets evaporated, leaving the decladded central part of the fiber coated with ash film. Similar procedures as discussed in Chapter 2, was followed in order to characterize each sensing probe. Experimental investigations establish the breakthrough of using ash immobilized cladding onto the decladded optical fiber as the RH sensing cladding. Proposed sensor exhibits linear response across a wide dynamic range of 4-90%RH with an optimum sensitivity of 9.8mV/%RH ($0.0076RH^{-1}$). For the dynamic performance (time-response), the optimized sensing probe was subjected to quick cyclic relative humidity (RH) change from 3% RH to 87% RH. The sensor exhibited an average response and recovery time of 0.013s and 0.0144s, respectively. Further, the sensor was tested for short-term and long-term stability performance. For analysing short-term stability performance, the sensor was exposed for about 30 minutes at RH levels, once stabilized at three humidity values. The maximum standard deviation of normalized intensity is observed to be ±3.65 mV. Thus, the maximum resolution of the sensor for RH detection is observed to be ±0.37%RH. Finally, to examine the long-term stability performance of the proposed sensor, experiments were repeated on four different days in a span of 16 days at three different humidities (15%RH, 55%RH, and 80%RH). In comparison to day one, the maximum variation in normalized output of the proposed sensor is observed to be less than 0.27% at all three RH levels. This shows the excellent repeatability and reliability of the developed optical fiber humidity sensor.

- **Chapter 10:** This chapter presents a summary and highlights of the optical fiber humidity sensors developed in the course of this research, employing intensity modulation through the evanescent wave (EW) absorption technique.

Above work has resulted in following publications:

(A) IN INTERNATIONAL JOURNALS

1. Sunil Mohan and Sunil K. Khijwania, “Highly sensitive GO-ZnO nanocomposite-based optical fiber Relative humidity sensor,” *IEEE Sensors Letters*, vol. 7, no. 9, pp. 1–4, 2023, doi: 10.1109/LSENS.2023.3301846.

2. Sunil Mohan, Sunil K Khijwania, Graphene oxide based optical fiber humidity sensor having linear response throughout a large dynamic range and optimum sensitivity", *Applied optics*, vol. 63, no. 1, pp 179-185, 2023, doi.org/10.1364/AO.507936.

3. Sunil Mohan, Sunil K. Khijwania, "Reduced graphene oxide (RGO) based optical fiber humidity sensor," *OFS-2020*, Th4.17, pp. 1-4, 2021, doi: 10.1364/ofs.2020.th4.17.

4. Sunil Mohan, F. Banoo, and Sunil K. Khijwania, "Graphene-Oxide Based Humidity Sensor Employing Few Micron Diameter Optical Fiber," *2022 Conference on Lasers and Electro-Optics, CLEO 2022 - Proceedings*, pp. 3–4, 2022, doi: 10.1364/cleo_at.2022.ath2k.3.

5. S. Mohan and Sunil K. Khijwania, "Graphene oxide Quantum dots (GQDs) based optical fiber humidity sensor," *OFS2022*, vol. 1, no. c, pp. 1–4, 2022.

6. Sunil Mohan, Sunil K Khijwania, "Highly-sensitive ultrafast Graphene oxide-based optical fiber humidity sensor", (Communicated).

7. Sunil Mohan, Sunil K Khijwania, "Highly sensitive fiber-optic humidity sensor based on reduced graphene oxide (rGO)", (Communicated).

8. Sunil Mohan, and Sunil K Khijwania, "Optical fiber humidity sensor employing Reduced Graphene Oxide Titanium Dioxide (rGO-TiO2) Nanocomposite", (Communicated).

9. Sunil Mohan, Sunil K Khijwania, "Novel GO-ZnO-Fe nanocomposite based ultrahigh sensitive optical fiber humidity sensor", (Communicated).

10. Sunil Mohan and Sunil K Khijwania, "Highly sensitive Blue Luminescent Graphene Oxide Quantum Dots (GQDs) based Optical Fiber Humidity Sensor (Communicated).

11. Sunil Mohan, P R Yashavanth, Soumen K. Maiti, Sunil Khijwania, "Highly sensitive biodegradable polymer-based novel optical fiber humidity sensor for human breath monitoring voiceprint recognition", (manuscript under preparation).

12. Sunil Mohan, Sunil K Khijwania, "Biowaste (ash from menthol boiling plant) based highly sensitive novel optical fiber humidity sensor having large dynamic range," (manuscript under preparation).

(B) IN INTERNATIONAL CONFERENCES

1. Sunil Mohan, Sunil K Khijwania, "Blue luminescent graphene oxide Quantum Dots (GQDs) based Optical Fiber Humidity Sensor," XLIV OSI Symposium on Frontiers in Optics & Photonics "FOP-21" 24-27 September 2021, IIT Delhi. (Oral presentation)

2. Sunil Mohan, Manish Singh Negi, Sunil K Khijwania, "A novel optical fiber humidity sensor employing Reduced Graphene Oxide Titanium Dioxide (rGO-TiO2) Nanocomposite", XLIV OSI Symposium on Frontiers in Optics & Photonics "FOP-21" 24-27 September 2021, IIT Delhi. (Oral presentation)

3. Sunil Mohan, Fatima Banoo, Sunil K Khijwania, "Graphene oxide-based humidity sensor employing few microns diameter PCS fiber," Conference on Lasers and Electro-Optics "CLEO" 15–20 May 2022, San Jose, California, United States. (Oral presentation)

4. Sunil Mohan, Sunil K. Khijwania, "Graphene oxide Quantum dots (GQDs) based optical fiber humidity sensor," 27th international conference on optical fiber senor "OFS-27", 29 August-2 September, 2022, Westin Alexandria (U.S.A.). (Poster presentation)

5. Sunil Mohan, Manish Singh Negi and Sunil K Khijwania, "rGO-TiO2 nanocomposite based optical fiber Relative humidity (RH) sensor, "25th Congress of the international commission of optics & 16th International Conference on Optics with in Life Science "*ICO-25* and *OWLS-16" 05 - 09 September* 2022, Technische Universität Dresden, Germany. (Poster presentation)

6. Sunil Mohan, and Sunil K Khijwania, "GO-ZnO nanocomposite-based optical fiber Relative humidity (RH) sensor," XLV symposium of OSI: Conference on optics, photonics & quantum optics "COPaQ 2022" 10-13 November, 2022, IIT Roorkee. (Poster presentation)

7. Sunil Mohan, Manish Singh Negi, Sunil K Khijwania, "Highly sensitive Optical fiber sensor for humidity measurement," "WRAP 2023" 07-09 December, 2023, IIIT Allahabad. (Poster presentation).

Chapter 2 : Graphene oxide-based optical fiber humidity sensor having a linear response throughout a large dynamic range and optimum sensitivity

2.1 Introduction

Precise control and monitoring of relative humidity (RH) is critically important in many scientific and industrial applications, including but not limited to structural health monitoring, semiconductor/electronic manufacturing, air-conditioning, food processing, medical/pharmaceutical industries, and environmental monitoring industries [3]. Several conventional (resistive and capacitive) RH sensors are commercially available, which exploit electrical properties of the sensing materials. However, major disadvantages of these sensors are their inability toward multiplexing, remote-sensing, and deployment in hazardous/ corrosive environments, and their susceptibility toward random electromagnetic radiations originated from other sources. An alternate and powerful solution that overcomes all these disadvantages is offered by optical fiber sensors. Additional distinct merits, such as very high sensitivity toward the applied perturbations/measurands, distributive sensing, biocompatibility, small volume, light weight, etc., have played a pivotal role in shifting the focus of research activities toward the development of optical fiber sensors for wide range of real-field applications. Today, optical fiber sensors are deployed for monitoring various parameters of interest spanning from physical and chemical to biochemical parameters, to name a few [31]. Numerous efforts have been made to develop optical fiber humidity sensors. Various sensing schemes, e.g., wavelength modulation through fiber Bragg gratings/long-period gratings [55], [56] phase modulation through optical fiber-based interferometric structures [59], [66] and intensity modulation through evanescent wave absorption, are employed to develop these sensors [7], [42]. These sensing schemes are indirect schemes in the sense that a suitable material is required to facilitate interaction of the optical signal (usually at 632.8 nm or at 1550 nm) with the RH perturbations applied to the fiber sensor. Various humidity sensitive hydroscopic materials, e.g., polyimide, poly (ethylene oxide)/cobalt chloride, agarose, chitosan, polyvinyl alcohol, and metal oxides, have been used not only for this purpose but also

to enhance the sensitivity of the RH measurement. As far as the performance characteristics of these sensors are concerned, it is observed that the sensor's response is either piece-wise linear or nonlinear throughout the reported dynamic range [7], [42]. This leads to a large scope of research for realizing optical fiber sensors with the widest possible linear dynamic range as well as an optimum sensitivity. As far as grating-based optical fiber sensors are concerned, temperature/strain cross-sensitivity imposes major limitations toward real-field applications. In addition, grating and interferometric sensors require sophisticated manufacturing techniques along with bulky and costly interrogation devices. A less costly and less complicated sensor is always preferred.

Recently, graphene and graphene derived materials have attracted significant research interest in the field of sensing because of their unique and excellent properties over the other materials [60]. Graphene oxide (GO), a two-dimensional nanomaterial, is one of the most important derivatives of graphene. The monolayer of GO contains sp2 and sp3 hybridized carbon atoms along with oxygen rich functional groups such as hydroxyl and epoxide groups on the basal plane, whereas carbonyl and carboxyl groups at the edge [74]. The structure, associated oxygen functional groups, and high surface area to volume ratio make GO film super-permeable and super adsorptive to water molecules [39]. This leads to an excellent dispersibility, hygroscopicity, and unique hydrophilicity [55], [60] making GO an outstanding candidate for RH sensing. Hence, researchers employed GO as the RH sensing medium in conjugation with different fiber geometries/configurations to develop an effective RH sensor [39], [55], [57], [58], [81], [82]. Huang *et al.* [39] reported an optical fiber RH sensor based on GO coated side-polished single-mode fiber. Whereas, Xiao *et al*. [33] reported another side-polished single-mode fiber (SP SMF) RH sensor that employed humidity sensitive reduced-GO film. In another research work, Wang *et al.* [57] employed an interferometric technique while reporting an optical fiber RH sensor. The sensor was based on an in-fiber Mach-Zehnder interferometer (MZI) coated with GO/PVA composite film. Liu *et al*. [58] reported another interferometric RH sensor that employed a GO-coated core-offset fiber MZI. Employing an infiber grating-based scheme, Dissanayake *et al*. [55] reported a GO coated long period grating (LPG)-based RH sensor. Wang *et al*. [48] reported a tilted FBG-based RH sensor. In another attempt, Xin *et al*. employed GO coated photonic crystal fiber (PCF) to develop an RH sensor [81]. Liu *et al*. reported an evanescent wave modulation scheme-based RH sensor employing a GO coated micro-capillary [43]. In another scheme, Gao *et al*. developed a single-mode fiber RH sensor employing reduced- GO coated hollow core fiber [69]. In another research work, Zhao *et al*. reported an RH sensor employing GO coated tapered single mode optical fiber having curved

geometry [82]. One of the very important and common observations in all these sensors is the limited dynamic range of RH measurement. The response of some of these sensors is observed to be either nonlinear or piecewise linear. In the latter case, linear response is observed only over a very short dynamic range. In both the cases, sensitivity is compromised in a large range of the humidity variations. Also, the response (humidification) time and recovery (desiccation) time, as reported for some of the sensors, are observed to be very high (ideally, it should be very low for the sensor to be ultrafast). Further, all the GO-based optical fiber sensors, reported in the literature, employed either the interferometric configuration, side-polished SMF/tapered SMF/grating structures, or microcapillary/ hollow-core fiber/PCF. These sensors are complicated in the sense that they require very complex manufacturing processes as well as costly/sophisticated interrogation devices. An optical fiber sensor that is simple to manufacture, having wide dynamic range, linear response throughout its dynamic range, optimum sensitivity, and fast response time is of great interest in real-field applications.

The main objective of the research reported in this chapter is to develop an optical fiber RH sensor with a high sensitivity, linear response over a wide dynamic range and superfast response and recovery times by employing simplest optical fiber sensing configuration. To fulfill the objective, an optical fiber humidity sensor is developed by employing GO diffused nanostructured sol-gel silica film of appropriate thickness and composition as a sensing cladding over the centrally decladded region of straight and uniform plastic-clad silica (PCS) multimode optical fiber. The proposed sensor exploits intensity modulation through evanescent wave absorption—one of the simplest techniques for developing optical fiber RH sensors. Such a simple sensor configuration, i.e., straight, and uniform optical fiber with GO diffused nanostructured sol-gel silica film as the sensing cladding in the central region of the fiber, is used for the first time to the best of author's knowledge for developing optical fiber RH sensors. Rigorous experimental investigations are carried out to establish the response characteristics of the proposed sensor. Throughout, a linear response over a dynamic range, as wide as 15.0%–95.3%RH, and an optimum sensitivity of 0.1036 dB/%RH are observed. Importantly, manifold sensitivity enhancement is observed for the sensor employing GO diffused nanostructured sol-gel silica sensing film in comparison to the sensor employing only pure silica nanostructured sensing film. In addition, the proposed sensor is observed to be extraordinarily fast while responding to the applied RH perturbations, which is depicted by the observed response time of 0.1436 s and recovery time of 0.1547 s. Repeatability and reversibility tests, conducted in extreme conditions over a span of 9 days, establish an absolutely invariable response of the sensor.

2.2 Experiment

2.2.1 Sol-gel process

The sol-gel process is a highly versatile and extensively employed technique for synthesizing hybrid and inorganic materials, such as composites, ceramics, and glasses. Typically, the sol-gel process involves the hydrolysis and condensation reactions of a metal alkoxide compound. Metal alkoxides, specifically silicon alkoxides like $Si(OC_2H_5)_4$, tetraethyl orthosilicate (TEOS), $Si(OCH_3)_4$ and tetramethyl orthosilicate (TMOS) are frequently employed in the synthesis of nanoporous glass matrices with interconnected pores formed by a three-dimensional SiO_2 network [83]. The sol-gel process comprises three steps: (1) sol formation, (2) gelation, and (3) drying. Initially a suitable amount of silicon alkoxides (for example TEOS), ethanol and water are mixed. Subsequently, a precise quantity of hydrochloric acid (HCl) is introduced into the solution while continuously stirring to adjust its pH. This process results in the formation of a homogeneous solution known as a sol. The sol is then allowed to undergo gelation for a period spanning several hours to days. During this stage, hydrolysis and condensation reactions occur, leading to the formation of siloxane polymers as depicted in the following:

Hydrolysis: Formation of silanol group (Si-OH)

$$Si(OC_2H_5)_4 + H_2O \rightarrow Si(OC_2H_5)_3(OH) + C_2H_5OH$$

Condensation: Formication of siloxane polymers

$$Si(OC_2H_5)_3(OH) + Si(OC_2H_5)_3(OH) \rightarrow (OC_2H_5)_3Si{-}O{-}Si(OC_2H5)_3 + H_2O$$

The aging process of the sol-gel method initiates poly-condensation reactions. This entails the crosslinking of silanol groups with siloxane, resulting in the formation of a SiO_2 nanostructure network. This process creates silanol groups on the surface of the network. The solvents can be removed by annealing the gel at higher temperatures through evaporation. A sensing agent added to the mixture at a specific point during the formation of sol can be securely trapped within the nanoporous glass matrix after gelation. Sol-gel-derived glass provides advantages with its porosity and accessibility, facilitating efficient transport diffusion of analyte molecules in and out from the porous sol-gel glass matrix. The chemical inertness of silica enables sensing probes based on such glasses to operate effectively in harsh environments. It also exhibits compatibility with numerous inorganic and organic reagents, allowing for the entrapment of diverse sensing agents within the nanostructure glass matrix. To design an OFS, a thin film of

sensing reagent doped sol-gel can be coated on the bare core of the fiber using dip-coating method. Numerous optical and optical fiber sensors based on sol-gel technology have been reported in literature [84]–[86].

2.2.2 Synthesis of graphene oxide

Graphene oxide was synthesized from natural graphite via the modified Hummer's method [87]. For this, an appropriate amount of graphite powder was added to the concentrated sulfuric acid (H_2SO_4) under constant stirring. Afterward, potassium permanganate ($KMnO_4$), a strong oxidizing agent, was slowly added to the solution. Stirring of the resulting solution was continued for more than 1 h. After proper oxidation of graphite, the excess amount of $KMnO_4$ was eliminated by slowly adding hydrogen peroxide (H_2O_2). The color of the solution changed from dark brown to light yellowish brown. The resulting solution was filtered, and the residue (filtrate) was treated with dilute hydrochloric (HCl) acid and then thoroughly washed multiple times with deionized (DI) water. The washed and then centrifuged solution carried purified GO, which was then dried in vacuum at a proper temperature to get the desired graphene oxide.

2.2.3 Characterization of Graphene Oxide

X-ray diffractometer (XRD, Rigaku TTRAX III) in Bragg–Brentano geometry, operating at 5kW with Cu-Kα radiation (λ = 1.5406 Å) is used for the structural characterization of synthesized GO at room temperature. XRD spectra are measured in the range of 2θ from 5° to

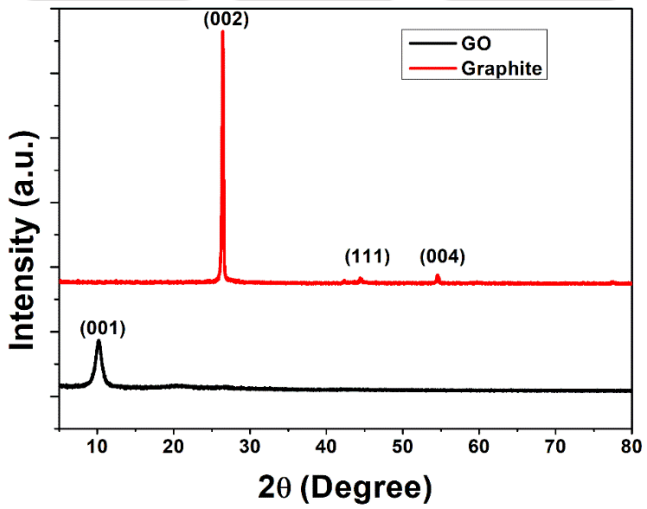

Fig 2.1 : *XRD spectra of Graphite and graphene oxide (GO).*

80°. Fig 2.1 shows the XRD spectra of graphite and GO. As can be observed, graphite exhibits an intense peak at $2\theta = 26.4°$ (interlayer spacing 0.337 nm) that corresponds to the (002) crystal

plane. On the other hand, GO exhibits an intense peak at $2\theta = 10.2°$ (interlayer spacing of 0.867 nm) that corresponds to the (001) crystal plane. This clearly shows that the oxidation of graphite. results in structural changes as it introduces oxygen-rich functional groups in the interlayer spacing, thereby increasing the interlayer spacing. In order to investigate further, elemental characterization of graphite and GO was carried out using energy dispersive X-ray (EDX, Zeiss Sigma, measured at 20kV) analysis. Results of EDX analysis are summarized in

Table 2.1 : *Results of elemental analysis of Graphite and GO using EDX.*

Elements	**Atomic %**	
	Graphite	*GO*
Carbon	87.2	63.5
Oxygen	8.2	31.5
Nitrogen	-	2.7
Sulphur	2.3	2.32
Silicon	0.82	0.84
Potassium	0.18	0.12

Table 2.1. It is evident from these results that the carbon percentage decreases from 87.2% (for graphite) to63.5% (for GO), whereas the oxygen percentage increases from 8.2% (for graphite) to 31.5% (for GO). This confirms the successful oxidation of graphite and the formation of GO.

2.2.4 Sensing probe preparation

Plastic-clad silica (PCS) multimode fiber (core *r. i.* 1.457, clad *r. i.* 1.404 and core diameter 125µm) was used to develop the proposed RH sensor. 60 cm length of this fiber was taken for preparing the sensor. Both the ends were polished to get optically flat end-faces in the transverse section of the fiber, which is critically important for achieving maximum power coupling efficiency from source to the fiber and fiber to the detector. Cladding was removed from the length of 5 cm in the central region of the fiber. GO was then synthesized through a solgel nanostructured matrix over this centrally decladded straight and uniform region of the fiber to fabricate the sensing film. For this synthesis of GO diffused silica matrix, silica sol was prepared by mixing tetraethyl orthosilicate (TEOS), DI water, ethanol, and hydrochloric acid in the ratio of 3:2:1:0.01. Suitable amount of water dispersed GO was mixed into the sol under constant stirring. In order to investigate the effect of sensing film composition on the sensor performance, amount of water dispersed GO in the sol was varied

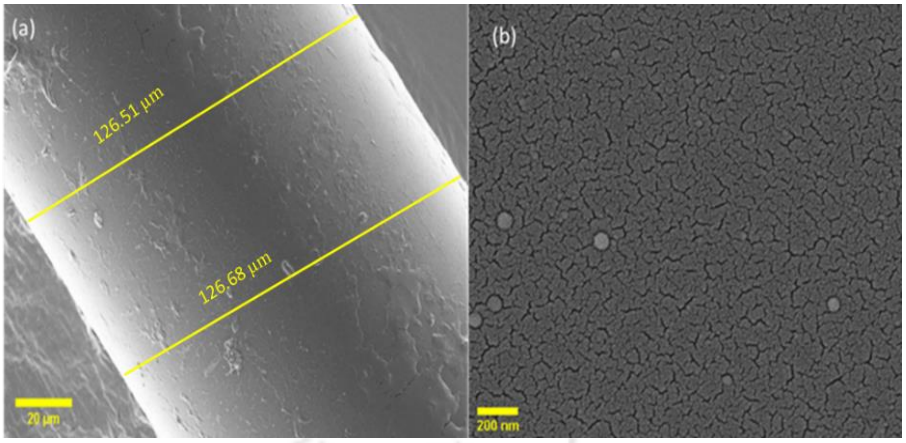

Fig 2.2 : *(a) FESEM image of the centrally decladded region of the fiber carrying GO defused silica sensing film (b) FESEM image of surface morphology of GO defused silica sensing film.*

in the order of 0.005g/ml, 0.010g/ml, 0.015g/ml. Dip coating method was used to deposit GO diffused nanostructured silica film onto the centrally decladded region of the fiber core for each sol solution. In order to further investigate performance of the sensor, multiple dip coating (1-dip, 2-dip, 3-dip and 4-dip) was employed in order to vary the thicknesses of the sensing film for each sol solution carrying different amount of diffused GO. All sensing probes were dried at room temperature for 48 hours, and afterwards, annealed at 100 °C for 2 hours in order to remove ethanol and water from the pores of the sensing film. Surface morphology, nanostructure and the thickness of deposited film were examined by FESEM. Fig 2.2(a) depicts, as an example, image of the 3-dip coated sensing region of the optical fiber having GO concentration that corresponds to 0.015g/ml. Average diameter in this region is observed to be ~126.60µm, which establishes an average thickness of the sensing film as 0.80µm. Surface morphology of the deposited sensing film for this probe is depicted in Fig 2.2 (b), which shows an interconnected high quality porous structure with moderate roughness.

2.2.5 Design and development of humidity chamber

A humidity chamber has been designed using a 1cm thick Perspex sheet to characterize the prepared sensing probes properly. The schematic diagram of the experimental setup is shown in Fig 2.3. The dimension of the chamber was 11 cm x 9 cm x 7cm. Inside the chamber, humidity level was precisely controlled by properly mixing dry and moist air through sophisticated flow meters (IEPL, Model 1355E). In this setup, air was initially divided into two separate channels. Air from one of the channels was passed through a water bath utilizing a flow meter to induce humidity, after which it was subsequently supplied to the humidity chamber. Air coming through the other channel was passed through an alumina-coated pipe and fed to the humidity chamber using another flow meter. A small outlet valve was made in

the humidity chamber in order to maintain the proper airflow. A commercial RH sensor (Totronic HygroClip 1HC2), having an accuracy of ±0.8%RH in the range of 0–100%RH, was fixed inside the chamber in order to monitor RH and temperature variations.

2.2.6 Characterization of the sensor

In order to investigate the response characteristics, sensor was fixed inside an in-house developed humidity chamber, maintaining the sensing region in the middle of the chamber (Fig. 2.3). Light from an He-Ne laser operating at 632.8 nm wavelength was coupled to the fiber. The other end of the fiber was connected to a photo- detector using a sub miniature version connector. Photodiode and the commercial sensor were interfaced with a computer through the data acquisition (DAQ) card and MATLAB program for real-time monitoring of the outputs of both the sensors. During the experimental investigations, RH was first reduced to the minimum level by passing dry air within the chamber. Afterward, RH was slowly increased in suitable steps to the maximum possible level by mixing controlled amount of humid air. Outputs from the fiber sensor and the commercial sensor were recorded as a function of time with a resolution of 1s.

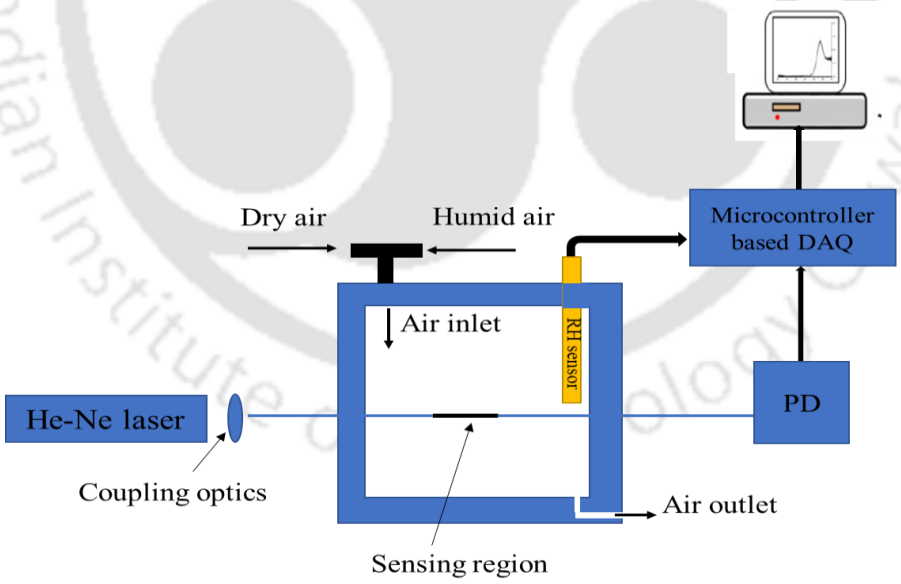

Fig 2.3 : *Schematic diagram of the experimental setup for the characterization of optical fiber humidity sensor.*

2.3 Result and discussion

Proposed sensor exploits the phenomena of intensity modulation through evanescent wave interaction with GO diffused nanostructured sol-gel thin sensing film in the cladding of the fiber. This sensor employs the simplest and easiest sensing configuration where the sensing film is synthesized onto the centrally decladded region of straight and uniform PCS optical fiber. In the process of optimizing sensor's response, the effects of composition as well as thickness of the sensing film were studied. Composition of the sensing film was varied by varying amount of water dispersed GO in the sol (in the order of 0.005g/ml, 0.010g/ml, 0.015g/ml) and thickness of the film was varied by employing successive dip-coating (1-dip,

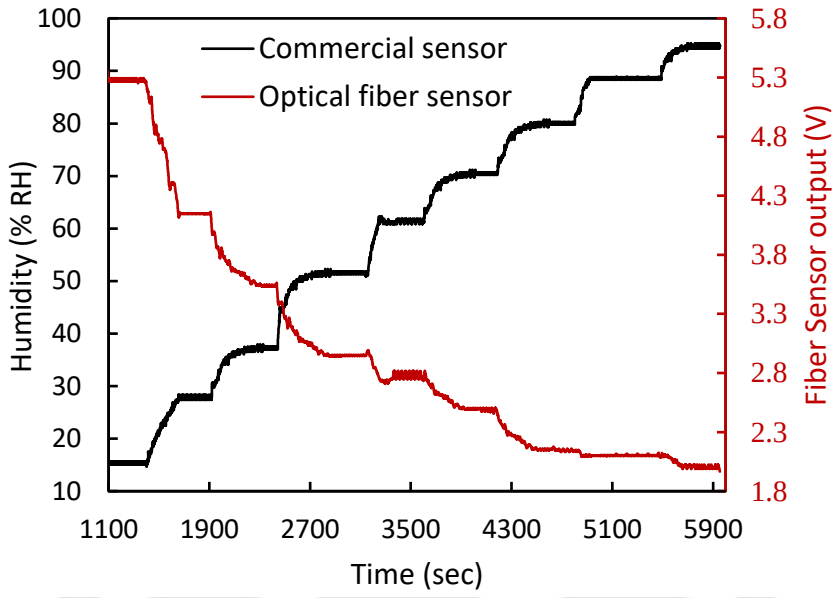

Fig 2.4 : *Time variation of the commercial humidity sensor and the optical fiber RH sensor (3-dip coated probe of 0.015g/ml water dispersed GO in the sol).*

2-dip, 3-dip and 4-dip) for each composition. In order to investigate response characteristics, outputs from the proposed and commercial sensors were monitored in real-time under varied humid environments. Throughout the experiment, temperature was kept constant at 25°C. As already established in our previous research [31], here also, best response characteristics were observed for 3-dip coated sensor irrespective of the film composition. Fig 2.4 depicts typical time-response of the sensor while increasing the humidity, as an example, for the sensing probe having film composition corresponding to 3-dip coating of 0.015g/ml water dispersed GO concentration in the sol. Here, the outputs of both the sensors are recorded as a function of time with a resolution of 1 s. Similar response was observed while decreasing the humidity. As can be observed from this result, fiber output decreases as humidity increases within the chamber.

Reason is, pure silica matrix, synthesized via sol-gel technique, is a porous nanostructure. When exposed to the humid environment, water molecules diffuse into the nano-scaled pores and get adsorbed. Immobilization of GO in the nanostructured silica film greatly stimulates the adsorption of water molecules within the sensing cladding. Rate of adsorption, and that ways, refractive index of the sensing cladding increases with the increase in RH. This results in the leakage of the guided power to the cladding modes in the sensing region; thus, facilitating comparatively intense intensity modulation. In order to proceed further, output of optical fiber sensor corresponding to the applied humidity (commercial sensor's output) was read from the stabilized portion of the response characteristics, depicted in Fig. 2.4. Maximum optical fiber output was observed at 2.44%RH. For the deeper understanding of the sensor's response,

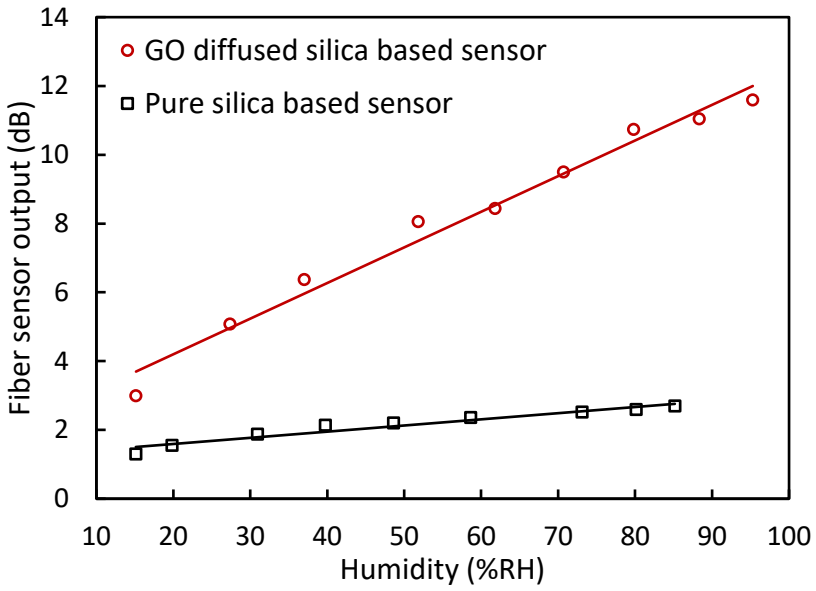

Fig 2.5 : *Experimentally observed response of the developed optical fiber RH sensor.*

over a dynamic range as wide as 15.0−95.3%RH. The sensitivity for humidification is observed to be 0.1036 dB/%RH. Similar response was observed for dehumidification. In order to investigate the optimum composition of the sensing film in accordance to [31], experiments were extended to other 3-dip probes of varying GO concentrations. It was observed that 0.015g/ml water dispersed GO in the sol constituted optimum composition for the sensing film in this study.

To analyze the effect of the presence of GO in the nanostructure silica matrix, optical fiber sensor based on pure sol-gel sensing film was also prepared. Response characteristics of this sensor is also plotted in Fig 2.5. The sensitivity for pure sol-gel based sensor is observed to be 0.009dB/%RH. This shows a manifold (~6 times) increase in the sensitivity for the proposed GO diffused nanostructured sol-gel silica film-based sensor in comparison to the pure sol-gel

based optical fiber sensor. The reason for excellent performance of the proposed sensor is the fact that GO is a good humidity sensing agent due to the presence of abundant hydrophilic functional groups at the surface, and its high surface-to-volume ratio. The incorporation of GO in the sol-gel silica nanostructured matrix increases the number of hydrophilic functional groups, and hence, the adsorption sites for the diffused water molecules within the composite material. This results in manifold increased adsorption of water in GO diffused nanostructured sol-gel silica film and hence, the refractive index of the sensing region, in comparison to the pure sol-gel nanostructure film.

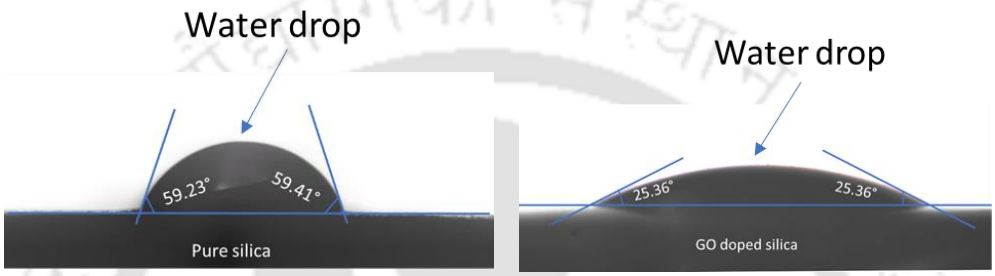

Fig 2.6 : *Contact angle measurement of water droplet on (a) pure sol-gel silica substrate (b) GO diffused nanostructured sol-gel silica substrate.*

To consolidate the hydrophilicity characteristics of the GO diffused nanostructured sol-gel silica film, contact angle (CA) measurements were performed using drop shape analysis for GO diffused nanostructured sol-gel silica substrate as well as pure sol-gel silica substrate at room temperature and 25%RH. As depicted in Fig 2.6, observed forward and backward CAs for pure sol-gel silica substrate are 59.23°and 59.41°, respectively, whereas forward and backward CAs for GO diffused nanostructured sol-gel silica substrate are observed to be 25.36°. Comparatively, the much lower contact angle observed for GO diffused nanostructured sol-gel silica substrate indicates absorption of water molecules within a fast response time (resulting in larger spread of water) and, hence, a better hydrophilicity for this case.

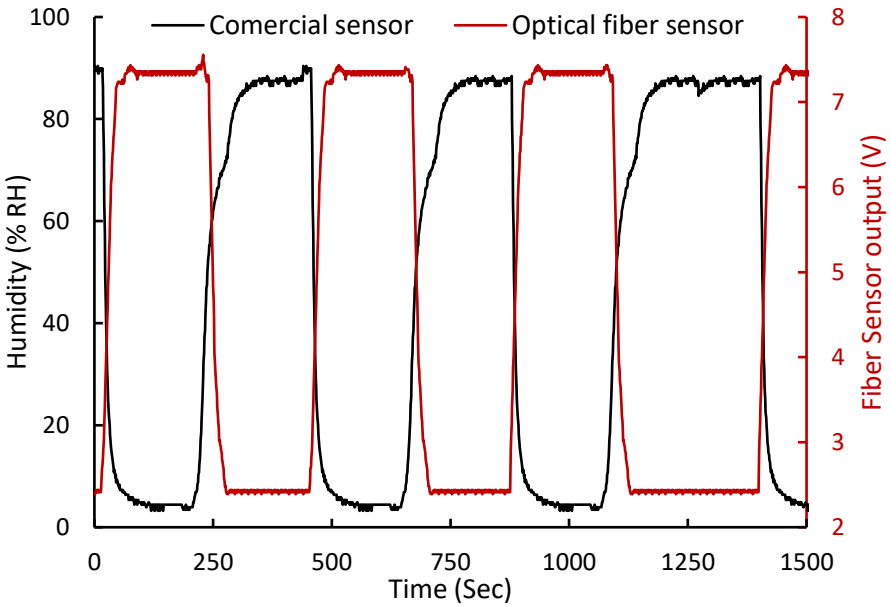

Fig 2.7 : *Time response behavior and the repeatability test for the optimized optical fiber humidity sensor against cyclic humidity perturbations.*

It is important to mention that not only the sensitivity and dynamic range, but detection speed is also a very critical parameter to evaluate the performance of a sensor towards its capability of monitoring dynamic and rapid evolution of ambient humidity. RH sensor having fastest response and recovery time with reversible response characteristics is of great importance. Hence, the dynamic performance and repeatability characteristics of the proposed sensor were investigated by exposing the sensor to the quick and cyclic RH step changes between minimum (~4%RH) and maximum (~88%RH) humidity values. The observed time response is depicted in Fig 2.6. The output of the proposed sensor changes almost instantly and smoothly during the forward (4%RH to 88%RH) and the reverse (88%RH to 4%RH) cycles of the humidity changes. Also, the fiber output is observed to be extraordinarily identical at extreme RH values during the humidification and desiccation cycles. This establishes highly repeatable and completely reversible nature of the proposed sensor. An average response time of 0.1436s during humidification and recovery time of 0.1547s during desiccation processes are observed from Fig 2.6, which is much lower than the response time of the commercial sensor.

Next, response characteristics of the proposed sensor is compared with the other GO based sensors, reported in literature employing various sensing schemes. For comparative analysis, Table 2 lists sensitivity characteristics along with response and recovery times for only those sensors that exhibit linear response over the observed dynamic range. As can be seen, linear

response is observed over a very narrow dynamic range for optical fiber RH sensors, employing various sensing configurations listed here. Overall, the maximum linear dynamic range (30% to 75%RH) is reported for the MZI based optical fiber sensor in [57], whereas an overall highest sensitivity (0.427 dB/%RH) is reported for side-polished SMF based sensor in [39]. In general, response and recovery times (wherever reported) are observed to be very high for GO based optical fiber RH sensors listed in Table 2.2. In comparison, widest dynamic range (15% to 95.3%RH) of throughout linear response is observed for the proposed sensor. This dynamic range is more than double of the dynamic range observed in [39], which is characterized with highest sensitivity. Further, the proposed sensor surpasses all as for as the time response is concerned and emerges with ultrafast response and recovery times (0.1436 s and 0.1547 s respectively) over the 84%RH width of the observed dynamic range. As for as the sensitivity of the proposed sensor is concerned, at the first hand, it appears to be on the lower side in Table 2.2. However, it is worth mentioning that all the sensors, reported in the literature and listed in Table 2.2 for comparative analysis, employ essentially single-mode fiber (SMF). Whereas the sensor reported in the present

Table 2.2 : *Response comparison of the reported sensor with other GO-based sensors.*

Authors	Sensing element	Linear Dynamic Range (% RH)	Sensitivity	Response time (sec)	Recovery time (sec)
Huang *et al.* 2018 [39]	SP SMF	58.5–92.5	0.427 dB/%RH	2.73	7.27
Xiao *et al.* 2014 [33]	SP SMF	75–95	0.31 dB/%RH	5	15
Liu *et al.* 2019 [43]	Micro capillary	30–70	0.211 nm/%RH	–	–
Wang *et al.* 2016 [48]	Tilted FBG	10–50	0.085 dB/%RH	–	–
Dissanayake *et al.* 2017 [55]	LPG	60–95	0.15 dB/%RH	–	–
Wang *et al.* 2016 [57]	MZI	30–75	0.193 dB/%RH	–	–
Liu *et al.* 2018 [58]	MZI	30–60	0.104 dB/%RH	–	–
Gao *et al.* 2016 [69]	Hollow core fiber	60–90	0.229 dB/% RH	5.2	8.1
Xin *et al.* 2020 [81]	PCF	30–70	0.128 nm/%RH	–	–
Zhao *et al.* 2019 [82]	Tapered SMF	84–95	0.361 dB/% RH	–	13.3
Proposed sensor	Straight and uniform PCS MMF	15–95.3	0.1036 dB/% RH	0.1436	0.1547

0.8288 dB/%RH if the PCS MMF is replaced by SMF in the present study. This sensitivity is almost double of the sensitivity achieved in [39]. Fastest response and recovery times and

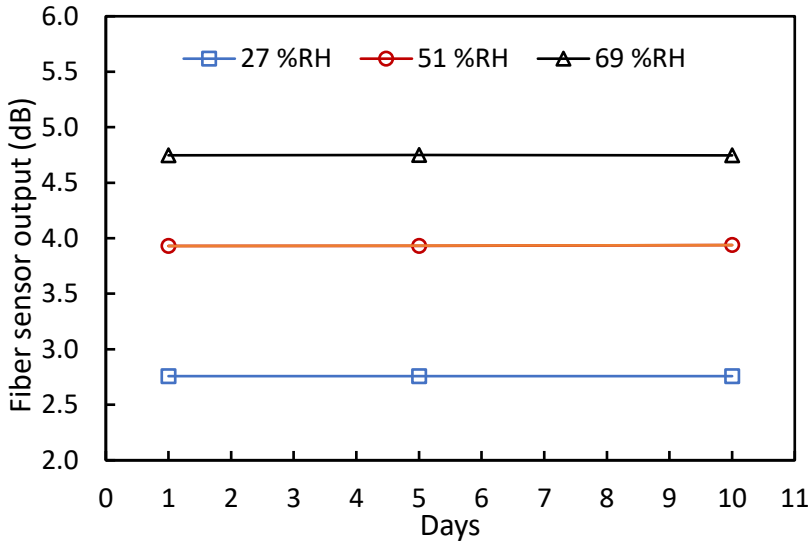

Fig 2.8 : Repeatability and reliability test: Fiber sensor output on three different days, each at interval of 4 days for 27%, 51% and 69%RH.

research employs PCS multimode fiber (MMF) having normalized frequency (V) 18.64. According to [88], [89], sensitivity of evanescent wave absorption based optical fiber sensor increases over 8 times if the PCS multimode fiber is simply replaced by standard SMF (V equal to 2.3). This means, expected sensitivity would be widest linear dynamic range covering measurement of RH at values as low as 15%RH and as high as 95.3%RH make the proposed sensor most distinct among other. Importantly, if PCS MMF is employed to develop the sensor, sensitivity increases approximately 70 times for the U-shape sensing probe in comparison to the straight and uniform sensing probe [90]. Thus, sensitivity of the proposed sensor can be tuned to 7.252 dB/%RH by replacing straight and uniform geometry of the PCS MMF with U-shaped geometry of the same fiber. This sensitivity is extraordinarily higher than the sensitivities reported in Table 2.2.

Finally, as the stability, repeatability and reliability are other critical parameters for RH detection, rigorous analysis was carried out to examine long-term performance of the proposed sensor. For this, experiments were repeated on three different days with an interval of 4 days at three different humidity levels (27%, 51%, and 69% RH) in a span of 9 days. Observed results are shown in the Fig. 2.7. Maximum variation in the proposed optical fiber sensor's output, compared to day one at all the three RH levels, is observed to be as low as 0.1%. This shows the excellent reliability and repeatability of the developed sensor. Thus, the reported

sensor employing intensity modulation through evanescent wave absorption facilitated by GO diffused nanostructured silica sensing film synthesized over a short length of centrally decladded straight and uniform optical fiber and having a fast, reliable, repeatable, and linear response achieved over almost the widest possible dynamic range is of great importance for real-field applications. Certainly, the sensitivity can be further increased by synthesizing the same nanostructured film onto a single-mode fiber or a U-shaped region of the same PCS optical fiber.

2.4 Conclusion

This Chapter describes the development of an optical fiber RH sensor employing evanescent wave absorption spectroscopy through graphene oxide (GO) diffused silica nanostructured thin sensing film synthesized over a 5cm long centrally decladded straight and uniform optical fiber. A detailed experimental investigation is carried out to analyse the sensor response/characteristics. Fiber sensor response is observed to be linear throughout a dynamic range as wide as 15% to 95.3% RH. The observed linear sensitivity for the fiber sensor is 0.1036dB/%RH. It is worth mentioning that the sensitivity can be further increased manifold by simply replacing the PCS multimode optical fiber used in present study with standard single mode fiber or by synthesizing the same nanostructured sensing film on a U-shaped geometry of the same optical fiber. Further, the developed sensor with shortest response and recovery times of 0.1436s and 0.1547s, respectively, is observed to be ultrafast among all the GO based optical fiber sensors reported in the literature. In addition, the sensor response is observed to be highly reversible, reliable, and repeatable. While applying RH perturbations, maximum fiber output variation over a span of over 9 days is observed to be of the order of only 0.1%. Hence, the proposed sensor is of great practical importance in monitoring dynamic and rapid evolution of ambient humidity perturbations. Next chapter of the thesis aims to augment sensitivity while possibly preserving the wide dynamic range of relative humidity measurement as observed in this chapter.

Chapter 3 : Highly sensitive fiber-optic humidity sensor based on reduced graphene oxide

3.1 Introduction

Several scientific studies have been reported in the literature with the aim of developing an affective all-optical sensor to measure relative humidity (RH). The unique and unparallel advantages of fiber optics, combined with their ability of remote sensing and multiplexing, have made optical fiber sensors an integral part of modern cutting-edge sensing technology. These facts motivated researchers and scientist worldwide, and huge amount of research and development are carried out to realize optical fiber sensor for monitoring numerous parameters of interest, exploiting various optical techniques in conjugation with fiber optics. Among all the techniques, intensity modulation through EW absorption exploiting different mechanical structures, such as, straight and uniform optical fiber [30], side polished single mode [33], U bend [38], [46] and Taper [37], [40], [44] is the most commonly employed technique for RH sensing. . These sensors exhibited either a wide dynamic range with throughout non-linear response, or, piecewise linear response over a very limited dynamic range. Further, being indirect sensor, they utilized hydrophilic material as RH sensing agent that was coated on the fiber core using appropriate immobilization techniques in sol-gel silica glass/polymer matrix. The sensor functions by absorbing moisture from the environment using hydrophilic materials, leading to alterations in the physical, chemical, and optical characteristics in the sensing region, allowing it to detect humidity. Although RH sensors based on hydrophilic materials have the advantage of high sensitivity over a wide range of RH detection, it takes a long time for the hydrophilic materials to reach saturation in adsorption of water molecules, resulting in longer response time to follow changes in the humidity perturbation. This was also witnessed in the research reported in the previous chapter, where the reported sensor employed GO diffused silica nanostructured thin sensing film on the small decladded section of a straight and uniform optical fiber. Since the discovery of graphene in 2004, when it was first isolated from graphite, it has attracted tremendous research interest due to its novel, exceptional electronic and photonic properties making it most desirable in wide range of applications. Graphene is a two-dimensional material, which is composed of one atom thick planar sheet of sp^2-bonded carbon

atoms that are perfectly arrange in a honeycomb lattice. Graphene oxide (GO) and reduced graphene oxide (rGO) are two very important derivatives of graphene. GO is widely employed in sensing technology due to its unprecedented advantages. However, relatively less research is devoted in exploring potential application of rGO. rGO stands out as a remarkable material for sensing applications owing to its exciting properties, derived from the parent material, graphene and its precursor, GO. The reduction of precursor (GO) partly restores the structure and properties of graphene in rGO. The properties of rGO, which in turn, affect the performance of rGO based devices depend on the reduction processes employed to obtain rGO. Nevertheless, rGO inherits excellent electrical conductivity, mechanical strength, and chemical stability of graphene while maintaining some of the advantageous features of GO, such as large surface- to-volume ratio and facile functionalization [91]. Further, rGO is also a promising hygroscopic material that exhibits hydrophilic properties that is mainly manifested by the adsorption of water molecules through hydroxyl and carboxyl groups on the surfaces and the edges [92]. There are examples where rGO is successfully employed in designing electronic gas sensor for the detection of NO2, NH3, H2O, CO, Cl_2 and H2 [92] as well as electronic RH sensor [92], [93]. However, only a very few optical fiber humidity sensors have been reported in the literature where rGO is employed as the RH sensing agent. In one of these, Xiao et al., [33] reported an optical fiber RH sensor by utilizing rGO-coated side-polished single-mode fiber (SP-SMF). The sensor response was observed to be linear over a dynamic range of 75-95%RH with a sensitivity of 0.31dB/%RH. On the other hand, Gao et al., [69] reported Fabry-Perot (FP) resonator employing SMF and rGO coated hollow-core fiber. A linear response over the dynamic range of 60-90%RH with a sensitivity of 0.229dB/%RH and response time as high as 5.2s (humidification) and 8.1s (dehumidification) are absorbed. In another research, Le et al. [94] reported rGO-overlaid two-mode microfiber knot resonator (TMM-KR) based optical fiber RH sensor. A nonlinear response over the dynamic range of 35-90%RH is observed for the sensor. Ahmad et al., [95] reported another optical fiber RH sensor that employed rGO-coated tapered single-mode fiber loop resonator (MLR) for monitoring humidity. A linear response over the dynamic range 30-50%RH with a sensitivity of 0.0537 nm/%RH was achieved for this sensor. These only available research works, reported in the literature, indicate further R&D scope of exploiting rGO to develop optical fiber RH sensor with better response characteristics. Sensors reviewed above involved complicated design structures and were characterized with moderate sensitivity, limited dynamic range and fast response/recovery times.

Research reported in this chapter is carried out with a motivation of improving critical performance characteristics by achieving improved sensitivity, response/recovery times and the dynamic range in comparison to what was achieved in the research carried out and reported in the previous chapter as well as the research works reviewed in this chapter by employing rGO and a simple optical fiber sensing structure. With this objective, an optical fiber RH sensor is developed employing reduced graphene oxide (rGO) immobilized nanostructured (sol-gel) silica sensing film on the centrally decladded straight and uniform multimode PCS optical fiber. A comprehensive experimental examination is carried out to optimize the sensor response by suitably controlling the thickness and composition of the sensing film. Notably, a much-improved sensitivity of 56.3mV/%RH (0.1262dB/%RH or 0.0104RH^{1}) over the linear dynamic range of 5-57%RH is observed for the optimized sensing probe. Significantly, a 7.6-fold improvement in sensitivity is observed for the sensor utilizing rGO immobilised nanostructured silica sensing film in comparison to the sensor employing only a pure silica nanostructured sensing film. Furthermore, the response of the optimized sensing probe is observed to be highly repeatable and fully reversible, having response time for humidification and dehumidification are 0.18s and 0.20s, respectively.

3.2 Experiment

3.2.1 Synthesis of reduced graphene oxide

Reduced graphene oxide (rGO) can be synthesized using various techniques. In the present work, chemical method [78] was employed to synthesize the rGO. To do so, a colloidal suspension of GO was obtained by dispersing GO in deionized water in an ultrasonic bath for 1 h. The solution was then transferred to a round bottom flask, and appropriate hydrazine hydrate was added to it. The solution was refluxed at 100°C for 24 hrs in an oil-bath using a water-cooled condenser. The brown-color solution was reduced to black colored solution. The final product was cooled, filtered, and washed with copious amounts of D.I. water and dried at 100°C for 24 hrs to obtain the rGO.

3.2.2 Characterization of reduced graphene oxide

X-ray diffractometer (XRD, Rigaku TTRAX III) in Bragg–Brentano geometry, operating at 5kW with Cu-Kα radiation (λ = 1.5406 Å) was used for structural characterization of synthesized rGO at room temperature. The XRD spectra were measured in the range of 2θ from 5° to 80°. Fig 3.1 shows XRD spectra of graphite, GO and rGO. As can be observed, graphite exhibits an intense peak at 2θ = 26.48° (interlayer spacing 3.37 Å) that corresponds to the (002)

crystal plane, whereas GO exhibits an intense peak at $2\theta = 10.29°$ (interlayer spacing 8.67 Å) that corresponds to the (001) crystal plane. The increase in interlayer spacing indicates the oxidation of graphite, while affecting the crystal structure. On the other hand,

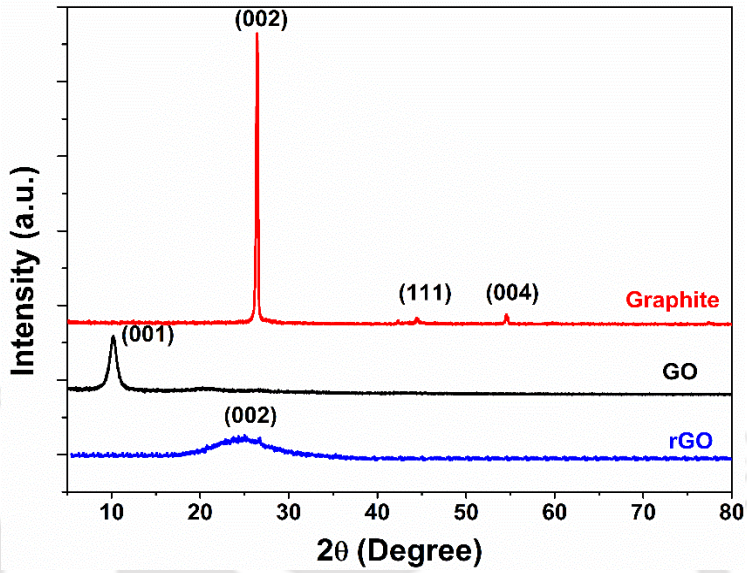

Fig 3.1 : *XRD of Graphite, Graphene oxide (GO) and reduced Graphene oxide (rGO).*

rGO exhibits a broad peak at $2\theta = 26.9°$ that corresponds to the (002) crystal plane. The presence of broad peak (002) for RGO implies that the crystal phase (002) is arranged randomly as compared to graphite and graphene oxide. In order to investigate further, elemental characterization of graphite, GO and rGO was carried out using energy dispersive X-ray (EDX, Zeiss Sigma, measured at 20 kV) analysis. Results of EDX analysis are summarized in Table 3.1. It is evident from these results that the carbon percentage increases from to 63.5% (for GO) to 86.2% (for rGO), whereas the oxygen percentage decreases from 31.5% (for GO) to 10.3% (for rGO). From these results, we can conclude that the reduction of GO to rGO successfully occurred in the presence of hydrazine hydrate.

Table 3.1 : *Result of elemental analysis of Graphite, Graphene oxide (GO), and reduced graphene oxide (rGO) using EDX.*

Elements	**Atomic %**		
	Graphite	**GO**	**(rGO)**
Carbon	87.2	63.5	86.2
Oxygen	8.2	31.5	10.3
Nitrogen	2.6	2.7	0
Sulfur	2.3	2.32	0.1
Silicon	0.82	0.84	0.80
Potassium	0.18	0.12	0

3.2.3 Sensing probe preparation

A piece of plastic cladding silica (PCS) fiber (Ceramoptec PWF125/225BN) with a length 60cm and core diameter of 125µm is used to develop an optical fiber RH sensor. In order to achieve sufficient power coupling from the source to the fiber sensor and fiber sensor to the detector, the end faces of the fiber were polished properly. Then about 5 cm of the cladding was dcladded from the central portion of the fiber. Central decladded portion of fiber was cleaned by proper sonication first in soap the DI water as per the standard procedure developed in the lab. A thin sensing rGO-doped silica film was coated over this centrally decladded straight fiber to fabricate the sensing probe. For this, silica sol was prepared by proper mixing of (TEOS), deionized water, ethanol, and hydrochloric acid in a 3:2:1:0.01 ratio [83]. After 36 hrs, an appropriate amount of rGO was mixed into the 20ml silica sol by proper stirring. The process of dip coating was employed to deposit an rGO doped silica nanostructured sensing film. In order to optimize the sensor performance, multiple sensing probes were prepared by varying chemical compositions (0.05g, 0.1g and 0.15g in 25ml silica sol) and film thickness (1-dip and 2-dip) for each chemical composition. All prepared sensing probes were left to dry for 48 hrs at room temperature and then annealed for a duration of 2 hrs at 110°C to remove any remaining trace of water and ethanol from the sensing probe. Surface morphology, nanostructure and the thickness of the developed films were examined by FESEM (Zeiss Sigma-300).

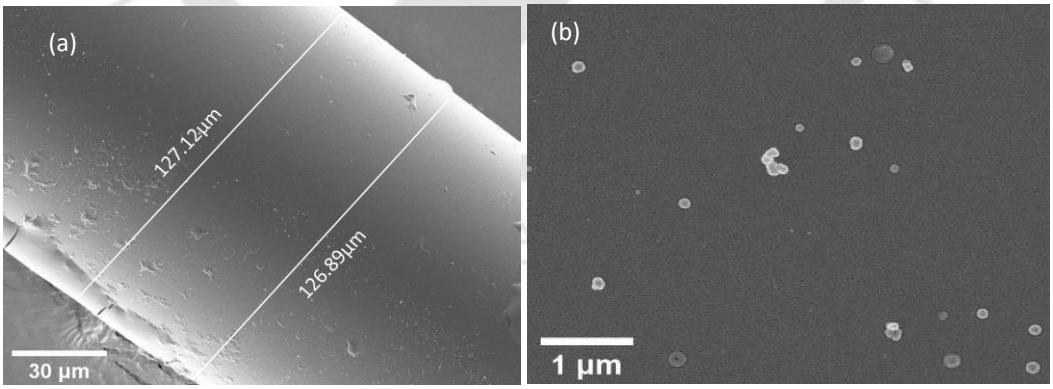

Fig 3.2 : *(a) FESEM picture of rGO doped silica coated fiber (b) FESEM picture of fiber rGO doped silica surface.*

Fig 3.2 (a) depicts, as an example, image of the 1-dip coated sensing region of the optical fiber having rGO concentration that corresponds to 0.1g rGO in 20ml sol. Average diameter in this

region is observed to be 127µm. This indicates that the average thickness of the sensing film is 1µm. Whereas, the average sensing film thickness of 2-dip coted fiber sensor is 2.15µm. The surface morphology of the deposited sensing film is depicted in Fig. 3.2 (b), which shows an interconnected high-quality porous structure with moderate roughness.

3.2.4 Characterization of the sensor

Similar procedures, as explained in Chapter 2, were followed to characterize each sensing probe.

3.3 Result and discussion

The proposed sensor exploits the phenomena of intensity modulation through EW interaction with rGO doped nanostructured sol-gel thin sensing film, synthesized onto the decladded region of a straight and uniform PCS optical fiber. Experiments were carefully carried out multiple time for increasing as well as decreasing humidity cycles for each sensing probe. In order to optimize the sensor's response, the impact of both the composition and thickness of the sensing film was investigated. The film thickness ranged from one dip to two dip, while the composition varied between 0.05g, 0.1g, and 0.15g in 20ml silica sol for each thickness. In order to examine response characteristics, real-time outputs from both the proposed and commercial sensors were monitored under varying humidity levels. Throughout the experiment, temperature was kept constant at 25°C. Typical response of the optical fiber

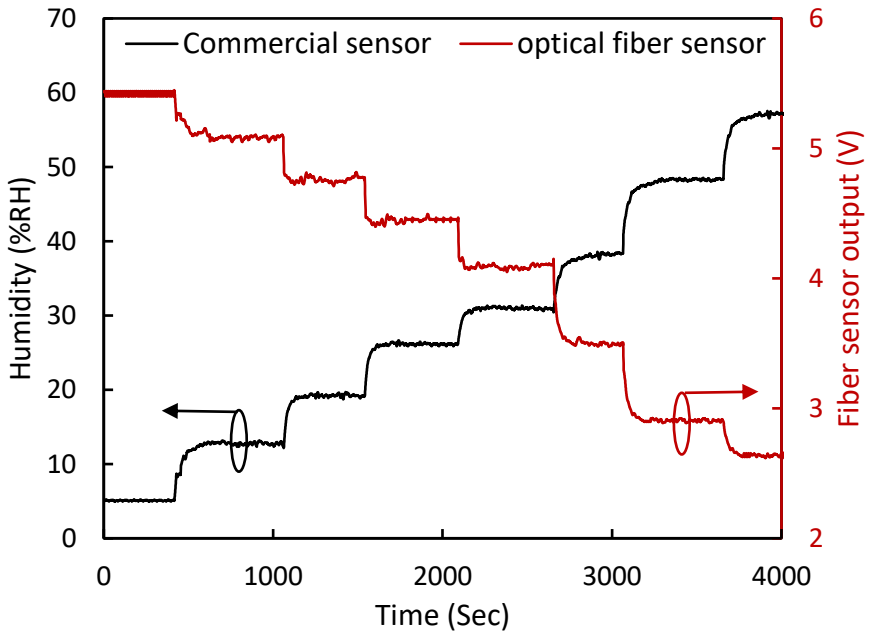

Fig 3.3 : *Time variation of a commercial humidity sensor and the fiber-optic humidity sensor having 0.1g rGO one dip thickness.*

RH sensor with rGO concentration of 0.1g with 1-dip thickness in the sensing film, as an example, is depicted in Fig 3.3. As can be observed from the time response of the sensor fiber sensor output decreases as RH increases in the chamber. Sensor followed the same response characteristics, of course, in reverse direction while decreasing the humidity Similar responses were observed for other sensing probes (having different film compositions and film thicknesses). Sensor's response characteristics can be explained by the fact that water molecules diffuse into the nano scaled pores of the pure solgel matrix and get absorbed into these pores. The rate of adsorption of water molecules that infiltrates into the nano-scaled pores of silica matrix is stimulated (greatly enhanced) owing to the presence of the rGO. Rate of adsorption, and that ways, refractive index of the sensing cladding increase with the increase in RH. This, in turn, leads to leakage of the guided power to the cladding modes in the sensing region and results in a more intense intensity modulation. To get deeper insight of the sensor response, fiber sensors output corresponding to the applied humidity was read from the stabilized portion of the response characteristics depicted in Fig 3.3 and plotted against applied RH perturbations for each film configurations. Fig 3.4 depicts the response of the sensing probe having film composition of 0.05g rGO in 20ml silica sol with varying film thicknesses. Since film in each case were deposited from the same solution, any difference in the response characteristics should be due to the difference in the film thickness. As can be

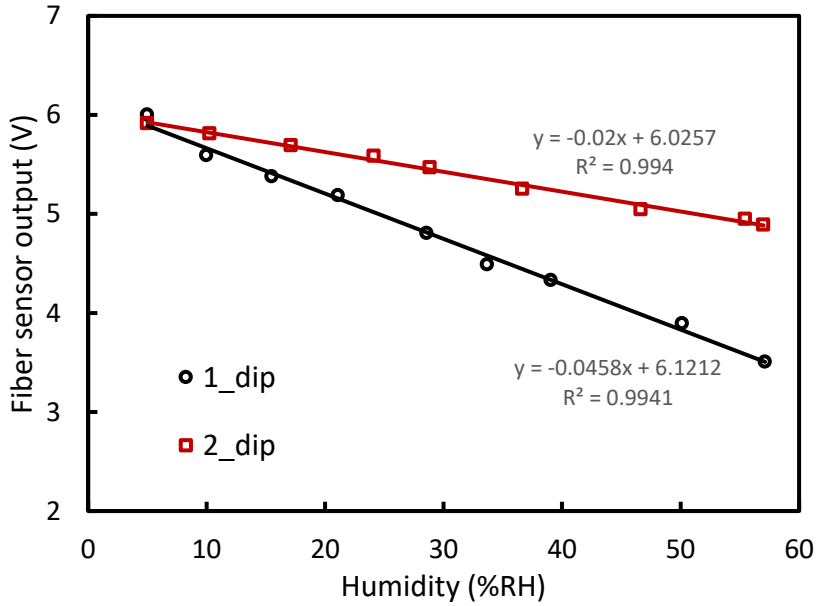

Fig 3.4 : *Experimentally observed Sensor response having film composition 0.05g rGO in 20ml of silica sol.*

observed from this figure, sensing probe of varying film thicknesses but having film composition fixed at 0.05g in 20ml silica sol shows a throughout-linear response over the

dynamic range of 5-57%RH, that is, observed linear dynamic range was unaffected by the variation of film thickness. A sensitivity of 45.8mV/%RH is observed for the sensing probe

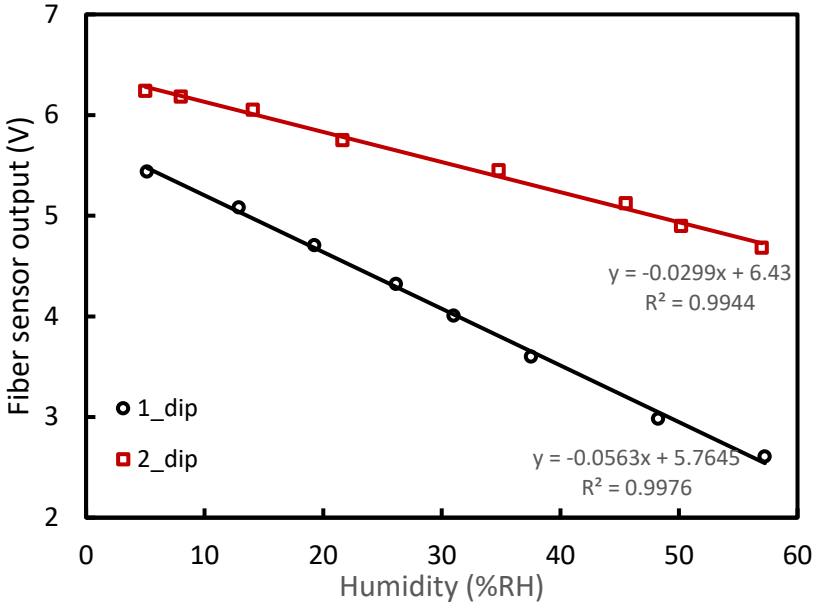

Fig 3.5 : *Experimentally observed Sensor response having film composition 0.1g rGO in 20ml of silica sol.*

having one dip film thickness, whereas, a sensitivity of 20 mV/%RH is observed for the sensing probe having two-dip film thickness. Consequently, sensitivity decreases 2.29 times as the film thickness is increased from one dip to two dip. As it is not feasible to reduce film thickness beyond 1µm (corresponding to 1-dip coating), above observation establishes the fact that there exists an optimum film thickness corresponding to the one-dip with 0.05g rGO in 20ml silica sol composition. Further, the response of the sensing probes having the other film composition (0.1g rGO in 20ml silica sol) are plotted in Fig 3.5. From the plot following observation can be made: (i) Both the sensors responded linearly over the dynamic range of 5-57%RH; (ii) A sensitivity of 56.3mV/%RH was observed for 1-dip coated sensing probe in comparison to the sensitivity of 29.9mV/%RH as observed for the 2-dip coated sensing probe; (iii) Once again sensitivity decreases over 1.88 times while reducing film thickness from 2 dip to 1 dip; (iv) Dynamic range remain unattached by the variation of film composition as well as film thickness; (v) Even increasing film composition from 0.05g rGO to 0.1 rGO in 20ml silica sol, optimum film thickness corresponds to 1-dip coating, and (vi) Increasing of rGO concentration in silica film enhances the overall sensitivity of the sensor for each film thickness.

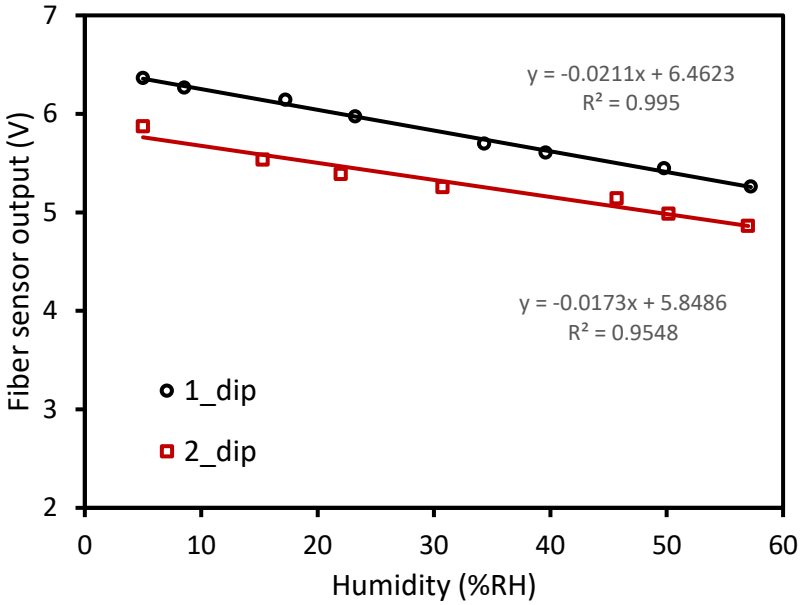

Fig 3.6 : *Experimentally observed Sensor response having film composition 0.15g rGO in 20ml of silica sol.*

The film composition was further changed from 0.1g to 0.15g in 20ml silica sol. The corresponding sensor's responses are plotted in Fig. 3.6. The sensing probe corresponding to one-dip film thickness again exhibits the best sensitivity. The following reasons can be attributed to the observation of optimum film thickness. For the 2-dip coating, the film thickness was much greater than that of the penetration depth of the evanescent wave. Hence, with the increase in humidity, water molecules that are diffused into the pores of the film could not penetrate into the volume of the film spanned by the evanescent wave to interact with the corresponding optical power in the evanescent wave. This reduced the sensitivity substantially.

Further, in order to understand the effect of film composition, response of sensors are compared in Fig. 3.7 for various film compositions keeping the film thickness fixed at the optimum value corresponding to 1-dip coating. As can be observed, an increment in film composition from 0.05g to 0.1g in 20ml silica sol improves sensitivity from 45.8 mV/%RH to 56.3 mV/%RH. However, increasing the rGO concentration from 0.1g to 0.15g in 20ml silica sol didn't pay any further dividend as sensitivity decreased from 56.3mV/%RH to 21.1mV/%RH, which is much less than that achieved for 0.05g rGO concentration. This establishes the existence of an optimum film composition which is observed to be 0.1g rGO in 20ml silica sol. Existence of optimum film configuration can be understood as following: Presence of nanocomposite concentration in sensing film beyond a certain level affects the porosity of sensing film, which obstructs the proper diffusion of water molecules into the

nanostructured sensing film. Hence, there is limited interaction between water molecules and the evanescent wave in the sensing region, reducing the sensitivity substantially. Next, in

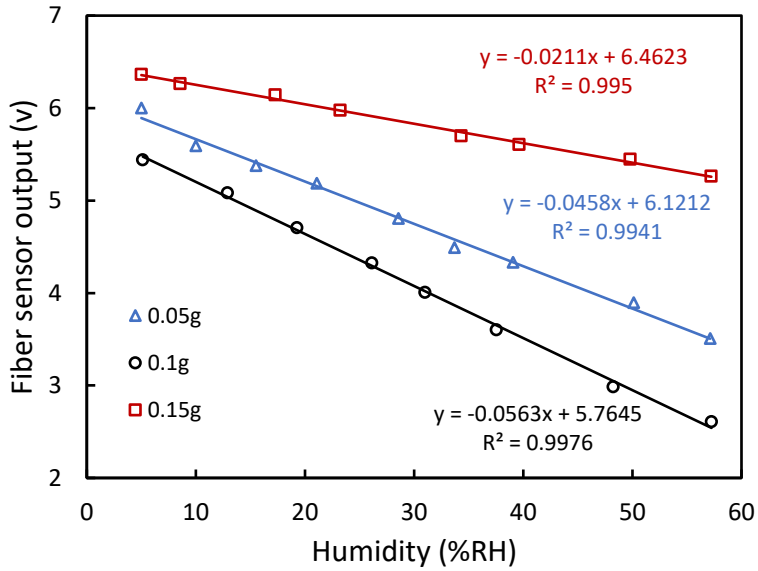

Fig 3.7 : *Sensor response compression one-dip coated probes with different film compositions.*

order to analyze the effect of the presence of rGO in the nanostructured silica matrix, optical fiber sensor based on pure sol-gel silica sensing film was also prepared and characterized. The responses of this sensor is plotted in Fig. 3.8. The sensitivity of pure sol-gel silica-based sensor is along with the response of the sensor with optimum film configuration (1-dip, 0.1g

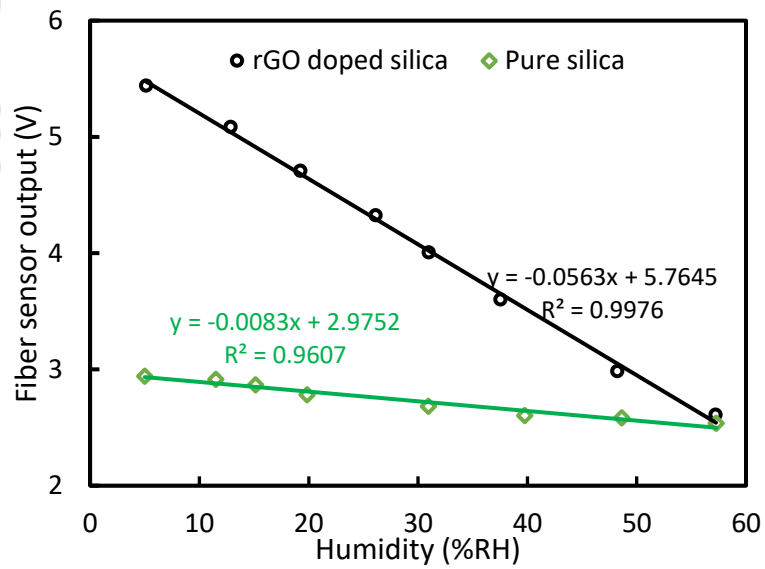

Fig 3.8 : *Experimentally observed sensors response having rGO doped silica and pure silica.*

rGO) is observed to be 8.3mV/%RH. This shows a manifold (6.4 times) increase in the sensitivity for the proposed rGO diffused nanostructured sol-gel silica-based sensor in comparison to the pure sol gel-based optical fiber sensor.

Besides sensitivity and dynamic range, detection speed is critical for assessing sensor performance while monitoring dynamic and rapidly changing ambient humidity. A sensor with the fastest response time, recovery time, and reversible response is of great importance. Hence, for the investigation of repeatability characteristics, optimized sensing probe was exposed to repeated and quick RH cyclic change between minimum and maximum humidity levels. The humidity chamber was first desiccated to 5%RH and then quickly humidified to 60%RH by passing humid air in the chamber. The observed sensor response is plotted in Fig.3.9. The optical fiber sensor output shows an instant and smooth change during the forward (3% to 60%RH) and the reverse (60% to 3%RH) cycles of the humidity change Also, the fiber output is observed to be extraordinarily identical at extreme RH values during the humidification and desiccation cycles. This established highly repeatable and completely reversable nature of the proposed sensor. An average response time of 0.18s during humidification and recovery time of 0.20s during desiccation process are observed from fig. 3.9.

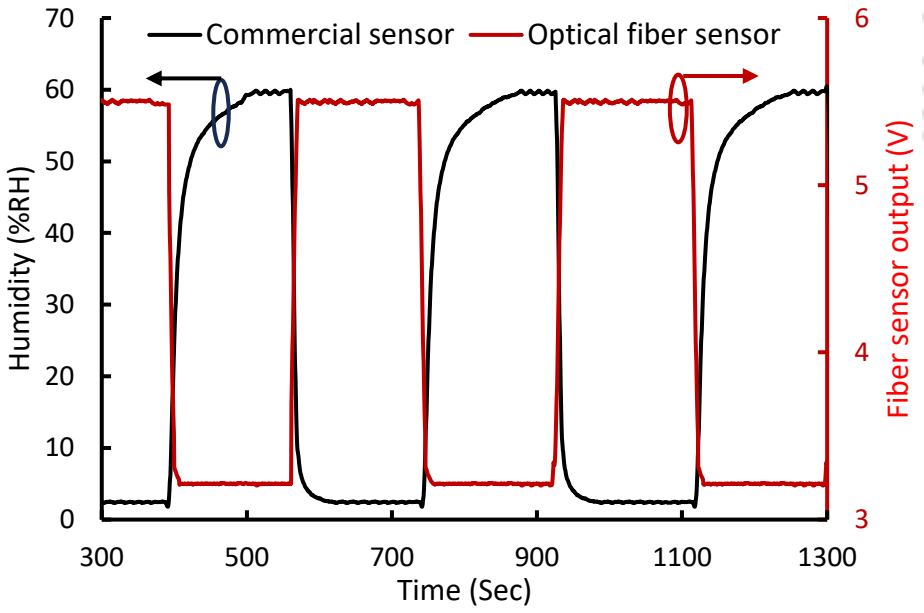

Fig 3.9 : *Time response behavior and the repeatability test for the optimized sensing probe during humidity perturbations.*

Next, the response characterisation of the optimized sensor is compared with GO/rGO based optical fiber RH sensors and other optical fiber RH sensors employing EW intensity

modulation scheme. For the comparative analysis, Table 3.2 lists sensitivity characteristics of those sensors that exhibit linear response over the observed dynamic range. A comprehensive

Table 3.2 : *Response comparison of optimized sensor with GO/rGO based optical fiber RH sensors and other optical fiber RH sensors employing EW intensity modulation.*

Authors	Humidity sensing material	Sensing element	Linear dynamic range (%RH)	Sensitivity
Wang *et al.*, 2016 [57]	GO	MZI	30–75	0.193 dB/%RH
Huang *et al.*, 2018 [39]	GO	SP SMF	58.5–92.5	0.427 dB/%RH
Zhao *et al.*, 2019 [82]	GO	S-taper SMF	~84–95	0.361dB/%RH
Zhong *et al.,* 2020 [38]	GO and PI	U-bend POF	**10-90**	0.0017RH^{-1}
Sun *et al.,* 2022 [96]	GO	Twisted weakly coupler	45–85	0.002RH^{-1}
Xiao *et al*., 2014 [33]	rGO	SP-SMF	75-95	0.31dB/%RH
Ahmad *et al*., 2016 [95]	rGO	Loop resonator	30-50	0.0537nm/%RH
Zhang *et al.*, 2020 [37]	NbS_2	Taper SMF	72–97	1.05dB/%RH
Batumalay, *et al*., 2015 [97]	ZnO	Taper POF	50-85	0.0258mV/%RH
Harith *et al*., 2020 [40]	ZnO nanorod	Taper POF	50-80	0.0172mV/%RH
Afsharipour *et al*., 2023 [46]	ZnO np	U-bend MMF	**10-80**	0.143mV/%RH
This work	rGO in sol-gel	Straight MMF	5-57	56.3mV/%RH 0.0104RH^{-1} 0.1262dB/%RH

list of the GO based optical fiber RH sensors is already presented in the previous chapter. Only the GO based optical fiber sensors that exhibited highest sensitivity and widest dynamic range are included in Table 3.2 for comparison. As can be observed, sensors employing various sensing elements in conjugation of GO and rGO [57], [39], [82], [96], [33], [95] along with sensors based on tapered SMF and POF [37], [97] have linear response over a very narrow dynamic range. U-bend MMF employing ZnO np has reasonably good dynamic range, but overall highest dynamic range is observed for U-bend POF employing GO with PI [38]. Dynamic range of the proposed sensor is lower than [38] and [46]. However, highest sensitivity is observed for the proposed sensor, which is 394 times higher in comparison to the previously reported highest sensitivity in the unit of mV/%RH in [46] and over 5 times higher in comparison to the previously reported highest sensitivity in the unit of RH^{-1} in [96] and ~6 times higher in comparison to [38] which reported widest dynamic range. It is worth mentioning that sensors reported in [38] as well as in [46] employed U-shaped MMF. In accordance to [90], if PCS MMF is employed to develop the sensor, sensitivity increases approximately 70 times for the U-shape sensing probe in comparison to the straight and uniform sensing probe. Thus, sensitivity of the proposed sensor can be tuned to 3941mV/%RH or 0.728 RH^{-1} by replacing straight and uniform geometry of PCS MMF with U-shaped

geometry of the same fiber. This sensitivity is extraordinarily higher than the sensitivities reported in Table 3.2. On the other hand, sensitivity of reported sensor in the unit of dB/%RH is observed to be lower than the sensitivity reported in [57] , [39] and [82]. As observed these sensors in [57] , [39] and [82] employ SMF or tapered SMF and characterized with a very narrow dynamic range. Sensor reported in the present work employs PCS MMF having normalised frequency (V) 18.64. As mentioned in Chapter 2, sensitivity increases over 8 times if PCS MMF is replaced by standard SMF (V equal to 2.3). This means expected sensitivity would be 1.0096dB/%RH of the PCS MMF is replaced by SMF in the present study. This sensitivity is 2.5 times higher than the sensitivity achieved in [39] and 2.5 times higher than the sensitivity achieved in [82] that employed tapered SMF. It's worth mentioning that sensor in [82] employed tapered fiber where the diameter is reduced from 125µm to 8.7µm. Tapering further enhance the sensitivity of the SMF based OFS. The expected sensitivity (1.0096 dB/%RH as mentioned above) even without tapering is still higher than the sensitivity achieved in [82]. These facts establish the superiority of the proposed sensor.

In order to ensure the reliability and repeatability of the sensing probe, a series of tests were conducted. For this, experiments were repeated on three different days with an interval of 4 days between first two experiments and an interval of 5 days between the second and third experiment at three different humidity levels (12%, 30%, and 48% RH) in a span of 10 days. The results obtained from these experiments are illustrated in Fig. 3.10. Upon analysis of the data, it was observed that the maximum variation in the output of the proposed optical

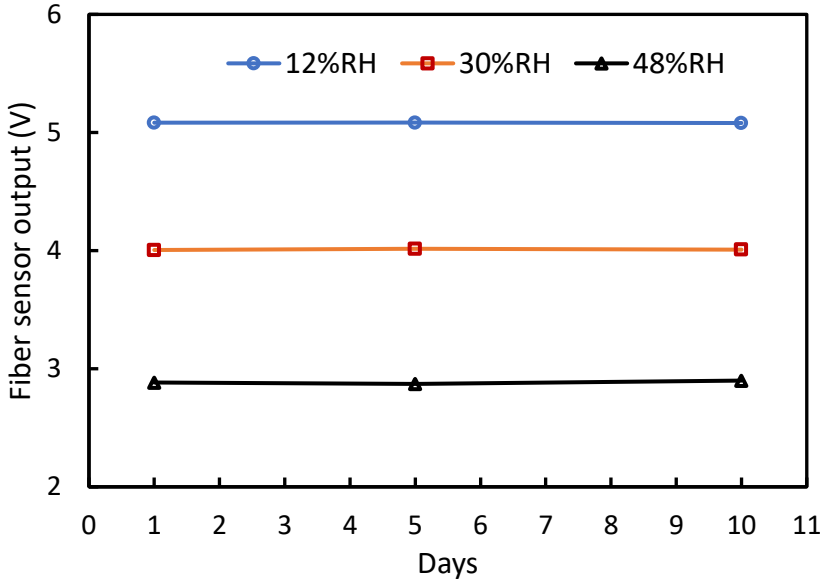

Fig 3.10 : *Repeatability and reliability test: Fiber sensor output on the three different days for 12%, 30%, and 48% RH.*

fiber sensor, compared to day one, at all the three humidity levels, is only 0.4%. This minimal difference indicates the outstanding reliability and repeatability of the developed sensor. The remarkable performance characteristics, specifically in terms of sensitivity enhancement of the sensor that employs intensity modulation through EW absorption facilitated by rGO diffused nanostructured silica sensing film synthesized over a short length of centrally decladded straight and uniform optical fiber is of great importance as far as real field applications are concerned.

3.4 Conclusion

In conclusion, a highly sensitive optical fiber sensor employing intensity modulation via evanescent has been successfully demonstrated in this chapter. A chemically synthesized rGO doped silica nanostructured sensing film was coated over the centrally decladded region of PCS fiber to realize the RH sensor. The response of the sensor was optimized by varying the composition (immobilized rGO concentration) of silica nanostructured sensing film as well as the thickness of the sensing film. An optical fiber sensing probe having composition 0.1g rGO in 20ml silica sol with the film thickness corresponding one-dip coating shows optimum response characteristics. A linear response over the humidity range of 5-57%RH with a sensitivity of 56.3mV/%RH ($0.0104RH^{-1}$) is achieved for the optimized sensor. It is worth mentioning that the sensitivity can be further increase manifold by simply replacing the PCS MMF used in present study with slandered SMF or by synthesizing the same nanostructured sensing film on a U-shaped geometry of the same optical fiber. Additionally, the sensor response is observed to be highly repeatable, reliable and reversible. Further, the response time and the recovery time are observed to be 0.18s and 0.20s respectively. Though, an enhanced sensitivity is achieved for the present sensor in comparison to the sensor developed and reported in chapter 2, the linear dynamic range could not be retained as wider as reported in chapter 2. This laid the foundation of the research work discussed in the next chapter.

Chapter 4 : Highly sensitive Blue Luminescent Graphene Oxide Quantum Dots (GQDs) based Optical Fiber Humidity Sensor

4.1 Introduction

Last chapter described the development of optical fiber RH sensor with rGO immobilised sol-gel silica nanostructure as a humidity sensing clad. A linear response over the dynamic range of 5-57%RH with a high sensitivity and improved time response was achieved. In order to reach the goal of the research of this thesis in realizing ultrafast optical fiber sensor with optimum sensitivity and linear response over widest possible dynamic range, a novel RH sensor is developed and reported in this chapter, which employed graphene quantum dots (GQDs) doped silica sol-gel nanostructure as an RH sensing cladding over the centrally decladded straight and uniform PCS multimode optical fiber. GQDs are zero-dimensional derivative of graphene oxide, characterized by their incredibly small lateral size, typically less than 10nm. Due to several unique and exciting (luminance, electrical, chemical, and optical) properties of GQDs, they have great potential for application in the field of sensing, photovoltaic cells, light-emitting diodes, bio-imaging, displays, and energy storage [98]. Like GO, GQDs have several oxygen-rich functional groups like hydroxyl and epoxide on their basal plane, with carbonyl and carboxyl groups at the edges. One of the most notable advantages of GQDs lies in their exceptional surface-to-volume ratio, surpassing even that of GO [99]. GQDs structure, coupled with their oxygen functional groups and high surface area to volume ratio, make them exceptionally permeable and adsorptive for water molecules. This results in outstanding dispersibility, hygroscopicity, and distinctive hydrophilicity, rendering GQDs a good candidate for relative humidity (RH) sensing applications. However, it's worth noting that only a limited number of optical fiber humidity sensors employing GQDs have been reported in the literature [56], [100], [101]. For example, Hou *et al*. [56] have proposed an fiber Bragg grating based RH sensor that employed GQDs doped polyimide (PI) coating. Proposed sensor responded linearly over a wide dynamic range 10-90%RH with a sensitivity of 3.26pm/%RH. In another research, Zhao *et al*., [101] reported a Fabry-Perot (FP)

interferometer as RH sensor that employed GQDs-PVA compound as the humidity sensing agent. For the development of the sensor, GQDs-PVA compounds were filled into the hollow core fiber (HCF), which is spliced at the end of a SMF with air cavity entrapped in between. A sensitivity of 117.25 pm/ %RH is observed over the linear dynamic range of 13.47- 81.34%RH. Further, Wang *et al.*, [101] have demonstrated an FP resonator based optical fiber RH sensor. This sensor employed two common single mode optical fibers, which were perfectly aligned to FP interferometer. The gap between the two aligned SMFs was filled with GQDs. The proposed sensor exhibits a linear response over a dynamic range of 11-85% RH, with a sensitivity of 0.567 nm/%RH. The fastest response during humidification and dehumidification was observed to be 5.5s and 8.5s, respectively. The GQD based sensors reported above are either FBG or interferometric-based. These sensors also require sophisticated and complex manufacturing process along with bulky and costly interrogation devices. As far as FBG based optical fiber sensors are concerned, temperature/strain cross sensitivity imposes major limitations toward real-field applications. A less costly and less complicated sensor is always preferred for real-field applications.

For the development of the proposed sensor in this part of research, a GQD diffused nonporous silica film was chemically synthesized over a short length and centrally decladded straight uniform multimode fiber. Performance characteristics of the developed sensor were comprehensively studied and optimized in terms of the sensing film configuration. A much-improved linear sensitivity of 0.2437dB/%RH over a dynamic range of 4%-70%RH is achieved for the optimized sensing probe. Equally importantly, sensor exhibited super-fast response time and recovery times of 0.025s during humidification and desiccation. The proposed sensor exhibits approximately double the sensitivity, along with a wider dynamic range and faster response, in comparison to the sensor reported in Chapter 3. In repeatability and reliability tests the maximum variation in output of the optimized fiber sensor is ±0.73% compared to the first day.

4.2 Experiment

4.2.1 Synthesis of graphene quantum dots (GQDs)

Graphene oxide quantum dots (GQDs) were synthesized using a hydrothermal method using citric acid [79]. First, an appropriate amount of citric acid (2.1g) was dissolved in 20 ml of mili-q water by proper stirring. After the complete dispersion of citric acid, a suitable amount of urea (1.8g) was added to the solution. After the complete dissolution of urea, a transparent solution was obtained. Then this solution was transferred into a 50 ml Teflon-lined stainless-

steel autoclave and heated at 200°C for five hrs. After that, this autoclave was allowed to cool down at room temperature, and the obtained solution was filtered with a 0.22µm pour-size vacuum filter. After that, this filtered solution was dialyzed through a dialysis membrane bag having pour size 1000 Da in water for 24 h. The water used in this dialysis process was changed every four hours. Then, the dialyzed quantum dots solution was dried at 100 °C for 24 h to get the desired GQDs. Obtained GQDs were again redispersed in a suitable amount of water.

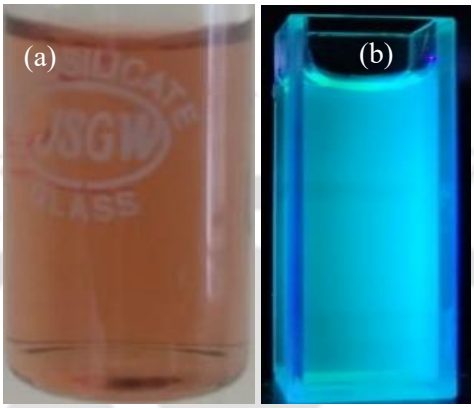

Fig 4.1 : *(a) Picture water dissolved GQDs in normal light (b) Picture water dissolved GQDs in UV light.*

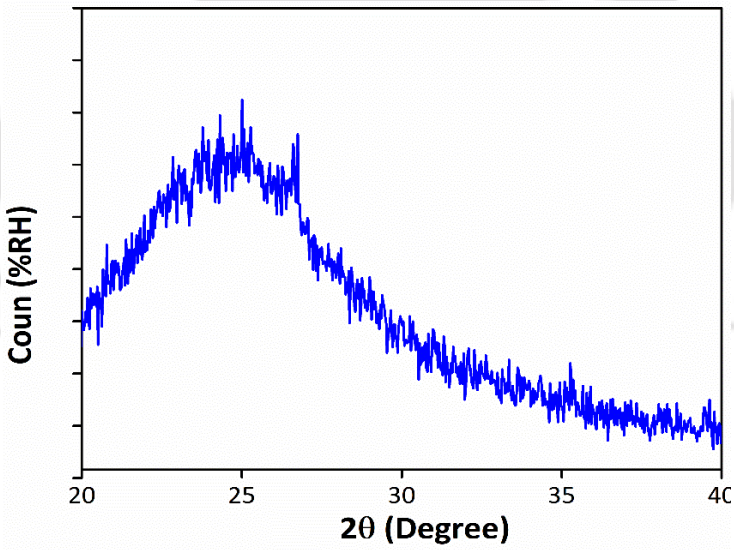

Fig 4.2 : *XRD of synthesized GQDs.*

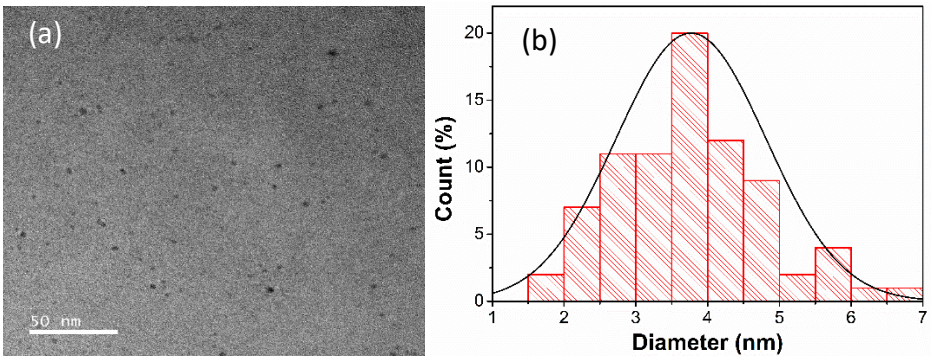

Fig 4.3 : *(a) FETEM of synthesized GQDs and (b) particle size distribution of GO-ZnO nanocomposite.*

4.2.2 Characterization of graphene quantum dots (GQDs)

Images of water-dispersed GQDs in normal light and UV light are shown in Fig. 4.1(a) and 4.1(b). An X-ray diffractometer (XRD, Rigaku TTRAX III), was used for the structural characterization of synthesized GQDs at room temperature. XRD spectra of synthesized GQDs are shown in Fig 4.2. The size and structural morphology of synthesized GQDs were examined by a FETEM. The FETEM picture of GQDs is shown in Fig 4.3 (a). Furthermore, the size distribution of particles in FETEM is shown in Fig 4.3 (b). It can be observed from Fig 4.3 (b) that the average diameter of developed quantum dots is 3.8±0.5nm.

4.2.3 Sensing probe preparation

Plastic cladding silica fiber with a length of 50 cm and a core diameter of 125 µm is used to develop an optical fiber RH sensor. The fiber has a core refractive index of 1.457 and clad refractive index of 1.404, which makes the critical angle of the fiber roughly equal to 75°. First, fiber ends are prepared properly to get optically flat end faces for maximum power coupling from the source to the fiber sensor and the fiber sensor to the detector. About 5 cm of the cladding was removed from the central portion of the fiber. The decladded portion of fiber was cleaned properly. A GQDs diffused silica film was chemically synthesized over a centrally decladded portion of the fiber. For the synthesis of GQDs diffused silica matrix, silica sol was prepared by mixing tetraethyl orthosilicate, deionized water, ethanol, and hydrochloric acid in the ratio of 3:2:1:0.01 [31]. After 36 hrs, a suitable amount of water dispersed GQDs was mixed into silica sol by proper stirring. The process of dip coating was employed to deposit GQD doped silica nanostructured sensing film. In order to optimize the sensor performance, multiple sensing probes were prepared by varying chemical compositions (75mg, 100mg and 125mg in 20ml silica sol) and film thickness (2-dip, 3-dip and 4-dip) for each chemical composition.

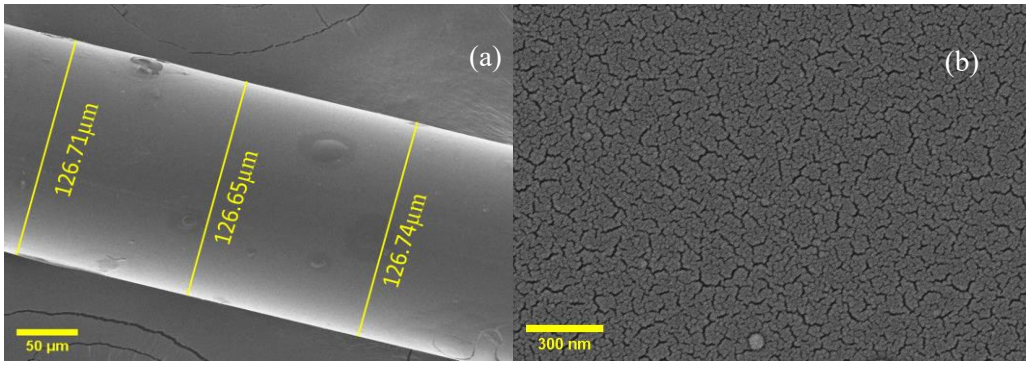

Fig : 4.4 *(a) FESEM image of the centrally decladded region of the fiber carrying GQDs immobilized sol-gel sensing film (3-dip coated with GQDs concentration corresponding to 100mg GQDs in 20ml sol). (b) FESEM pattern of surface morphology of the sensing region.*

All sensing probes were dried first at room temp for 48 hrs, then annealed for 2 hrs at 110°C to remove the trace water and ethanol from the sensing film. Surface morphology, microstructure, and film thickness of the developed films were examined by FESEM (Sigma-300). Fig 4.4(a) illustrates, as an example, image of 3-dip sensing region of the optical fiber having GQDs concentration that corresponds to 100mg GQDs in 20ml sol. Average diameter in this region is observed to be 126.7µm, which establishes the average thickness of the sensing film as 850nm. The surface morphology of the deposited sensing film is depicted in Fig 4.4 (b), which shows an interconnected high-quality porous structure with moderate roughness.

4.2.4 Characterization of sensor

Similar procedures, as explained in Chapter 2, were followed to characterize each sensing probe.

4.3 Result and Discussion

The proposed sensor exploits the phenomena of intensity modulation through EW interaction with GQDs doped nanostructured sol-gel thin sensing film, synthesized onto the decladded region of a straight and uniform PCS optical fiber. Experiments were carefully carried out multiple times for increasing as well as decreasing humidity cycles for each sensing probe. In order to optimize the sensor's response, the impact of both the composition and thickness of the sensing film was investigated. The film thickness ranged from two dip to four dip, while the composition varied between 75mg, 100mg and 125mg in 20ml silica sol for each thickness. In order to examine response characteristics, real-time outputs from both the proposed and commercial sensors were monitored under varying humidity levels. Throughout the experiment, temperature was kept constant at 25°C. Typical response of the optical fiber

RH sensor employing film thickness corresponding to 3-dip coating andh GQDs concentration corresponding to 100mg GQDs in 20 ml of silica sol, as an example, is depicted in Fig 4.5. As can be observed from the time response of the sensor depicted in plot, fiber sensor output decreases as the humidity inside the chamber increases. Similar behaviour

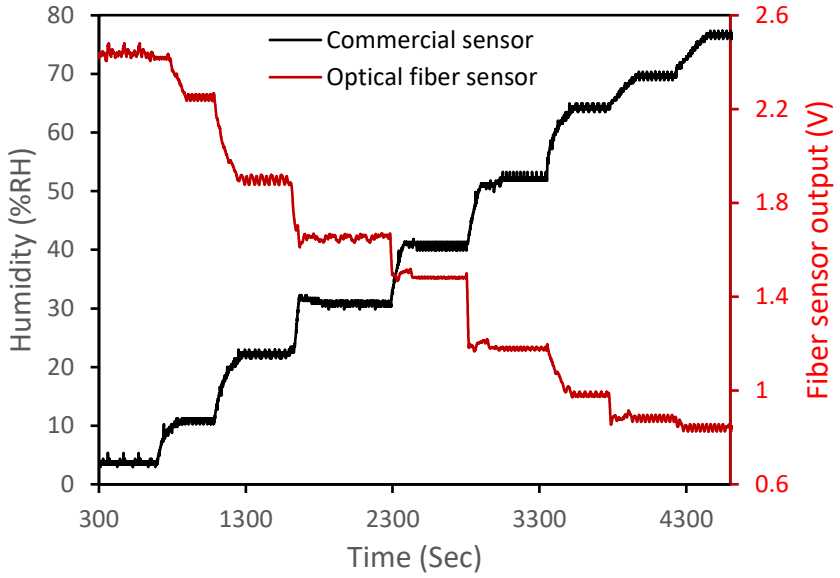

Fig : 4.5 *Time variation of the commercial humidity sensor and the optical fiber RH sensor.*

was observed for other sensing probes. Sensor's response characteristics can be explained by the fact that water molecules into the nano-scaled pores of the pure solgel matrix and get absorbed into these pores. The rate of adsorption of water molecules that infiltrates into the nano-scaled pores of silica matrix is stimulated (greatly enhanced) due to the presence of the GQDs. Rate of adsorption, and that ways, refractive index of the sensing cladding increase with the increase in RH. This, in turn, leads to leakage of the guided power to the cladding modes in the sensing region and results in a more intense intensity modulation. The response of all the developed sensors having different film thicknesses and different film compositions is examined rigorously. To get detailed information about the effect of film composition, output of optical fiber sensor is plotted against applied %RH in dB ($dB = log10(I_{3\%RH}/I_{\%RH})$). Fig 4.6 depicts the effect of GQDs concentration variations in the silica sol-gel matrix for the sensor having fixed film thickness corresponding to 2-dip coating. As can be observed, all sensors show a linear response over 3% RH to 70 % RH. A sensitivity

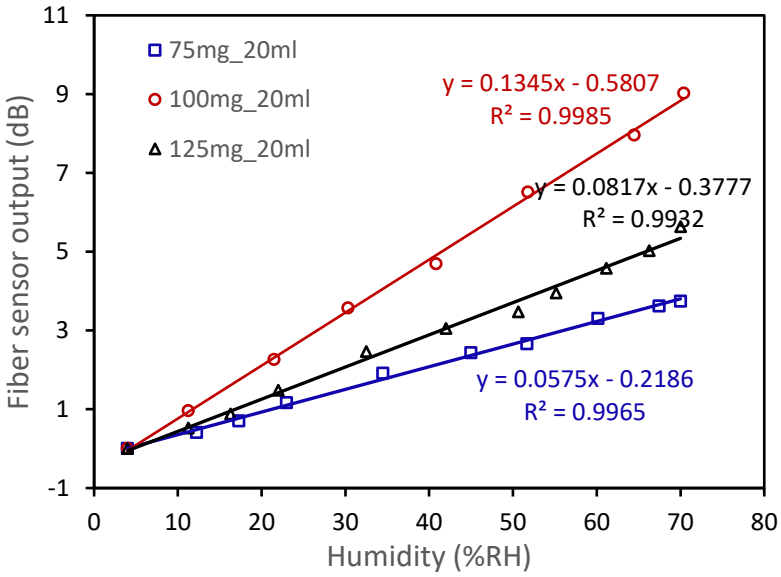

Fig 4.6 : *Experimentally observed sensor response of the optical fiber sensor having 2dip coating thickness.*

of 0.0575 dB/% RH is observed for the sensor having film composition of 75mg in 20 ml sol. An increase in GQDs concentration from 75mg to 100mg improves the sensitivity from 0.0575dB/%RH to 0.1345dB/% RH, which is over 2.3 times higher than the previous one. Further increase of GQDs concertation in silica matrix does not follow the same trend. The sensor with film composition of 125mg in 20 ml silica sol has a sensitivity of 0.0817dB/%RH. Hence, film composition of 100 mg in 20ml silica sol is observed to be the optimum for developing an optical fiber sensor. Further, the outputs of the sensing probes having fixed film thicknesses corresponding to three-dip coating with varying concentration of immobilized GQDs are plotted against the applied humidity in Fig 4.7. As can be observed from this plot, an increase in dip thickness in coated film does not affect the dynamic range of the sensor. The overall sensitivity of the developed sensor increases with the increase in thickness. The sensitivity for the sensor with film composition 75mg in 20 ml sol is 0.1294 dB/%RH (which is 3 time higher than 2dip sensor with the same composition). Again, an increase in GQD concentration in silica matrix 75mg in 20 ml to 100mg in 20 ml improves the sensitivity, which is 0.2437dB/%RH. Further, an increase in GQDs concentration of 125mg in 20 ml silica matrix again decreases sensitivity substantially. The sensitivity of the 3-dip coated sensor having a concentration of 125mg in 20ml is observed to be 0.1543dB/%RH. The film thickness was further increased from three dip to four dip. Response of the sensor having film thickness corresponding to 3-dip coating with varying GQDs concentration are plotted in Fig 4.8. Overall, the sensitivity of the 4-dip sensor

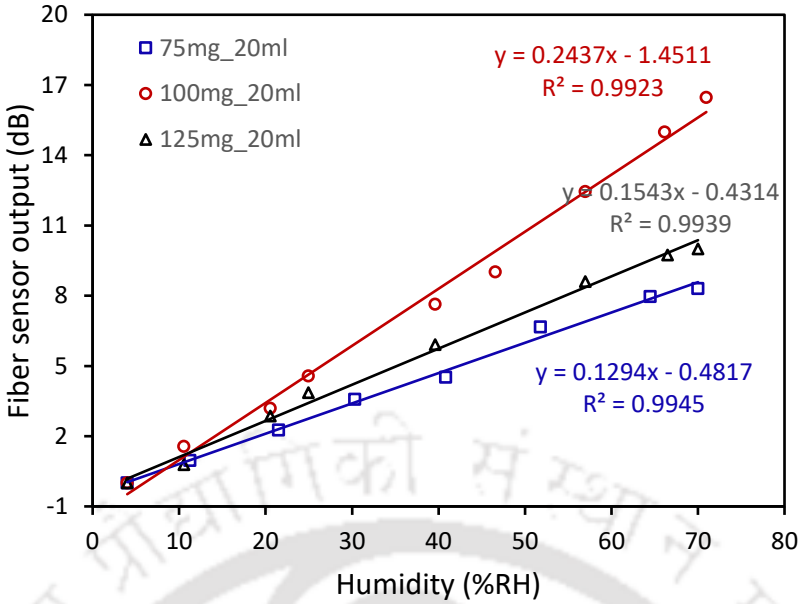

Fig 4.7 : *Experimentally observed sensor response of the optical fiber sensor having 3 dip coating thickness.*

decreases in comparison of the 3-dip coated sensor. Again, the sensor having a film composition of 100mg in 20ml silica sol shows the best sensitivity, which is 0.1367 dB/%RH. Above results establish the existence of an optimum film composition along with the optimum film thickness for the present sensor. An overall best sensitivity of 0.2437dB/%RH is observed for the sensor that comprised a sensing film having optimum film thickness corresponding to 3-dip coating and optimum film composition corresponding to the GQDs concentration of 100mg in 20ml silica sol. The following reasons can be attributed to the observation of optimum film thickness and composition. Response of the sensor depends on the two physical parameters of the sensing film: the thickness and the porosity of the sensing film. In the case of two-dip, the film thickness is much less than the penetration depth of the evanescent wave. So, a very limited number of GQDs are present in the silica matrix that could interact with an evanescent wave. Hence, with the increase in the humidity, water molecules that are diffused into the film's pores can interact with limited number GQDs, resulting in a limited absorption of the optical power carried by the evanescent field in the sensing region. The thickness of the sensing film corresponding to the three-dip is approximately equal to the penetration depth of the evanescent wave. This means more GQDs in sensing film are now available to interact with the evanescent wave. This led to a higher sensitivity as compared to the two-dip coated probe. But in the case of four dip coated sensor, the thickness of sensing film is much more than the penetration depth of the evanescent wave. Therefore, only a limited number of water molecules are able to penetrate

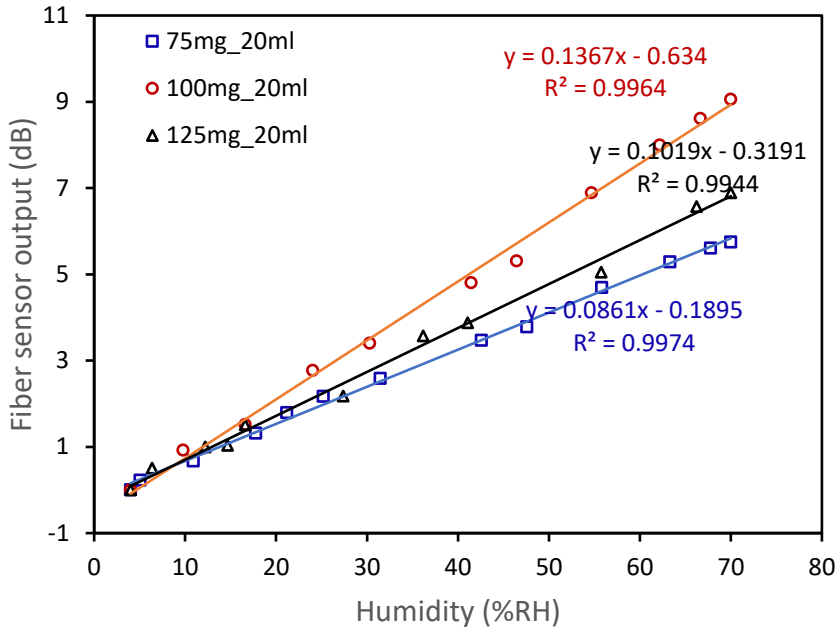

Fig 4.8 : *Experimentally observed sensor response of the optical fiber sensor having 4 dip coating thickness.*

that region of sensing film spanned by the evanescent wave to interact with the corresponding optical power in the wave. Hence, the sensing probe with four dip-coating is less sensitivethan three dip coated sensors. Further, the sensitivity is observed increasing with GQD concentration in the sensing film. This is because, with the increasing concentration in sensing film, the more GQDs are available to interact with the evanescent wave. But

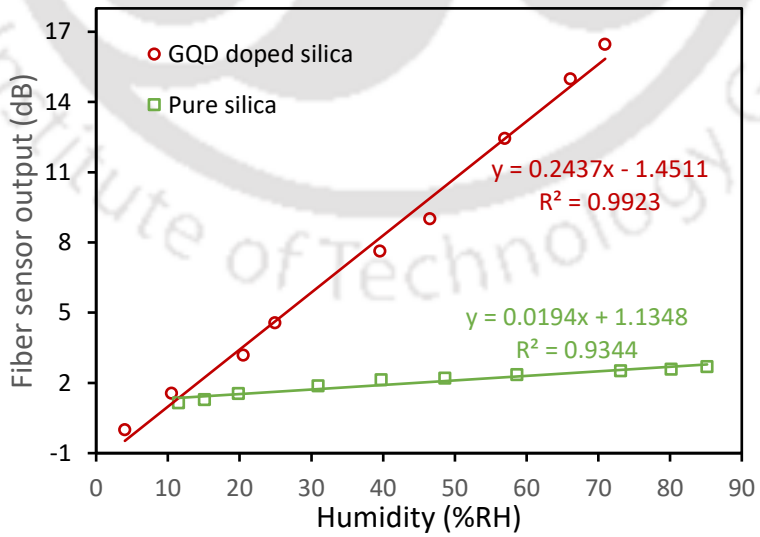

Fig 4.9 : *Response comparison optimized of GQD-based optical fiber RH sensor with sensor based on pure silica.*

increasing GQDs concentration in sensing film beyond a certain level affects the porosity of the sensing film, which obstructs the proper diffusion of water molecules into the nanostructured sensing film. Hence, there is limited interaction between water molecules and evanescent wave, reducing the sensitivity substantially. The sensing probe having thicknesses corresponding to three dip coating with 100mg GQDs in 20ml silica sol is of the order of the penetration depth, and hence, comprises the optimum film composition. Which, in tern, leads to a maximum evanescent wave interaction while varying humidity in the chamber.

Further, in order to analyse the effect of the presence of GQDs in nanostructure silica film, an optical fiber sensor based on pure sol-gel nanostructured sensing film was also prepared and characterized. The response characteristics of this sensor along with the response characteristics of the optimized GQDs sensor are plotted in Fig. 4.9. The sensitivity for pure sol-gel based sensor is observed to be 0.0194 dB/%RH. This shows a manifold (12.5 times) increase in the sensitivity for the proposed GQDs diffused nanostructured sol-gel silica film-based sensor in comparison to the pure sol-gel-based optical fiber sensor.

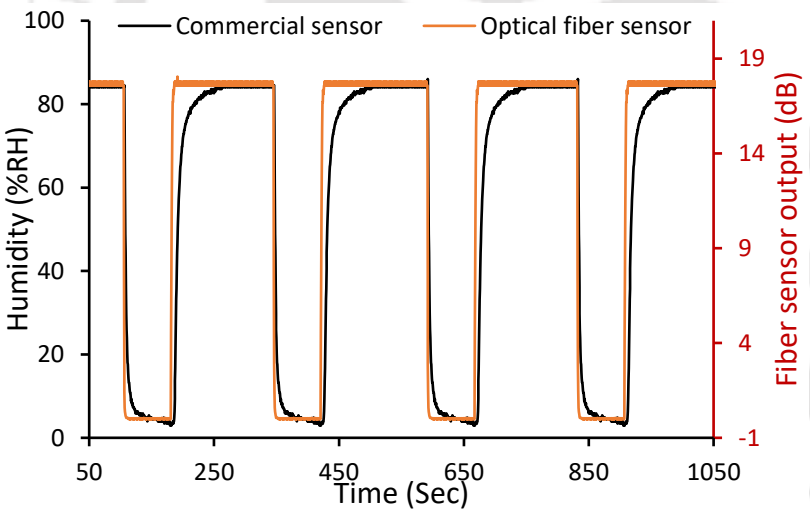

Fig 4.10 : *Time response behavior and the repeatability test for the optimized fiber-optic humidity sensor against cyclic humidity perturbations.*

Further, the optimized sensing probe's dynamic performance and repeatability characteristics were investigated. The sensor was exposed to the cyclic RH variations between ~4%RH and ~83%RH. The observed response is shown in Fig 4.10. As can be observed from the figure, the output intensity of the optical fiber sensor almost instantly and smoothly changes during the forward (3%RH to 83%RH) as well as the reverse (83%RH to 3%RH) cycles of the humidity change. Average response time (humidification) and recovery

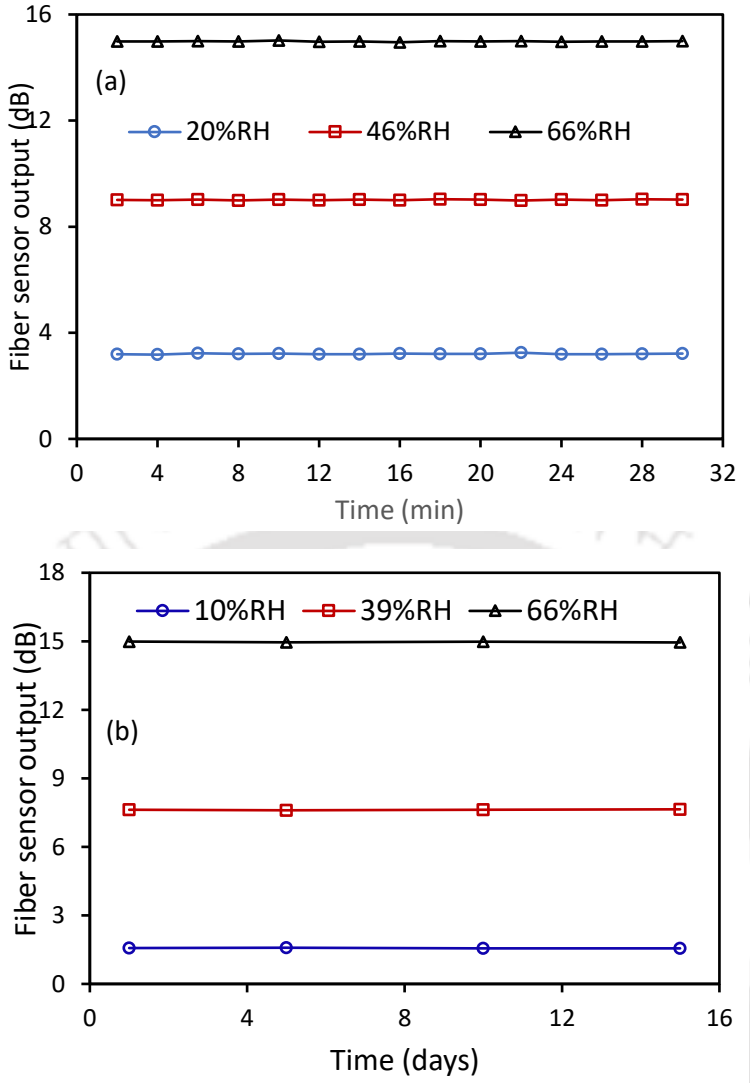

Fig 4.11 : *(a) Short term stability (b) Long-term stability, repeatability, and reliability test: Fiber sensor output on the three different days, each at an interval of 4, 5, and 5 days for 62%, 84% and 94%RH.*

time (desiccation) are observed to be 0.025s. The time response is observed for the proposed sensor establishes it superfast in comparison to the other optical fiber GQD based RH sensors as well as the sensors developed and reported in the previous chapters of this thesis.

Finally, stability, repeatability, and reliability are other critical parameters for RH detection, rigorous analysis was carried out to examine the short and long-term performance of the proposed sensor. For analyzing short-term response, the sensor was exposed for about 60 minutes at different RH levels, once stabilized at three typical values: 20% RH (low), 46% RH (medium), and 66% RH (high) shown in Fig 5.11(a). The standard deviations of intensity are observed to be ± 0.016 dB/%RH, ± 0.0149dB/%RH, and ±0.0148, respectively, at 20%RH, 46%RH, and 66%RH levels. Hence, the maximum resolution of the sensor for RH detection is

observed to be ±0.069%RH, which indicates the excellent stability and accuracy of RH detection. For this, experiments were repeated on four different days with an interval of 4 days at three different humidity levels (10%, 39%, and 66% RH) in a span of 15 days. Observed results are shown in Fig. 5.11(b). Maximum variation in the proposed optical fiber sensor's output, compared to day one at all three RH levels, is observed to be as low as 0.73%. This shows the excellent reliability and repeatability of the developed sensor. Thus, the reported sensor employing intensity modulation through evanescent wave absorption facilitated by GO diffused nanostructured silica sensing film synthesized over a short length of centrally decladded straight and uniform optical fiber and having a fast, reliable, repeatable, and linear response achieved over almost the widest possible dynamic range is of great importance for real-field applications.

4.4 Conclusion

This chapter describes the development of all-optical fiber-based humidity sensors that employ an evanescent wave-based intensity modulation scheme. To realize the humidity sensor, GQDs diffused nanostructured silica film was synthesized over the centrally decladded PCS optical fiber. The sensor was rigorously investigated by varying the various parameters (film composition and thickness) that can influence the sensor's response. Developed sensor with composition of sensing film having 100mg GQDs in 20ml silica sol-gel composition and thickness of 3-dip coating is characterized with the optimum response. A linear dynamic range of 4-70%RH with a sensitivity of 0.2437dB/%RH and resolution of ±0.069%RH are observed for the optimized sensor. The response time of optimized sensing probe is 0.025s observed during humidification and desiccation. Though the sensitivity, dynamic range and response/recovery times are all improved, the scope for further improvement of sensor's response is observed to be still wide open, which lead the foundation of the research reported in the next chapter.

Chapter 5 : Novel GO-ZnO & GO-ZnO-Fe nanocomposite-based ultrahigh sensitive optical fiber humidity sensor

5.1 Introduction

The last chapter described the development and experimental investigations of optical fiber RH sensors based on EW intensity modulation employing graphene quantum dots (GQDs). A good sensitivity over a wide dynamic range while maintaining a fast response time was successfully achieved. To further enhance the sensitivity while maintaining linearity over a wide dynamic range of RH, another novel sensor is developed employing simplest fiber geometry and incorporating a different sensing reagent, GO-ZnO nanocomposite. The motivation behind the utilization of this nanocomposite is the fact that GO is a 2D nanomaterial that exhibits exceptional super-permeability and super-adsorptive capabilities towards water molecules, resulting in excellent dispersibility, hygroscopicity and unique hydrophilicity. On the other hand, ZnO also exhibits a sensitive hydroscopic nature exploited for the development of optical fiber RH sensors. For example, Aneesh *at al*., [30] employed a ZnO nanoparticle (np) immobilized porous silica matrix as the sensing cladding over a centrally decladded plastic-clad silica (PCS) fiber for the development of RH sensor. A linear response over a wide dynamic range of 4-96%RH with a sensitivity of $0.0013RH^{-1}$ was observed. Whereas Azad *et al.*, [35] proposed ZnO nanorods-coated etched optical fiber as the RH sensor. The sensor response was observed to be piecewise linear with a good linear sensitivity only in the 30-55%RH range. In another article, Harith et al. [38] employed tapered POF and aluminium doped ZnO nanostructure to develop an RH sensor. The sensor response was observed to be linear over a dynamic range of 50-80%RH with a sensitivity of 0.0295mV%RH. Liu et al. [102] employed ZnO nanorods grown on thinned silica fibers using a hydrothermal method to develop an optical fiber RH sensor. A nonlinear response over the wide dynamic range of 10-95%RH was observed. Hence, GO-ZnO nanocomposite is expected to enhance the sensitivity of RH measurement. It is important to mention that GO-ZnO nanocomposite is used for the first time to the best of the author's knowledge. For the development of the sensor, GO-ZnO

nanocomposite-doped nanostructured silica sol-gel film was synthesized onto the centrally decladded PCS fiber. Rigorous experimental investigations demonstrate that the sensing probe demonstrates a linear response over a dynamic range of 17-91%RH, with a sensitivity of 33.6 mV/%RH, and response time and recovery time are 0.33s and 0.45s, respectively. Maximum variation in the proposed optical fiber sensor's output is observed to be as low as ±0.79% during a long-time stability test. Furthermore, the response is observed to be highly repeatable and fully reversible

The GO-ZnO nanocomposite-based sensor shows a reasonably wide dynamic range with a very high sensitivity. In order to further enhance sensitivity while keeping the sensor response linear, possibly over a wide RH with better response time, another novel sensor is developed while employing another nanocomposite, which is obtained by incorporating Fe in GO-ZnO nanocomposite. For the development of the sensor GO-ZnO-Fe nanocomposite doped silica sol-gel film was synthesized over the centrally decladded PCS fiber. It is worth mentioning here that the GO-ZnO-Fe is also used for the first time to the best of the author's knowledge. The GO-ZnO-Fe nanocomposite-based sensing probe shows a linear response over the dynamic range of 17−80%RH with a sensitivity of 60.6 mV/%RH. The average response and recovery times of the GO-ZnO-Fe nanocomposite-based sensor is observed to be 0.031s. As can be observed, the incorporation of Fe in GO-ZnO nanocomposite almost doubles the sensitivity and improves the response time, making the sensor response 10 times faster. Furthermore, a maximum fiber output variation during the long-term stability test is observed to be ±0.37%. The response of the proposed sensor is observed to be very fast, reversible, and repeatable.

5.2 Experiment

5.2.1 Synthesis of GO-ZnO nanocomposite

For the synthesis of GO-ZnO nanocomposite [103], 0.1 g of GO was dispersed in 40 mL of DI water using ultrasonication to form a GO suspension. Furthermore, 1.0 mM of zinc chloride ($ZnCl_2$) and 10.0 mM of sodium hydroxide (NaOH) were sequentially mixed in the GO suspension. The resulting mixture was sealed in a 60-mL glass tube and kept stationary at 90 °C for 6 h. Afterward, it was allowed to cool at room temperature. The composite was then filtered, washed multiple times with distilled water and ethanol, and finally dried at 80 °C for 24 h.

5.2.2 Synthesis of GO-ZnO-Fe nanocomposite

GO-ZnO-Fe nanocomposite was synthesized using the hydrothermal method, as discussed in [75]. For the synthesis of GO-ZnO-Fe nanocomposite, first Fe doped was prepared. First, 20 ml of 1M zinc acetate solution was prepared, and then 50mg of iron nitrate was dissolved into it by proper steering. After that, 10ml of 1M NaOH solution was added to the solution dropwise, and then a yellow precipitate was formed. The precipitate was first centrifuged and then washed with copious amounts of water. The final product was dried in an oven at 100°C for 1h. For GO-ZnO-Fe nanocomposite preparation First, 0.5g GO and 0.5g Fe doped ZnO dissolved in water separately. Then, the GO solution was mixed with Fe-doped ZnO solution. After that, the prepared mixture was transferred to a Teflon autoclave and placed in a furnace for a 7 hrs at 180° C. The mixed solution was centrifuged and washed with acetone and water. The final product was dried in an oven at 100 ºC for 6 hrs.

5.2.3 Characterization of nanocomposites

X-ray diffractometer (XRD, Rigaku TTRAX III) in Bragg–Brentano geometry, operating at 5kW with Cu-Kα radiation (λ = 1.5406 Å) is used for the structural characterization of synthesized GO, GO-ZnO nanocomposite as well as GO-ZnO-Fe nanocomposite. XRD spectra are shown in Fig. 5.1. GO exhibits an intense peak at 2θ = 10.29° (interlayer spacing of 8.67 Å) that corresponds to the (001) crystal plane. For GO-ZnO as well as GO-ZnO-Fe nanocomposite, diffraction peaks appeared at 32.7°, 35.2°, 37.2°, 47.9°, 57.1° and 64°. These peaks actually correspond to (100), (002), (101), (102), (110), (103), and (112) crystalline planes of ZnO. Importantly, (001) peak is completely absent in both GO-ZnO and GO-ZnO-Fe nanocomposite. This shows the formation of exfoliated GO sheets due to the nucleation and growth of ZnO and Fe-doped ZnO nanocrystals onto the GO sheets, confirming the successful formation of nanocomposites [104]. Field emission transmission electron microscope (FETEM, JEOL-2100F) measurement is also performed in order to study the size distribution within the developed nanocomposite. Fig. 5.2 (a) depicts typical FETEM image, whereas, Fig. 5.2 (b) illustrates size distribution within the developed GO-ZnO nanocomposite, which is predominantly in the range of 5-10nm with average particle distribution of 7.5±0.06nm. Whereas, FETEM pictures of prepared GO-ZnO-Fe nanocomposite and their particle distribution are shown in Fig 5.3 (a) and 5.3(b). The size of GO-ZnO-Fe nanocomposite ranged from 3nm to 13nm with an average diameter of 8.2±0.05nm.

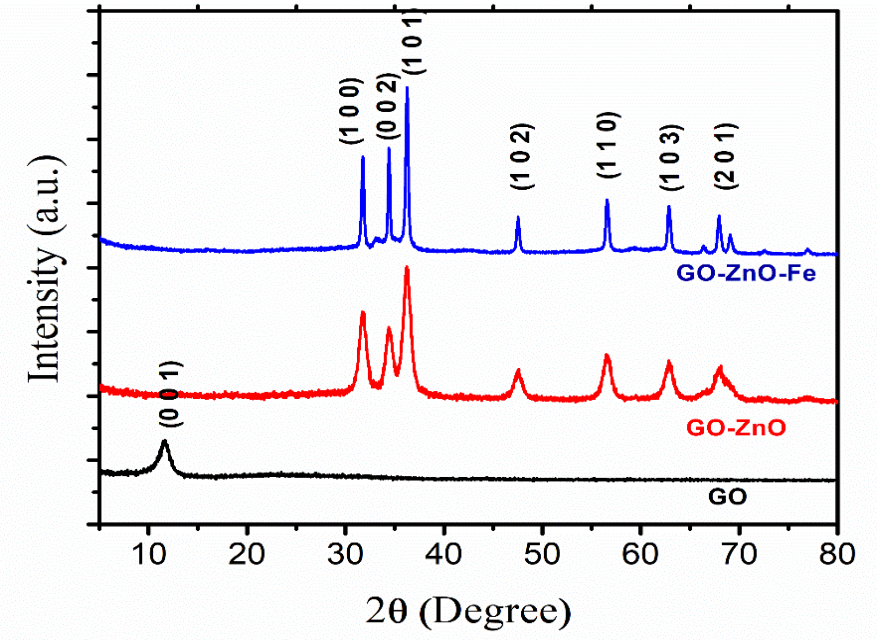

Fig 5.1 : *XRD of GO, GO-ZnO and GO-ZnO-Fe.*

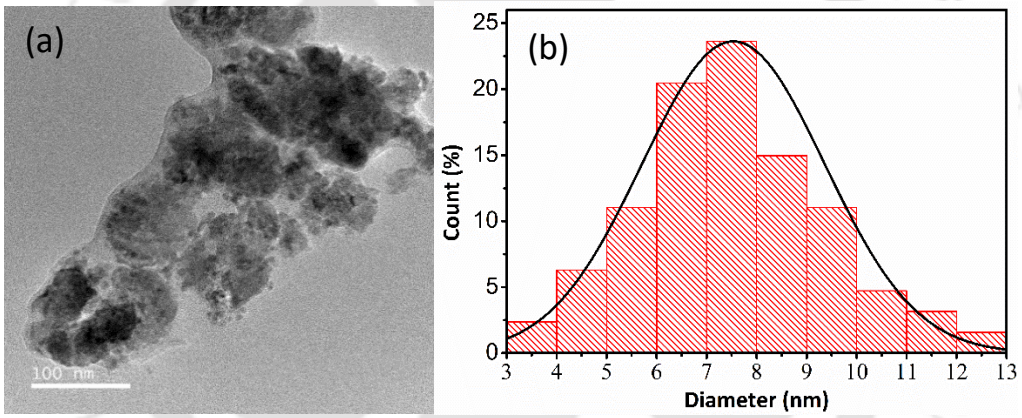

Fig 5.2 : *(a) FETEM pic of nanocomposite and (c) particle size distribution of GO-ZnO nanocomposite.*

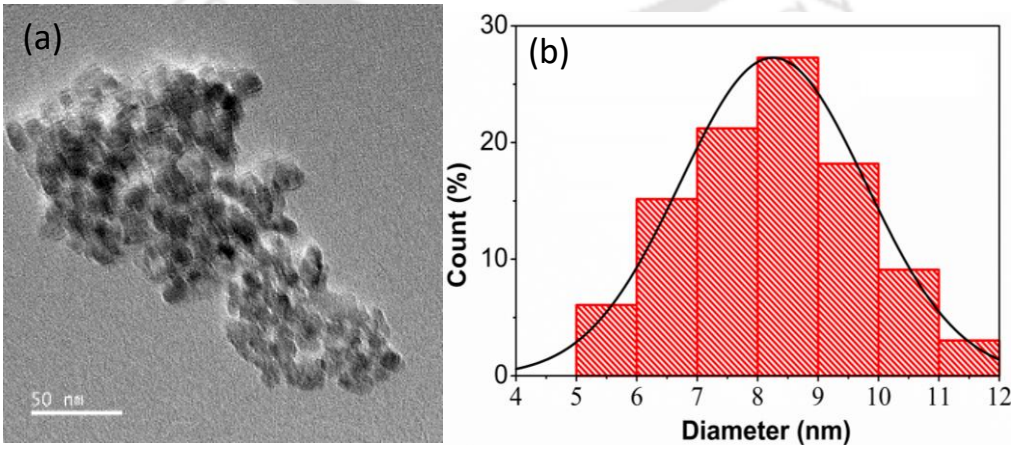

Fig 5.3 : *(a) FETEM pic of nanocomposite and (b) particle size distribution of GO-ZnO-Fe nanocomposite.*

5.2.4 Sensing probe preparation using GO-ZnO nanocomposite

PCS multimode optical fiber of 200-μm core diameter is used to develop the RH sensor. Total length of 60 cm was taken and both the ends of the fiber were polished in order to achieve maximum power coupling efficiency. Afterward, cladding was removed from the central region of the fiber over a length of 5 cm. GO-ZnO nanocomposite-diffused sol-gel nanostructured film was chemically synthesized over this decladded region of the fiber. To do this, sol was prepared by mixing tetraethyl orthosilicate, deionized water, ethanol, and hydrochloric acid in the ratio of 3:2:1:0.01. Suitable amount of water dispersed GO-ZnO nanocomposite was mixed into the sol under constant stirring. The resulting sol was used to deposit a thin sensing film onto the centrally decladded straight and uniform region of the fiber using dip-coating method at a predetermined speed. The sensing probe was dried at room temperature

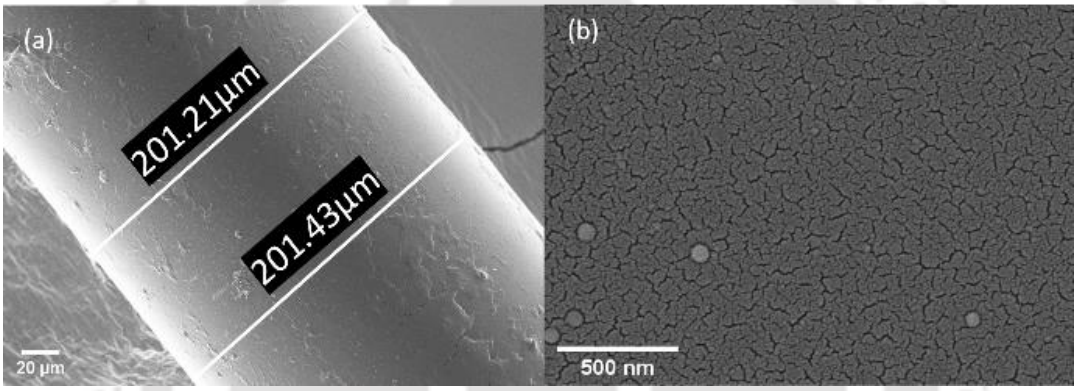

Fig 5.4 : *(a) FESEM image of the centrally decladded region of the fiber carrying GO-ZnO nanocomposite immobilized sol-gel sensing film. (b) FESEM pattern of surface morphology of the sensing region.*

for two days and then annealed at 110 °C to remove residual water and ethanol from the pores of the film. Surface morphology, microstructure, and the thickness of deposited film were examined by FESEM. Fig 5.4 (a) depicts an image of the coated region of optical fiber. The average diameter in this region is observed to be 201.30 μm, which establishes an average thickness of the sensing film as 0.66 μm. The surface morphology of the deposited sensing film is depicted in Fig 5.4 (b), which shows an interconnected high-quality porous structure with moderate roughness.

5.2.5 Sensing probe preparation using GO-ZnO-Fe nanocomposite

A piece of plastic cladding silica fiber having same configuration as utilized for the development of GO-ZnO based nanocomposite-based sensor is used for the preparation of GO-ZnO-Fe based optical fiber RH sensor. The GO-ZnO-Fe doped silica sensing film was

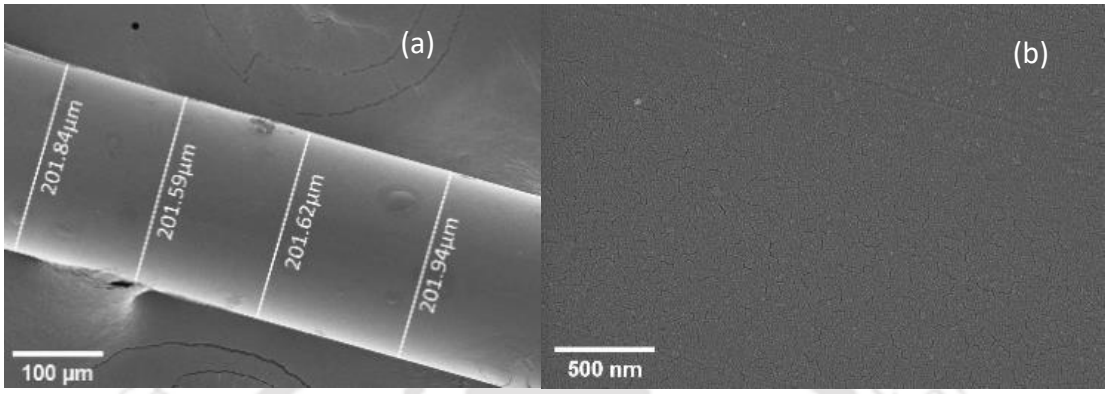

Fig 5.5 : *(a) FESEM image of the centrally decladded region of the fiber carrying GO-ZnO-Fe nanocomposite immobilized sol-gel sensing film. (b) FESEM pattern of surface morphology of the sensing region.*

chemically synthesized over the decladded portion fiber for the development of GO-ZnO-Fe based sensing probe. Fig 2(a) illustrates an FESEM image of the coated area of the optical fiber, where the average diameter was measured to be 201.67µm, which establishes an average thickness of the sensing film of 835nm. The surface morphology of the deposited sensing film is depicted in Fig 2(b), which shows an interconnected high-quality porous structure with moderate roughness.

5.2.6 Charecterization of sensor

Similar procedures, as explained in Chapter 2, were followed to characterize each sensing probe.

5.3 Result and Discussion

5.3.1 Response of GO-ZnO nanocomposite-based sensor

The proposed sensor exploits the phenomena of intensity modulation through EW interaction with GO-ZnO nanocomposite immobilized nanostructured sol-gel thin sensing film, synthesized onto a straight and uniform optical fiber probe under varied humid environment. In order to investigate performance characteristics, real-time monitoring of the output from the proposed and commercial sensors was carried out, keeping the temperature constant at 25 °C.

As an example, typical response of the sensor is depicted in Fig 5.6(a) while increasing the humidity inside the chamber. As can be observed from the response, fiber sensor output decreases as humidity increases. The reason is, when the sensor is exposed to a humid environment, water molecules diffuse into the nanostructure and get adsorbed on the nanocomposite. This increases the refractive index of the sensing cladding of the fiber. Rate of adsorption, and that way, the refractive index of the sensing cladding increases with the increase

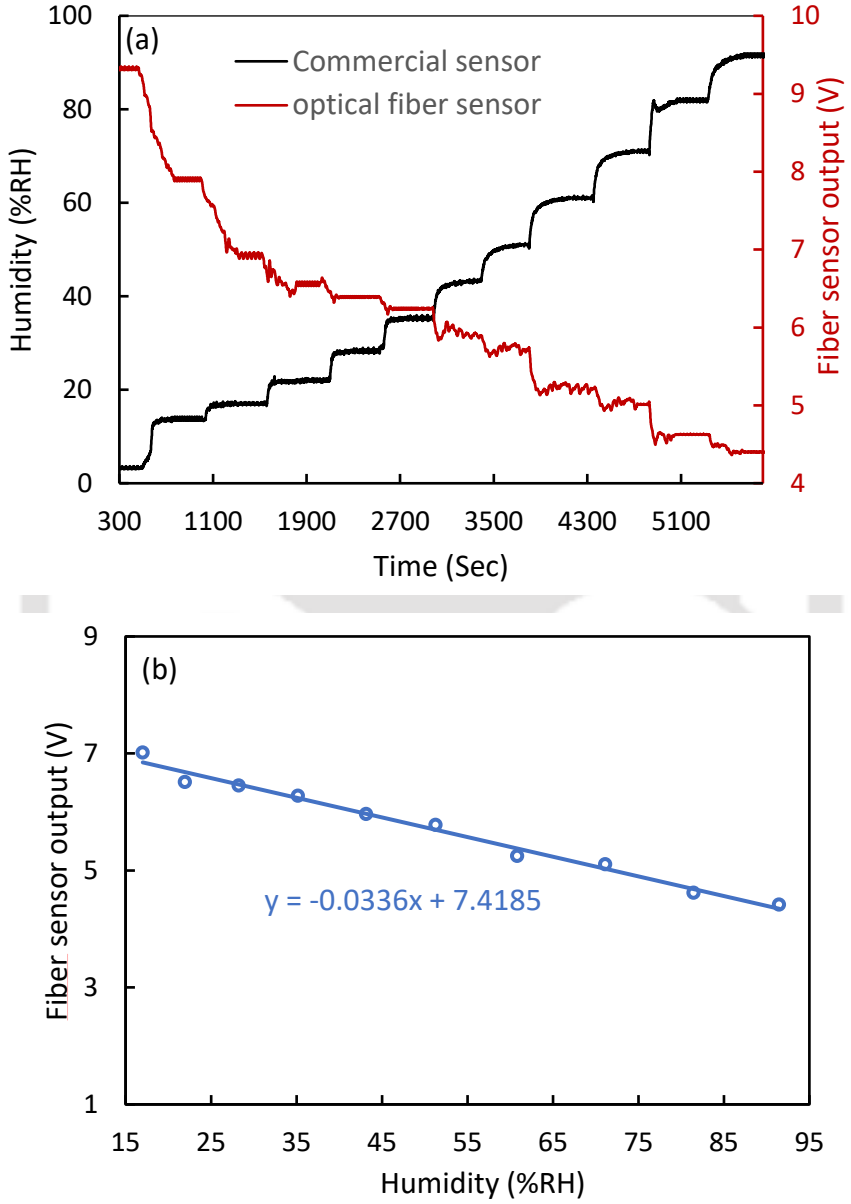

Fig 5.6 : *(a) Response of commercial sensor and that of the proposed GO-ZnO based sensor (b) Experimental responses of the proposed GO-ZnO based sensor.*

in RH. This results in the leakage of the guided power to the cladding modes in the sensing region. In order to get a deeper insight, the fiber sensor's output is plotted against %RH in Fig

5.6 (b). As can be observed, the proposed sensor responds linearly to the applied RH perturbations over the dynamic range of 17%−91%RH with a high sensitivity of 33.6mV/%RH.

Next, the response characteristics of the proposed sensor are compared with the other sensors that employed EW intensity modulation scheme. Table 1 lists the linear sensitivity characteristics of various sensors used for comparative analysis. As can be observed, sensors based on side-polished SMF (SP-SMF) [33], taper SMF [37], and taper polymer-optical fiber (taper POF) [40] [97] have linear response over a very limited dynamic range. U-bend POF [38] and MMF [46] have reasonably good dynamic range, but overall highest dynamic range is observed for straight MMF-based sensor [30]. The dynamic range of the proposed sensor is slightly lower than that in [38] and [30] . However, the highest linear sensitivity is observed for the proposed sensor, which is over three times greater than that in [30] and ~235 times higher in comparison to the previously reported highest sensitivity in [46]. It is worth mentioning that sensor that employed tapered fiber, the diameter was reduced from 125 to 8.7μmmaking the sensor extremely delicate. Importantly, sensitivity increases approximately 70 times for the U-shaped sensing probe in comparison to the straight and uniform sensing probe [30], Chapter 2. This means the expected sensitivity would be $0.25RH^{-1}$ (2352 mV/%RH) if the straight and uniform optical fiber probe of the proposed sensor is replaced with a U-shaped probe of the same fiber. This sensitivity is extraordinarily higher than the sensitivities reported in Table 5.1.

Table 5.1 : *Response Comparison of the Developed Sensor with Reported Sensors Employing EW Absorption Scheme*

Author & Ref.	Sensing element	Dynamic range %RH	Sensitivity
Xiao et al., 2014 [33]	SP SMF	75-95 (20)	0.31dB/%RH
Zhang et al., 2020 [37]	Taper SMF	72–97(25)	1.05dB/%RH
Zhong,et al., 2020 [38]	U bend POF	10-90(80)	$0.0017RH^{-1}$
Aneesh et al.,[30]	Straight MMF	4-96 (92)	$0.0012RH^{-1}$
Batumalay, *et al*., 2015 [97]	Taper POF	50-85 (35)	0.0258mV/%RH
Harith et al., 2020[40]	Taper POF	50-80(30)	0.0295mV/%RH
Afsharipour et al.,2023[46]	U bend MMF	10-80(70)	0.143mV/%RH
Proposed sensors	Straight MMF (GO-ZnO)	17-91 (74)	33.6mV/%RH ($0.0037RH^{-1}$)

Next, the fiber sensor was exposed to repeated and quick RH step changes between the minimum and maximum humidity values to investigate the dynamic performance and repeatability characteristics. The humidity chamber was first desiccated to 5%RH and then quickly humidified to 80%RH. The observed time response is depicted in Fig. 3(d). The output of the proposed sensor changes almost instantly and smoothly during the forward (5%RH to

80%RH) and the reverse (80%RH to 5%RH) cycles of the humidity variations. An average response time of 0.33 s during humidification and recovery time of 0.45 s during desiccation processes are observed from Fig. 3(d), which are much lower than the response time of the commercial sensor. Finally, repeatability and reliability tests were carried out. For

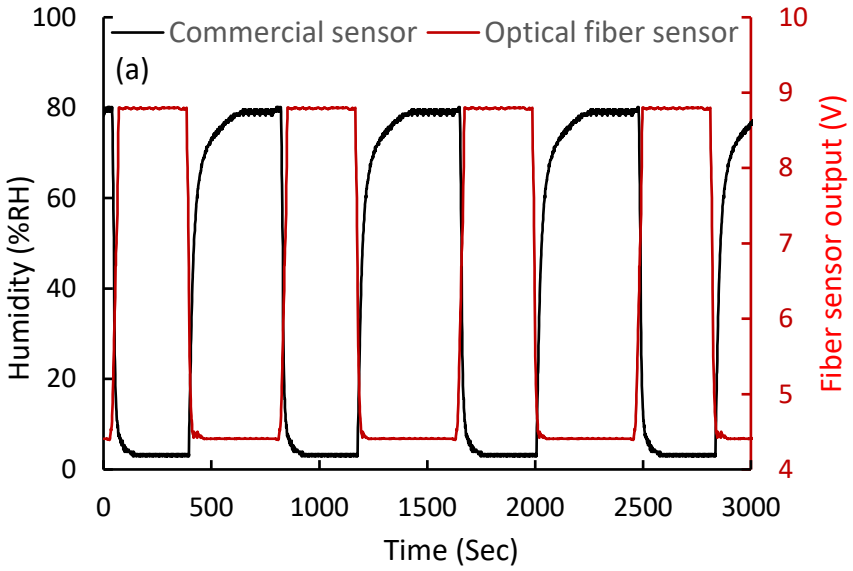

Fig 5.7 : *Time response test under cyclic RH perturbation for GO-ZnO nanocomposite-based sensor.*

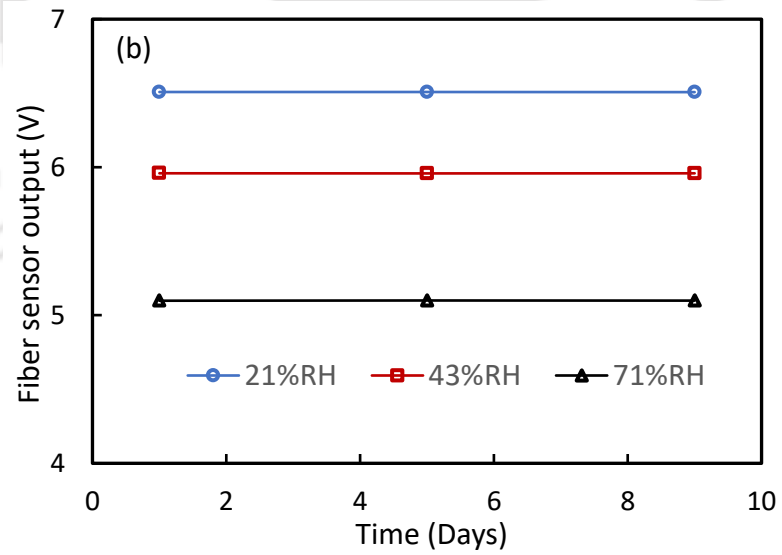

Fig 5.8 : *Repeatability and reliability test: Fiber sensor output on the three different days, each at an interval of 4 days at 21%, 43%, and 71% RH for GO-ZnO nanocomposite-based sensor.*

this, experiments were repeated on three different days with an interval of 4 days at three different humidity levels (21%, 43%, and 71%RH) in a span of 10 days. Observed results are depicted in Fig. 3(e). Maximum variation in the proposed optical fiber sensor's output, compared to day one at all three RH levels, is observed to be as low as ±0.79%. This shows the

excellent reliability and repeatability of the developed sensor. Thus, the excellent performance characteristics of the proposed GO-ZnO nanocomposite-based sensor, employing straight and uniform optical fiber, are of great importance for real-field applications.

5.3.2 Response of GO-ZnO-Fe nanocomposite-based sensor

The GO-ZnO nanocomposite-based sensor exhibits a reasonably wide dynamic range with very high sensitivity. In order to further enhance the sensitivity while maintaining linear sensor response over a wide dynamic better response time, another novel optical fiber RH sensor was developed by employing GO-Zn-Fe nanocomposite. The typical time response of GO-ZnO-Fe based optical fiber RH is depicted in Fig 5.9(a). Just like the GO-ZnO sensor, the output of the GO-ZnO-Fe sensor also decreases as humidity levels increase within the chamber. In order to get a deeper understanding of the sensor's performance, the fiber sensor's output is plotted against the relative humidity percentage (%RH) in Fig 5.9(b). As can be observed, sensor shows a linear response over the dynamic range of 17% to 80%RH, with a sensitivity of 60.6mV/%RH and a very good R^2 value of 0.9993. Further, for comparative analysis, the response characteristics of two additional optical fiber sensors with ZnO doped silica and pure silica film are plotted in Fig 5.10. As can be observed from this plot, sensor employing GO-ZnO-Fe nanocomposite doped silica sensing film exhibits maximum sensitivity of 60.6mV/%RH. Over 1.8 times, 3.7 times, and 11.88 times sensitivity enhancement are observed for the proposed sensor in comparison to the sensitivity observed for GO-ZnO nanocomposite, ZnO np doped silica, and pure silica-based optical fiber RH sensors, respectively. Similarly, sensor employing GO-ZnO nanocomposite doped silica sensing film exhibits sensitivity, which is over 6.7 times and 2 times higher in comparison to the sensitivities observed for pure sol-gel and ZnO nanoparticle doped sol-gel based optical fiber sensors, respectively. The excellent performance of the proposed sensors can be attributed to several factors. Firstly, GO itself is a good humidity sensing agent due to the presence of abundant hydrophilic functional groups at the surface, and its high surface-to-volume ratio [74]. The incorporation of ZnO nps into GO sheets increases the number of hydrophilic functional groups on the surface of the composite material. Stacked GO and ZnO

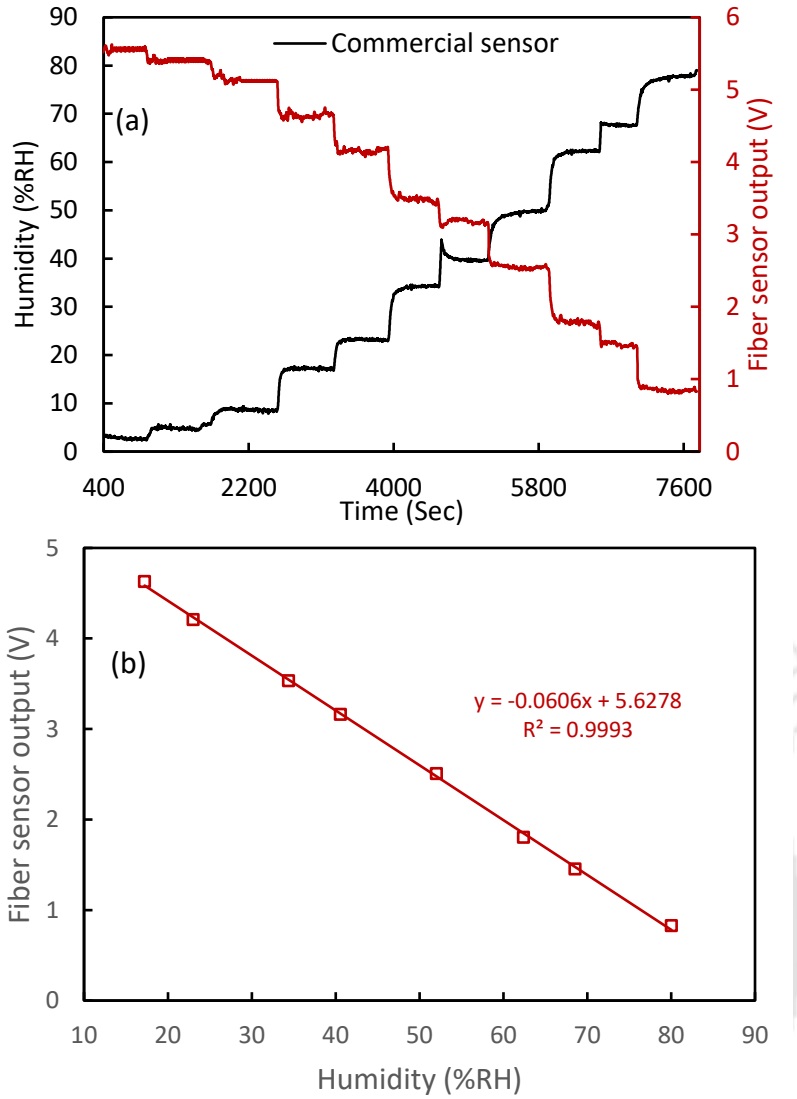

Fig 5.9 : *(a) Response of commercial sensor and that of the proposed GO-ZnO-Fe based sensor (b) Experimental responses of the proposed GO-ZnO-Fe based sensor.*

increases the adsorption sites for the diffused water molecules [76]. This results in manifold increased adsorption of water in GO-ZnO nanocomposite and hence, the refractive index of the sensing region, in comparison to the pure sol-gel and ZnO np-doped sol-gel nanostructures. Further polarization of the nanocomposite also affects the sensitivity of the nanocomposite towards the RH. The inherent polarization characteristics of graphene oxide (GO) primarily depend on the separation distance between its two layers. This separation allows charged molecules to congregate at the interface between the layers, leading to polarization effects. The introduction of ZnO, leads to the exfoliation and improved dispersion of GO nanosheets. This enhances the extent of interfacial polarization. The introduction of Fe in GO-ZnO nc further enhances the polar nature of nanocomposite [76]. Hence, GO-ZnO-Fe is more polar in comparison to pristine GO, ZnO np, and GO-ZnO

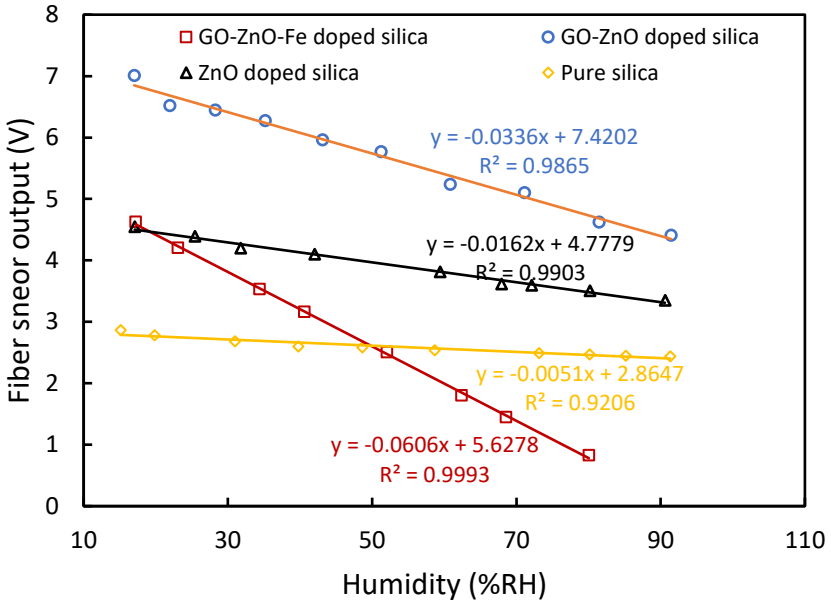

Fig 5.10 : *Experimentally observed responses of optical fiber RH sensors.*

nanocomposite. As a result, the GO-ZnO-Fe nanocomposite doped silica exhibits significantly increased water adsorption compared to both pure silica and ZnO nanoparticle-doped silica.

It is crucial to note that, apart from sensitivity and dynamic range, the detection speed is also very critical for assessing a sensor's efficacy in monitoring the quick and dynamic changes in ambient humidity. An RH sensor with the quickest response and recovery times and reversible response characteristics holds significant importance. The fiber sensor was exposed to repeated and quick RH step changes between the minimum and maximum humidity values to investigate the response time and repeatability characteristics. The humidity chamber was first desiccated to 3%RH and then quickly humidified to 83% RH. Data coming from commercial sensors and optical fiber sensors were recorded at intervals of 0.5s. Fig 5.9 demonstrates that the fiber sensor exhibits nearly instantaneous and smooth changes in output between the minimum and maximum values during both the both forward cycle (3% RH to 83% RH) and the reverse cycle (83% RH to 3% RH). Which shows highly reversible and repeatable nature of sensor. An average response and recovery time of 0.031s is observed. It is important to highlight that the response times of the fiber sensor for the forward and reverse humidity cycles are significantly lower than those of the conventional sensor.

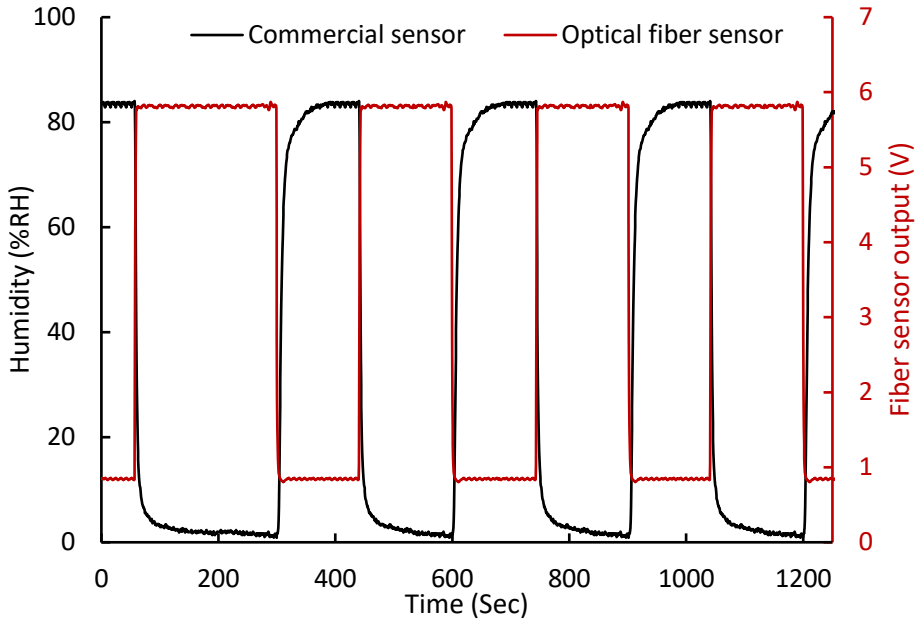

Fig 5.11 : *Time response test under cyclic RH perturbation for GO-ZnO-Fe nanocomposite.*

Stability, repeatability, and reliability are other critical parameters for RH detection. Rigorous analysis was carried out to examine the short-term and long-term performance of the proposed sensor. For analyzing short-term response, the sensor was exposed for about 30 minutes at RH levels, once stabilized at three typical values: 10% RH (low), 35% RH (medium), and 68% RH (high) shown in Fig 5.10 (a). The standard deviations of intensity are observed to be ±4mV, ±4.6mV, and ±4.9mV, respectively, at 10%RH, 35%RH, and 68%RH levels. Hence, the maximum resolution of the sensor for RH detection is observed to be ±0.078%RH, which indicates the excellent stability and accuracy of RH detection. For analysing long-term responses, experiments were repeated on five different days. With an interval of 4, 5, 5, and 5 days, thus spanning a total of 20 days. The experiment was performed at four different %RH (10%RH, 30%RH, 50%RH, and 68%RH). The results obtained from these tests are presented in Fig 5.10(b). Notably, compared to the initial measurement on day one, the maximum variation in the output of the optical fiber sensor was observed to be an impressively low value of 0.4% across all four RH levels. This shows the exceptional reliability and repeatability of the developed sensor. Thus, the reported sensor employing EW intensity modulation facilitated by GO-ZnO-Fe nanocomposite diffused in sol-gel silica nanostructured film synthesized over a short length of centrally decladded straight and uniform optical fiber and having a fast, reliable, repeatable, and linear response achieved over almost the widest possible dynamic range is of great importance for real-field applications.

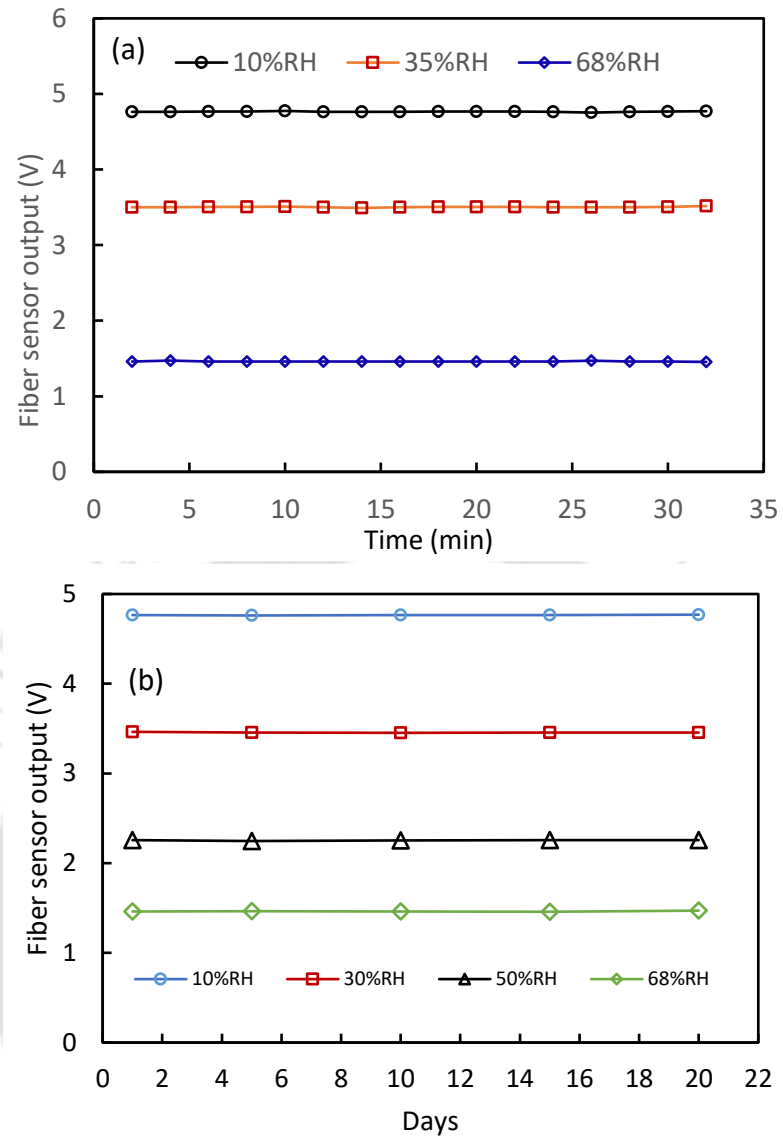

Fig 5.12 : *(a) Short-term stability test (b)Long term stability, Repeatability and reliability test: Fiber sensor output on the five different days, each at an interval of 4, 5, 5 and 5 days for 10%, 30%, 50% and 68%RH.*

5.4 Conclusion

In conclusion, this chapter reports two novel optical fiber humidity sensors employing separately GO-ZnO nanocomposite and GO-ZnO-Fe nanocomposite doped sol-gel silica nanostructured sensing film over a centrally decladded region of straight and uniform optical fiber. Rigorous experimental investigations are carried out for both the reported sensors. GO-ZnO nanocomposite-based sensor exhibits a linear response over the dynamic range of 17-91%RH with a significantly enhanced sensitivity of 33.6mV/%RH. This sensor is observed to be highly reversible, stable, and fast, with average response and recovery times of 0.33 and

0.45 s, respectively. With the objective of further enhancing the sensitivity and response time of this sensor while keeping the dynamic range intact, another nanocomposite is exploited by incorporating Fe in GO-ZnO nanocomposite. The GO-ZnO-Fe nanocomposite-based sensor shows a linear response over the 17−80%RH dynamic range with a sensitivity of 60.6mV/%RH. The average response and recovery times of the GO-ZnO-Fe nanocomposite-based sensor is observed to be 0.031s. Incorporation of Fe in GO-ZnO nanocomposite almost doubles the sensitivity and improves the response time, making the sensor response more than 10 times faster. Further, the response characteristics of the both the sensors are compared with the sensor that employs pure sol-gel silica and ZnO nps doped sol-gel silica nanostructured sensing films. GO-ZnO-Fe nanocomposite-based sensor is observed to be 11.88, and 3.7 times sensitive in comparison to the pure silica and ZnO nanoparticles-based sensors. Though the sensitivity, dynamic range as well as response time all improved, it is felt that the scope of improving repose and recovery time is still there. Hence, research is further extended to develop another optical fiber sensor as discussed in chapter 6.

Chapter 6 : Ultrahigh sensitive rGO-TiO2 nanocomposite-based optical fiber sensor for humidity measurement

6.1 Introduction

Chapter 5 described, the development of two sensors based on GO-ZnO nanocomposite and GO-ZnO-Fe nanocomposite. A wider dynamic range with optimum sensitivity and far better response time was achieved for the sensors. In order to investigate further the optimization possibilities and to make a comparative study, another novel sensor is developed by employing a reduced graphene oxide titanium dioxide (rGO-TiO_2) nanocomposite. rGO is a derivative of GO with a lesser number of oxygen functional groups in comparison to GO. rGO exhibits mechanical, optoelectronic, and conductive properties similar to pristine graphene due to its heterogeneous structure. This structure consists of a graphene-like basal plane with structural defects and enriched with areas containing oxidized chemical groups. rGO is already used for the development of optical fiber RH sensor in chapter 3. On the other hand, TiO_2 nanoparticles are also used for the development of optical fiber humidity sensors [25], [31], [42]. Herrero *et al.,* [25] proposed ant TiO_2 overlayed side polished single mode fiber based optical fiber RH sensor. The observed dynamic range of the developed sensor was 0-15%RH. In an another article Aneesh *et al., ,*[31] demonstrated a highly sensitive optical fiber RH sensor employing TiO_2 nanoparticle doped silica coated over centrally declared fiber. A linear response over wide dynamic range of 24-95%RH with sensitivity of 27.1 mV/%RH. Whereas, Huang *et al.*, [42] reported an optical fiber humidity sensor based SiO_2/TiO_2 bi-film coated straight fiber. A piecewise linear response over the RH range 15-95% RH was observed.

Hence, the combination of rGO and TiO_2 in the nanocomposite is anticipated to significantly augment the sensitivity of relative humidity (RH) measurements. For the development of the sensor, rGO-TiO_2 nanocomposite (comprising rGO and TiO_2) doped silica sol-gel nanostructured sensing film is synthesized over a centrally decladded straight and uniform plastic-clad silica (PCS) fiber. The proposed sensor exploits EW intensity modulation. In order to get an optimum response, rigorous experimental investigation is carried out by varying sensing film compositions. The optimized sensing probe shows linear response over a

wide dynamic range of 3-70%RH with a sensitivity of 103mV/%RH ($0.0145RH^{-1}$), which is observed for the first time to the best of the author's knowledge. In addition, the response time of the proposed sensor is observed to be 0.025s for humidification and desiccation, both.

6.2 Experiment

6.2.1 Synthesis of rGO-TiO_2 nanocomposite

For the synthesis of reduced graphene oxide-titanium dioxide (rGO-TiO_2) nanocomposite, first, graphene oxide (GO) was synthesized via modified Hummer's method as discussed in Chapter 2. The desired graphene oxide was obtained by slow centrifugation. In order to prepare rGO-TiO_2 nanocomposite [80], 0.5 mL of $TiCl_4$ was added to 40 mL of deionized water. Resulting solution was stirred for 20 min, and then slowly dropped into 5 mL of 30% H_2O_2 solution and stirred for 5min. Afterwards, 5mM of NaOH solution was added to the above solution until pH of the solution was measured to be 4. Next, 10 mg of GO was added to the mixed solution separately and stirred for 30 min. The prepared mixture was then placed in an autoclave and subjected to a solvothermal reaction at 140°C for 6 hours. The resulting black product was washed multiple times with ethanol and distilled water and then dried at 60°C for 12h.

6.2.2 Characterization of rGO-TiO_2 nanocomposite

An X-ray diffractometer (XRD, Rigaku TTRAX III), was used for the structural characterization of synthesized nanocomposite at room temperature. Further, size of the-synthesized nanocomposite was examined by a field emission transmission electron microscope (FETEM, JEOL-2100F). XRD spectra of synthesized GO, rGO and rGO-TiO2 are shown in Fig. 6.1(a). The (001) crystal plane of GO exhibits a strong peak at 10.5°, with an interlayer spacing of 8.67 Å, whereas the interlayer spacing for graphite is 3.37 Å. The increased interlayer spacing suggests the oxidation of graphite, which affects its crystal structure. Upon reduction of GO, a broad peak at $2\theta = 25.29°$ appears for (002) crystal phase of rGO. The presence of this broad peak suggests that the arrangement of the (002) crystal phase in rGO is random compared to graphite and graphene oxide. The XRD pattern of the rGO-TiO2 nanocomposite shows peaks at 25.41°,38.2°,48.25°,54.66°,62.74°, 75.4° and 75.3°, which correspond to (101), (004), (200), (105), (211), (204) and (116) crystalline planes of anatase TiO_2. could be attributed to the fact that the Importantly, (001) peak is completely absent in rGO-TiO_2 nanocomposite, whereas, the primary rGO peak at $2\theta = 25.29°$ nearly coincides with the main peak of anatase TiO_2 (101) at 25.41°. This shows the formation of

exfoliated GO sheets due to the nucleation and growth of TiO2 nanocrystals onto the GO sheets, confirming the successful formation of the nanocomposite [80], [105]. The FETEM image of the rGO-TiO2 is depicted in Fig. 6.1(b), and the corresponding size distribution of the particles is presented in Fig. 6.1(c). The size of particles is predominantly in the range of 5-12nm with average particle distribution of 8.2±0.1nm.

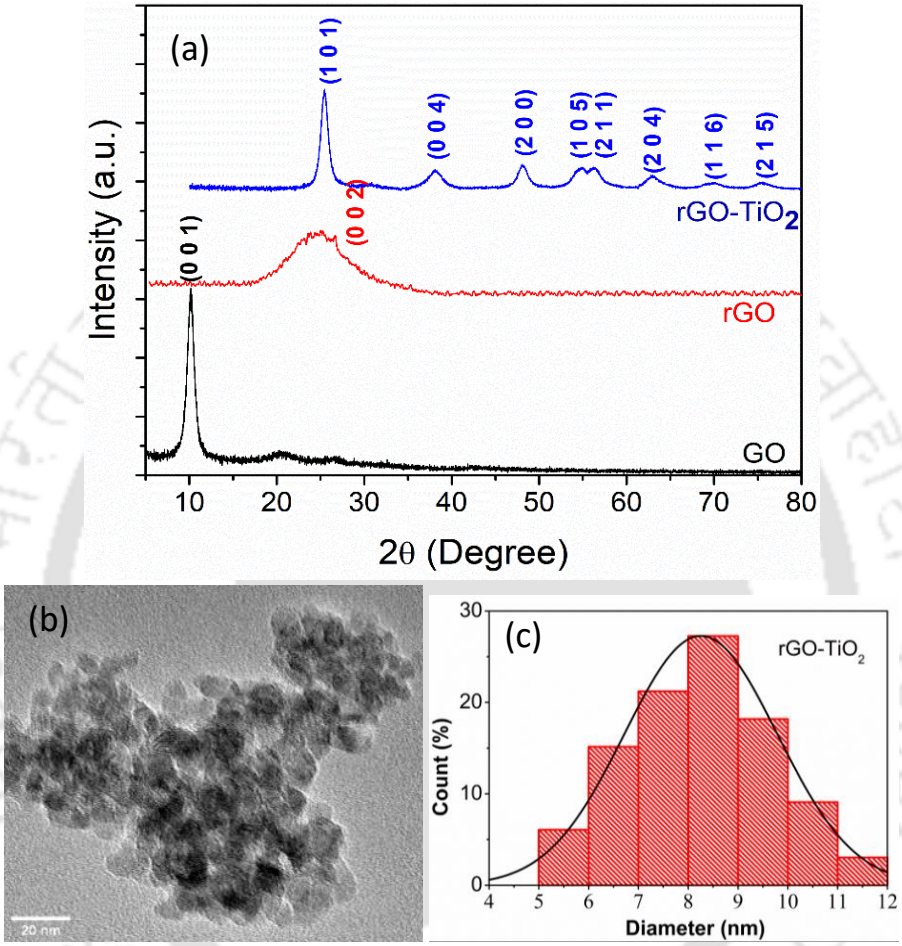

Fig 6.1 : *(a) XRD of GO, rGO and rGO-TiO2 nanocomposite (b) FETEM picture of rGO-TiO2 nanocomposite and (c) Size distribution within the nanocomposite.*

6.2.3 Sensing probe preparation

A piece of plastic cladding silica fiber (PCS) having a core diameter of 200µm and length of 50cm (200/380T, Ceramoptec) is used for sensing probe preparation. The core and cladding refractive index of the fiber are 1.457 and 1.404, respectively. First, fiber ends are polished properly to get optically flat end faces for maximum power coupling from the source to the fiber sensor and fiber sensor to detector. About 5 cm of the cladding was removed from the central portion of the fiber. The decladded portion of fiber was cleaned properly by sonicating it first in soap solution and then in water multiple times. An rGO-TiO_2 diffused silica film was

chemically synthesized over a centrally decladded portion of the fiber. For the synthesis of rGO-TiO_2 diffused silica matrix, silica sol was prepared by mixing tetraethyl orthosilicate, deionized water, ethanol, and hydrochloric acid in the ratio of 3:2:1:0.01. After 36h, a suitable amount of rGO-TiO_2 was mixed into silica sol by proper sonication. Prepared sol was coated over the decladded portion of the fiber by dip coating method. As already

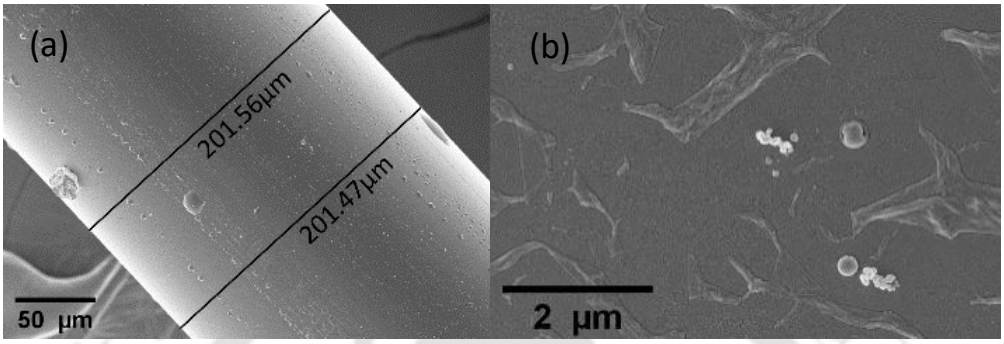

Fig 6.2 : *(a) FESM picture of rGO-TiO2 doped silica coated fiber (b) FESEM picture of surface in sensing region.*

established in our previous research works [31], Chapter 2, and Chapter 4, best response characteristics were observed for the sensing probes having sensing film thickness approximately 0.8µm which corresponds to the thickness of three dip coated decladded fiber. Hence, multiple sensing probes with 3-dip film thickness were prepared using varying film compositions to optimize the sensor's performance characteristics. All sensing probes were dried first at room temperature for 2 days and then annealed for 2h at 110°C to remove the trace water and ethanol from the sensing film. The surface morphology, microstructure, and film thickness of the 3dip coated probe were analyzed using FESEM (Sigma-300). Fig 6.2(a) illustrates an image of the coated area of the optical fiber, where the average diameter is measured as 201.51µm. This establishes an average thickness of the sensing film as 757.75nm. The surface morphology of the deposited sensing film is depicted in Fig 6.2(b), which shows high-quality porous structure with moderate roughness.

6.2.4 Charecterization of the sensor

Similar procedures, as explained in Chapter 2, were followed to characterize each sensing probe.

6.3 Result and discussion

For proper experimental investigation, all the developed sensing probes were carefully

characterized at different humidity levels during ascending and descending humidity cycle. For example, the time response of the developed sensing probe having film thickness 3-dip with composition 0.15g nanocomposite in 20ml silica sol is depicted in Fig 6.3(a). From the result it can be conclude that the fiber sensor output decreases with an increase in humidity inside the chamber. This can be physically understood as following: water molecules being diffused into the nano scaled pores of the rGO-TiO_2 doped silica matrix get adsorbed in these pores. Increase in the humidity increases adsorption of water vapor and condensed in the pores of the sensing film. This leads to a change of refractive index in the sensing region carrying nanocomposite

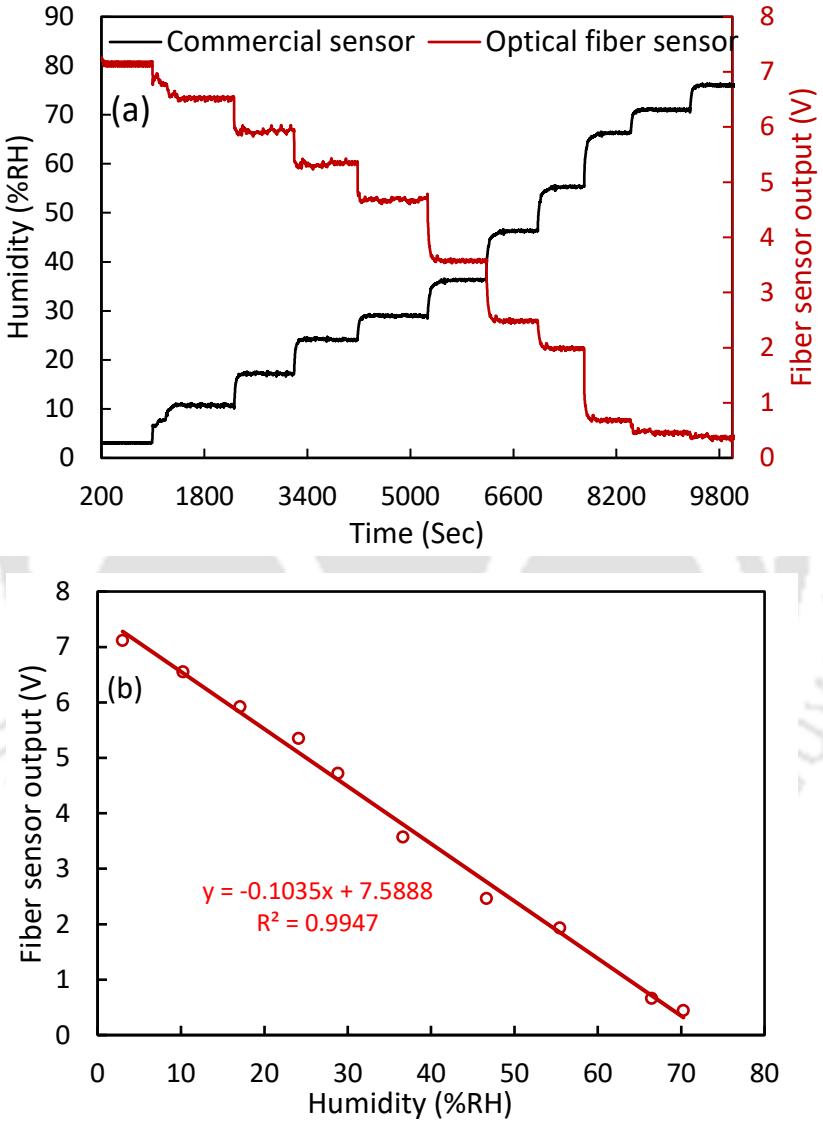

Fig 6.3 : *(a) Response of commercial sensor and that of the proposed sensor (b) Experimental response of proposed sensor.*

doped silica film. Corresponding leakage of the guided power to the cladding modes results in a comparatively intense intensity modulation. In order to get a deeper insight, the fiber sensor's

output is plotted against %RH in Fig. 6.3 (b). As can be observed, the proposed sensor responds linearly to the applied RH perturbations over the dynamic range of 3−70%RH with sensitivity of 103.5mV/%RH. In order to investigate the effect of film composition on sensors performance, the responses of the sensor employing varying film compositions as 0.1g, 0.15g, and 0.2g nanocomposite in 20ml silica sol and film thickness fixed at optimum value of 3-dip coating are plotted in Fig 6.4. As can be observed, sensor employing 0.1g film composition shows a linear response from 3% to 70%RH with a sensitivity of 61.6mV/%RH. An increment in film composition from 0.1g to 0.15g nanocomposite in 20ml silica sol improves sensitivity to 103.5mV/%RH, which is 1.6 times higher than the sensitivity observed in the case of the sensing probe having

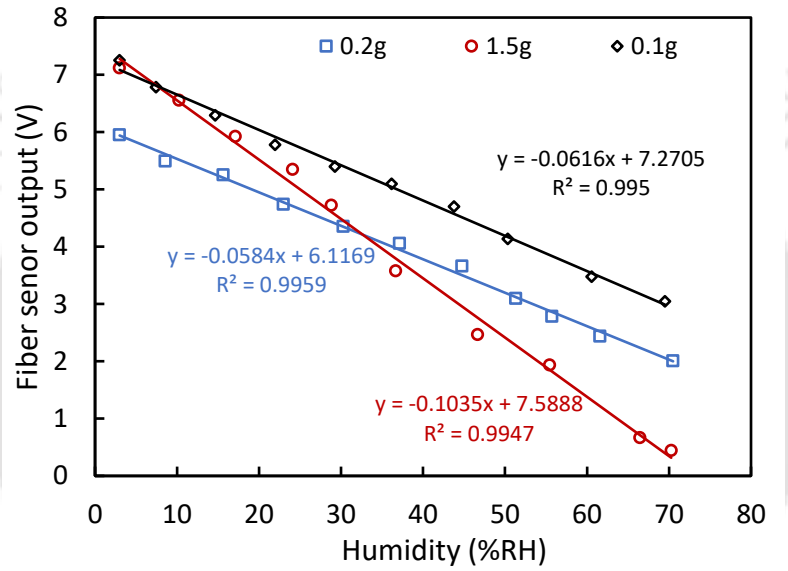

Fig 6.4 : *Responses of the sensing probes having different film compositions.*

0.1g nanocomposite in the film. This is due to the fact that the number of nanocomposite molecules available to react with humidity is 1.5 times greater. However, further increment of nanocomposite from 0.15g to 0.2g in film composition do not exhibit the same trend. The sensitivity of the probe having 0.2g nanocomposite in 20ml silica sol is 59.1mV/%RH. This shows the existence of an optimum film composition along with the 3-dip film thickness for the present sensor which is observed to be 0.15g nanocomposite in 20ml sol. The existence of optimum film composition can be understood as following: presence of nanocomposite concentration in sensing film beyond a certain level affects the porosity of sensing film which obstructs the proper diffusion of water molecules into the nanostructured sensing film. Hence, there is limited interaction between water molecules and evanescent wave, reducing the sensitivity substantially. Further, for the comparative analysis two more sensors employing

pure silica nanostructured and TiO_2 nps doped silica nanostructured sensing film are developed and experimentally investigated. The sensitivity of the TiO_2nps doped silica-based sensor is observed to be 27.1mV/%RH, whereas the sensitivity of the pure silica-based sensor was 5.1mV/%RH. This shows that the sensitivity of the proposed sensor is 20.29 times higher than the sensitivity of pure sol-gel silica nanostructured sensing film, and 3.81 times higher than the sensitivity of TiO_2 np doped sol-gel silica nanostructured sensing film. The exceptional performance of the proposed sensor can be attributed to several factors. Firstly, rGO itself serves as an excellent humidity sensing agent with high surface-to-volume ratio. Additionally, combination of stacked rGO and TiO_2 provides a greater number of adsorption sites for the diffusion of water molecules. Consequently, the refractive index of the sensing region in the proposed sensor experiences a manifold increase, leading to its outstanding performance in humidity sensing applications.

Next, dynamic performance of the fiber sensor was examined by subjecting it to the repeated and rapid changes in relative humidity (RH) between 2% and 83%. To achieve this, the sensor is quickly humidified to 83% RH by passing air from the mouth through the pipe into the chamber. Data coming from commercial sensor and optical fiber sensor were recorded at interval of 0.5s. The time response of the sensor is

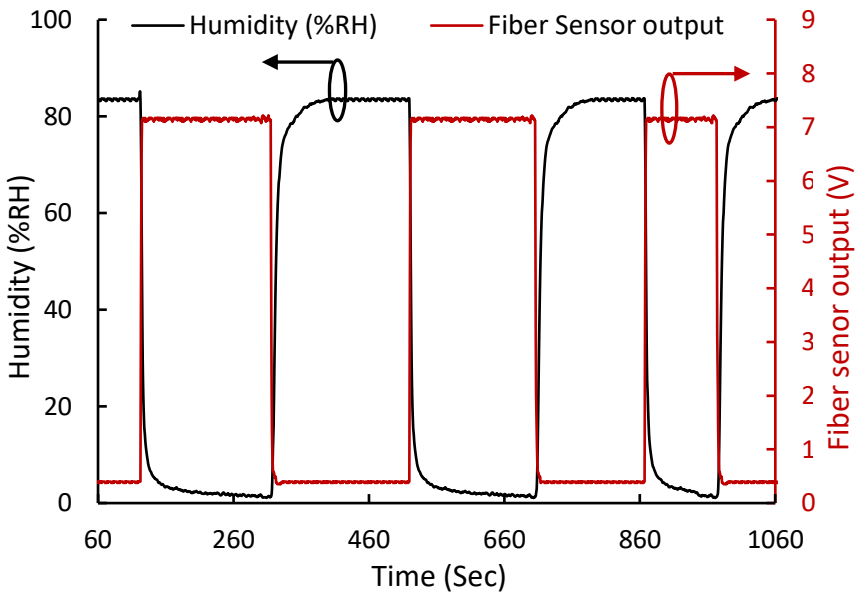

Fig 6.5 : *Time response behavior of humidity sensor against cyclic humidity.*

illustrated in Fig 6.5. The figure clearly demonstrates that the fiber sensor exhibits nearly instantaneous and smooth changes in output between the minimum and maximum values during both the forward cycle (2% RH to 83% RH) and the reverse cycle (83% RH to 3% RH) of humidity. This shows a highly reversible and repeatable nature of the proposed sensor. An

average response and recovery time of 0.025s are observed for the sensor.

Stability, repeatability and reliability are other critical parameters for RH detection. Rigorous analysis was carried out to examine short-term and long-term performance of the proposed sensor. For analysing short-term response, sensor was exposed for 30 minutes at RH levels, once stabilized at three typical values: 10% RH (low), 30% RH (medium), 60% RH (high) and 70%RH (high) as shown in Fig 6.6(a). The standard deviations of output intensity are observed to be ±10.2mV, ±8.4mV, and ±10.2mV respectively, at 10%RH, 30%RH and 60%RH levels. Hence, maximum resolution of the sensor for RH detection is

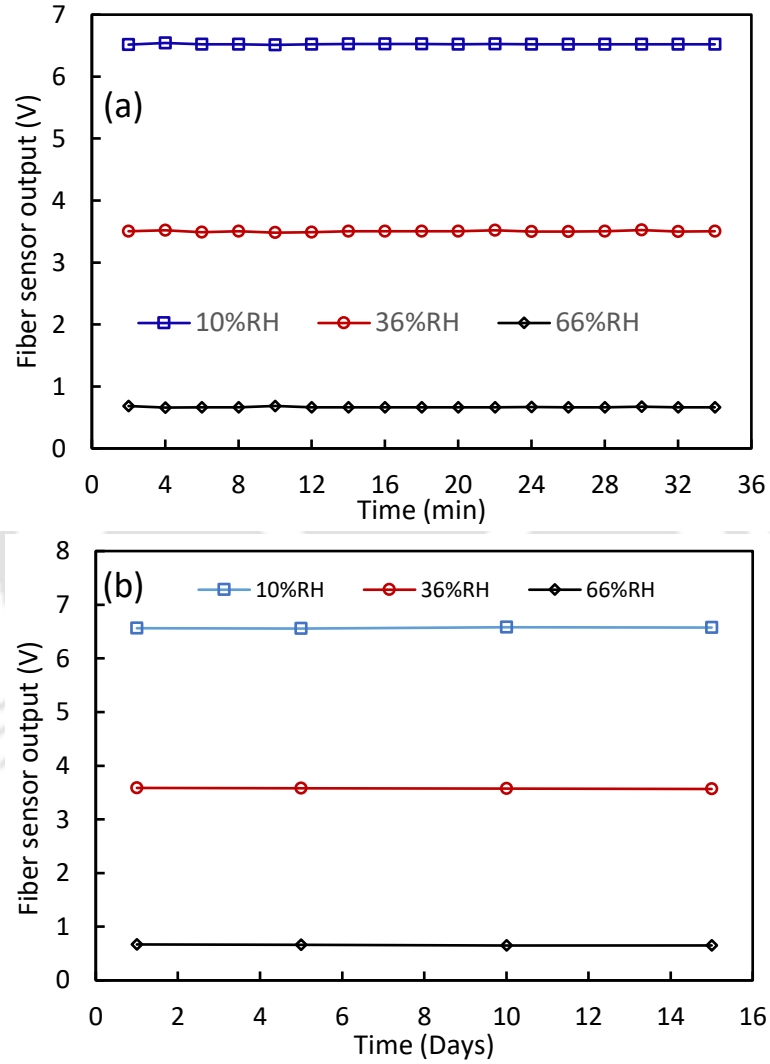

Fig 6.6 : *(a) Short term stability test (b) Long-term stability, repeatability, and reliability test: Fiber sensor output on the three different days, each at an interval of 4, 5, and 5 days for 10%, 36% and 66%RH.*

observed to be ±0.099%RH, which validates the excellent stability and accuracy of RH detection. For analysing long-term response, experiments were repeated on four different days.

With an interval of 4, 5 and 5 days, thus spanning a total of 15 days. The experiment was performed at three different %RH (10%RH, 36%RH and 66%RH). The results obtained from these tests are plotted in Fig 6.6 (b). Notably, the maximum variation in the output of the optical fiber sensor, compared to the initial measurement on day one, was observed to be an impressively low value of ±0.4%. across all three %RH levels. This shows the exceptional reliability and repeatability exhibited by the developed sensor. Therefore, the remarkable performance characteristics of the proposed sensor, which employs rGO-TiO2 nanocomposite doped sol-gel silica nanostructured sensing film onto the decladded region of straight and uniform optical fiber, hold significant importance for real-field applications.

6.4 Conclusion

Research in this chapter presents the successful development of a simple optical fiber relative humidity (RH) sensor. The sensor incorporates a reduced graphene oxide-titanium dioxide (rGO-TiO2) nanocomposite diffused silica nanostructured sensing cladding, covering the centrally decladded region of the fiber. Comprehensive experimental studies establish that the sensor exhibits a linear response over a wide dynamic range of 3-70%RH, making it suitable for a diverse range of applications. Notably, the sensor demonstrates an ultrahigh sensitivity of 103.5 mV/%RH, ensuring accurate and precise RH measurements. Moreover, the proposed sensor showcases exceptional reversibility and stability with an average response and recovery time of 0.025s, enhancing its practicality and reliability. These findings highlight the potential of the proposed optical fiber RH sensor as an efficient and effective tool for humidity monitoring. Its simplicity, high sensitivity, linearity, and fast response make it a valuable asset in various industries, such as environmental monitoring, agriculture and air conditioning. The sensor's ability to maintain stability and reversibility further contributes to its practicality and long-term use. It is evident that, the reported sensor showing an increase in sensitivity with reduced dynamic range and improved response time in compared to the sensor reported in Chapter 5. Response time of the developed sensor still needs to be improved for several real-field applications, such as, breath monitoring and voice print recognition, which forms the basis for the research work discussed in the next chapter.

Chapter 7 : Ultrafast highly-sensitive Graphene oxide (GO) based optical fiber humidity sensor

7.1 Introduction

As discussed in the previous chapter, a very high sensitivity over a wide dynamic range is achieved by employing rGO-TiO_2 nanocomposite doped silica sensing cladding over the centrally decladded optical fiber. Nevertheless, response time of the sensor still needs to be improved for several applications, as an example, for human breath monitoring and voice print recognition to name a few. Sensor reported in Chapter 6 exploited EW intensity modulation to detect changes in humidity levels. RH sensors based on this technique employ chemically synthesized cladding over a short section of decladded core of an optical fiber to facilitate interaction of guided light with the measurand. Performance of such sensors critically depends on the penetration depth (d_p) of the guided modes (or fractional power in the cladding). For straight and uniform optical fiber, d_p is typically of the order of the wavelength of the light propagating within the fiber. This short region where measurand interacts with the optical signal limits the performance of evanescent-wave absorption-based sensors employing straight and uniform fiber geometry. Over the years, several researchers have utilized various structures, e.g., U-bend fiber [38], side polished single-mode fiber [33][106], and taper fiber [107] to improve the response of RH OFS. Nevertheless, nonlinear response, limited dynamic range or piecewise linear sensitivity and very high response and recovery times remained major limitations. One way to increase the penetration depth (or fractional power in the cladding) is reducing the core diameter of the fiber [108]. This can be achieved by chemical etching [109]. For example, Azad et al. [35] have reported an optical fiber RH sensor using ZnO nanorod coated etched optical fiber. Good sensitivity over a limited dynamic range of 30–55%RH and recovery time as high as 7 s were observed for this sensor.

In recent years, carbon-based nanomaterials, such as graphene, graphene oxide (GO), and reduced graphene oxide (rGO), have attracted great attention of researchers due to their exciting electrical, mechanical, and optical properties. Recently, GO and rGO are extensively

used for developing conventional as well as optical fiber RH sensors employing various schemes. As an example, response and recovery times, as high as 10.5s and 41s, along with nonlinear response remained major challenges for conventional sensor employing GO [110]. On the other hand, Zhong et al. [38] utilized polyimide and GO coating on a U-shaped plastic optical fiber (POF) for RH measurement. A sensitivity of 0.0017 RH^{-1} over a dynamic range of 10–90%RH along with response and recovery times as high as 145 s and 155 s were observed in this case. Syuhada et al. [107] reported PVA-GO coated tapered optical fiber RH sensor, observing nonlinear intensity response with 147s and 293s as response and recovery times. Sun et al. [96] reported GO/PVA coated double-tapered twisted fiber (DTTF) structure for RH measurement. Observed linear dynamic range, sensitivity, response and recovery times were 45–85%RH, 0.002 RH^{-1}, 1.9s and 5.7s respectively. In another sensor employing rGO and hollow core fiber (HCF), a dynamic range of 60-90%RH, response time of 5.2s and recovery time of 8.1s were observed[69]. Unfortunately, all the sensors mention above showed limited dynamic range, nonlinear response or low linear sensitivity and very high response/recovery times. Wider dynamic range, optimum sensitivity and importantly, ultrafast response are critical in monitoring dynamic evaluation of RH.

This chapter reports an optical fiber RH sensor based on GO coated reduced-to-few-micron core-diameter (RFMCD) straight and uniform sensing region. Sensor employs intensity modulation via EW absorption technique. Reduced-to-few-micron core-diameter substantially enhances fractional power in the cladding and subsequently improves the response characteristics of the sensor. Rigorous experimental investigations are carried out to establish the response characteristics of the proposed sensor. This sensor outperforms other sensors due to its ultrafast response time of 50ms over a dynamic range as wide as 3−94%RH. In addition, sensor response is observed to be linear throughout the observed dynamic range. An optimum sensitivity of 0.0115%RH^{-1} and an excellent accuracy of RH detection (reflected by maximum resolution of 0.049%RH) are observed for the proposed sensor. Repeatability and reversibility tests, conducted in extreme conditions over a span of 16 days, establish an invariable response of the sensor.

7.2 Experiment

7.2.1 Sensing probe preparation

Fig. 7.1 depicts the fabrication of graphene oxide coated reduced-to-few-micron core-diameter straight and uniform sensing probe. For the sensing probe preparation, first, Graphene

oxide was synthesized from natural graphite via modified Hummer's method as discussed in Chapter 1. Afterwards, reduced-to-few-micron core-diameter straight and uniform sensing probe was prepared in order to strengthen evanescent-wave, and hence, fractional power in the cladding of the sensing region. To do so, plastic-clad silica (PCS) multi-mode fiber (200/380T, Ceramoptec) of core diameter 200µm was used. Total length of 50cm was taken and both the fiber ends were polished in order to achieve maximum power coupling efficiency from source to sensor and sensor to detector. Approximately 2.5cm length of the fiber was decladded from the central region. The decladded region of the fiber was fixed inside a specially designed etching chamber as shown in Fig 7.1(a). HF etching method [109] in a pre-controlled and precise manner was deployed to reduce the core diameter of the

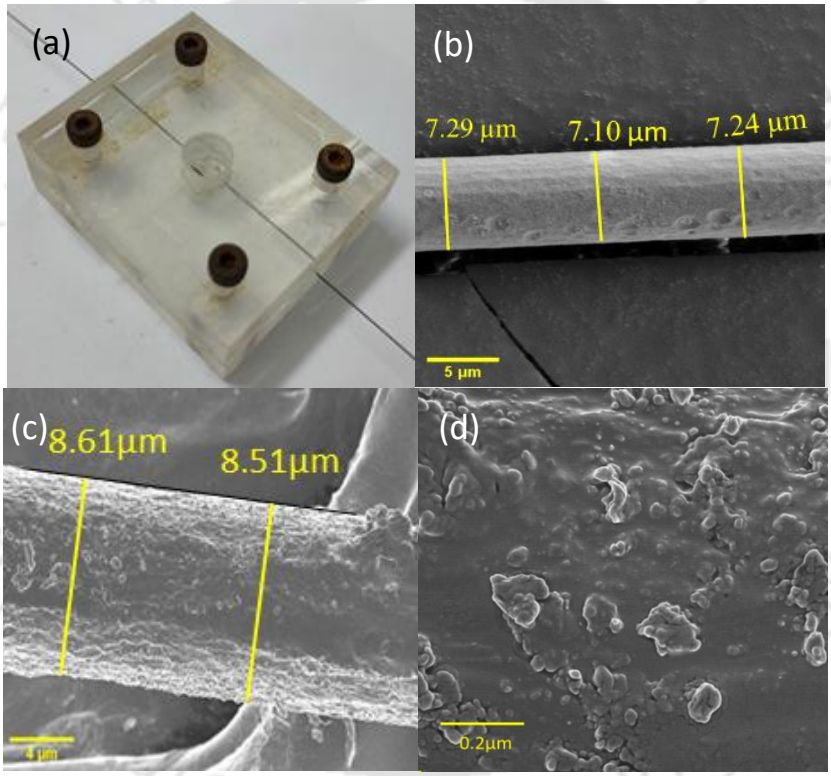

Fig 7.1 : *(a) Fiber in etching chamber; FESEM image of (b) etched optical fiber, (c) GO coated etched optical fiber; and (d) zoomed FESEM image of the surface of the sensor.*

decladded region. Etching end-results were examined by the Field Emission Scanning Electron Microscope (FESEM) (Zeiss, Sigma 300). Image of the etched fiber is shown in Fig 7.1(b). As can be observed, a good degree of uniformity with an average core diameter of ~7.21µm (~96.4% reduction) is achieved for the etched region of the fiber. Afterwards, GO was synthesized over the etched portion of the fiber. For this, GO was first dispersed in ethanol. Then, the reduced-to-few-micron core-diameter region of the fiber was carefully immersed in

the GO dispersed ethanol solution and kept at 80°C in an oven. Drying the probe at 80° results in the evaporation of ethanol and hence, a uniform GO film on the decladded and etched region of the fiber is coated. The prepared sensing probe was kept in a desiccator under partial vacuum for two days to remove the trace alcohol and water from the GO film. Surface morphology and the thickness of the deposited GO film were examined by FESEM. Figures 7.1(d) and 7.1(e) depict images of coated optical fiber and its surface, which establish that GO film is firmly fixed onto the fiber surface. The thickness of the GO film is observed to be 0.675µm. In order to optimize sensor response, multiple sensing probes having different film thicknesses were prepared by changing the amount of GO in ethanol (0.5g GO in 40ml, 0.5g GO in 80ml and 0.5g GO in 160ml ethanol).

7.2.2 Characterization of sensing probe

Response characteristics of the developed sensor were investigated by fixing the sensor inside a humidity chamber, humidity level was precisely controlled by properly mixing dry and moist air through sophisticated flow meters. Commercial RH sensor (Totronic HygroClip

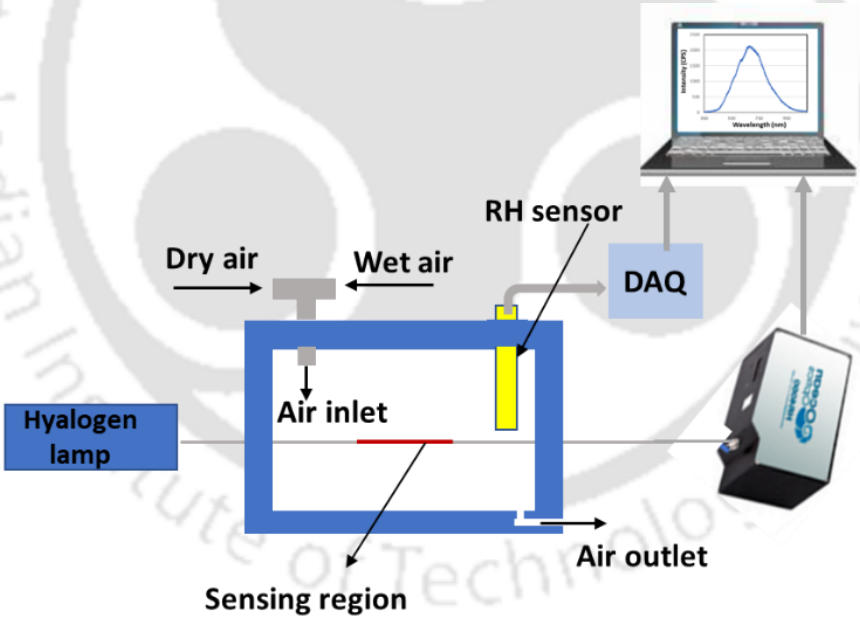

Fig 7.2 : *Experimental setup for characterization of optical fiber RH sensor.*

1HC2), having an accuracy of ±0.8%RH in the range of 0–100%RH, was fixed inside the chamber in order to monitor RH and temperature variations. During the characterization of the sensor, light from a halogen light source (Ocean optics, HL-2000-FHSA) was launched from one end of the fiber and the distal end was connected to the spectrometer (Ocean optics RH4000, resolution 0.02nm). Commercial sensor and the spectrometer both were interfaced

with computer through data acquisition (DAQ) card and MATLAB program. Effect of humidity was monitored in real- time by recording the transmitted spectrum. For this, the humidity level was, first reduced to the minimum level by injecting dry air inside the chamber. Afterwards, the humidity level was slowly increased in suitable steps by mixing controlled amount of moist air inside the chamber. Sensor's response was investigated only after the stabilization of RH within the chamber during humidification as well as desiccation. Throughout the experiment, temperature within the chamber was maintained at 24°C.

7.3 Result and discussion

The proposed sensor exploits the phenomena of intensity modulation through evanescent wave interaction within the thin GO sensing film, deposited onto a centrally decladded straight and uniform reduced-to-few-micron core of a multimode PCS optical fiber. In the process of optimizing sensor's response, multiple sensing probes with varying thicknesses of GO-based sensing film were prepared. To do so, the amount of GO in ethanol was varied as 0.5g GO in 40ml, 0.5g GO in 80ml and 0.5g GO in 160ml ethanol, and each GO dispersed solution was used for synthesizing thin GO film. In order to investigate response characteristics, outputs from the proposed and commercial sensors were monitored in real- time under varied humid environments. The spectral response characteristics for the sensing probe having film composition/thickness, as an example, corresponding to 0.5g GO in 80ml ethanol, are depicted in Fig. 3 (a) while increasing the humidity in a range of 3–94%RH. The responses are recorded at fixed and stable RH levels. A similar response was observed while decreasing the humidity. As can be observed, optical fiber output is substantially reduced at low humidity. With increasing RH, the intensity of the guided light increases uniformly over the whole range of spectrum (from 300nm to 1100nm). GO is rich in oxygen-containing functional groups. If exposed to a humid environment, dissociated water molecule makes a weak hydrogen bonding with these oxygen-rich functional groups. As a result, water molecules are easily absorbed by the two-dimensional multilayers of GO where they act as Electron acceptors. With the attachment of water molecules, the surface charge carrier density of GO increases, causing the Fermi level of the GO to rise above the Dirac point. This results in the block of interband transitions and a subsequent reduction in the conductivity of the GO
sensing film [111]. Hence, the effective refractive index of the GO sensing film decreases as adsorbed water molecules increase when humidity is increased [112]. With the decreasing

cladding refractive index, penetration depth in the sensing region decreases owing to the tight confinement of the mode-field in the core region. Therefore, the interaction between the EW

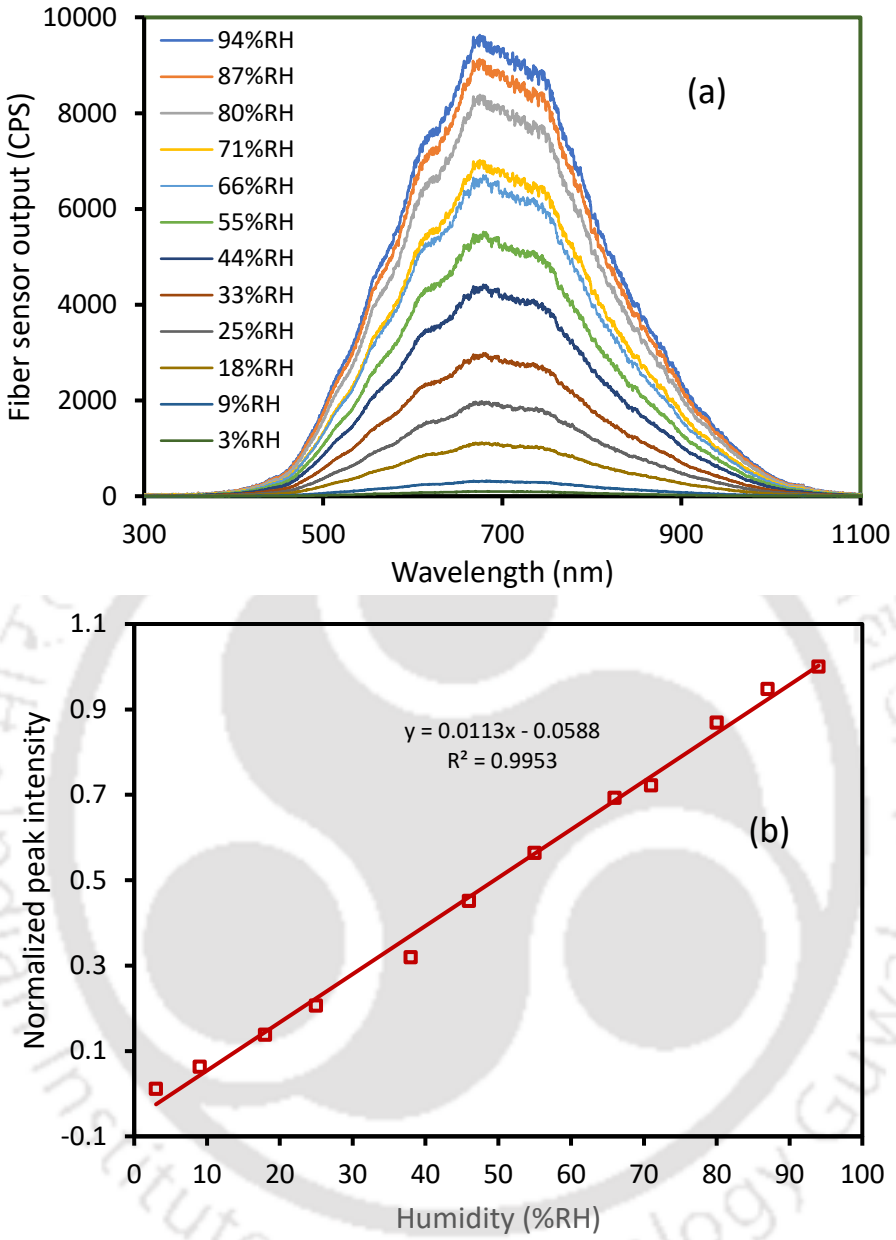

Fig 7.3 : *(a) Experimentally observed spectra of fiber output for different RH, (b) Experimentally observed sensor response.*

and water-molecule-adsorbed GO sensing film gets exceedingly poor with increasing RH levels. Hence, at high humidity, guided optical power is less affected. On the other hand, penetration depth of evanescent-wave in the sensing region is large when RH is low. This facilitates greater interaction between the evanescent-wave and water molecule adsorbed GO sensing film, leading to a greater absorption of guided optical power in the sensing region. Hence, intensity of the output spectra is very low at low RH levels. The performance of the proposed sensor relies on the thickness of the sensing film.

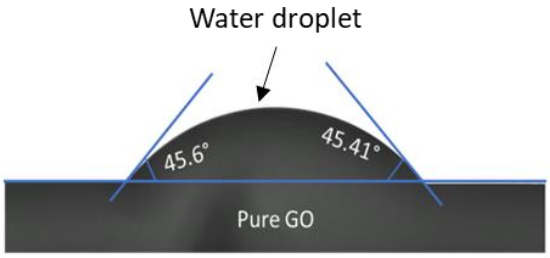

Fig 7.4 : *Contact angle of water drop on GO surface.*

In order to get a better understanding of the response characteristics, optical fiber output is extracted from Fig. 7.3(a) at various wavelengths and plotted against applied RH variations. Typical response of the proposed sensor, as an example at 630nm, is depicted in Fig. 7.3(b). As can be observed, fiber output increases as humidity increases. Importantly, the sensor exhibits throughout-linear response over a dynamic range as wide as 3–94%RH with the sensitivity of $0.0115RH^{-1}$ and linearity as high as 0.9949. Exactly the same response is observed at other wavelengths, too. 630nm wavelength, hence onward, is chosen as the benchmark wavelength for analyzing sensor's performance owing to its closeness with, He-Ne laser for designing a futuristic prototype. Importantly, in order to achieve optimum response for the sensor, thickness of the sensing film must be of the order of the penetration depth of the evanescent wave in the sensing region. In the present research, this is achieved for the sensing probe prepared with 0.5mg GO dispersed in 80ml of ethanol.

Apart from sensitivity and dynamic range, detection speed is a very critical parameter to evaluate the performance of a sensor towards its capability of monitoring the dynamic and rapid evolution of ambient humidity. RH sensor having the fastest response time and shortest recovery time, reversible response and detection with high precision is of great importance. Hence, the dynamic performance and repeatability characteristics of the proposed sensor were evaluated by exposing it to the quick and cyclic RH step changes between minimum (5%RH) and maximum (83%RH) humidity values. The humidity of the chamber was first desiccated to 5%RH and then quickly and repetitively humidified to 83%RH by passing human breath from the mouth. During this cyclic change, the peak intensity of fiber sensor output spectra was recorded. The observed time response of the developed sensor is depicted

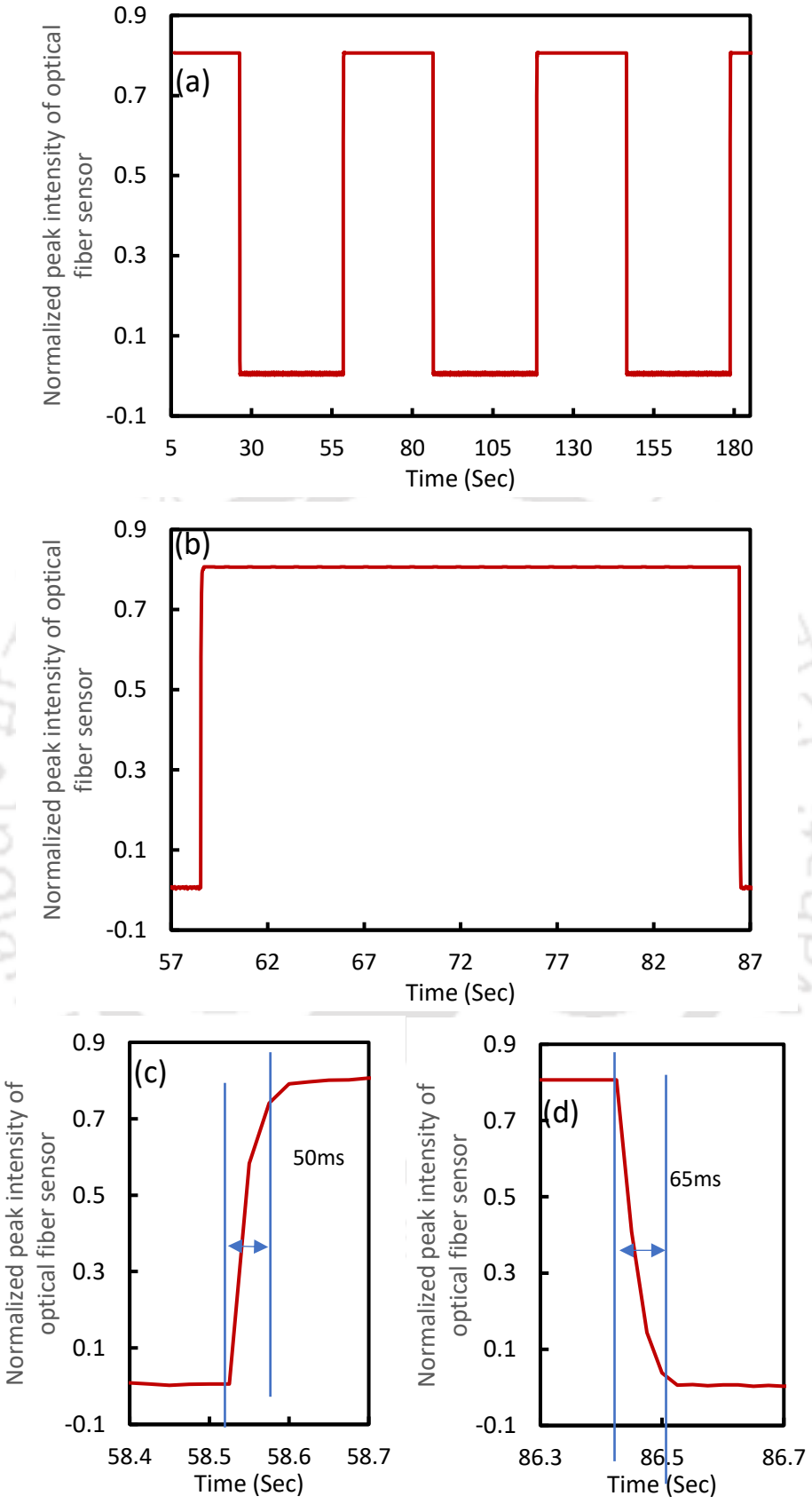

Fig : 7.5 *Time response of the developed sensor for (a) cyclic humidity perturbations, (b) single cycle, (c) humidification and (d) dehumidification.*

in Fig. 7.4(a), whereas Fig. 7.4(b) depicts a zoomed-in response for a single cycle. As can be observed, fiber output intensity instantly and smoothly changes during forward and reverse humidity cycles without any hysteresis, reflecting completely reversible response of the proposed sensor. Enlarged views of the response in Fig. 7.4(c) and Fig. 7.4(d) of a single cycle in Fig. 7.4(b) show an extraordinarily sharp rise-time (50ms) during humidification and quick fall-time (65ms) during dehumidification. Identical rise and fall times are observed for other cycles too. The ultrafast response of the developed sensor is mainly attributed to the hydrophilic nature of GO film, order of the penetration depth of the evanescent wave in the sensing region and the thickness of the sensing film. To consolidate the hydrophilicity characteristics, contact angle (CA) measurements were performed using drop shape analysis for GO film at room temperature and 25%RH. As depicted in Fig. 7.4, observed forward and backward CAs for GO sensing film are observed to be 45.6° and 45.41°. The low contact angles indicate absorption of water molecules within a fast response time (resulting in larger spread of water) and hence, a better hydrophilicity for this case.

Table 7.1 : *Comparison of Dynamic range, Response time and Recovery time of Proposed sensor with Other Reported Sensors.*

Author & Ref.	Sensing element	Dynamic range (%RH)	Response (s)	Recovery (s)
Li *et al.*, 2017 [106]	SP-SMF	40–85	0.85 (47–73%RH)	0.85
Syuhada *et al.*, 2021 [107]	Taper fiber	20–99	147 (20–99%RH)	293
Gomez *et al.*, 2018 [36]	Straight POF	10–75	1.5 (10–90%RH)	-
Zhong, *et al.*, 2020 [38]	U bend POF	10–90	145 (10–90%RH)	155
Wu *et al.*, 2020 [113]	FBG	35–95	174 (11–60%RH)	231
Shao *et al.*, 2021 [71]	PCF	30–90	0.4 (30–90%RH)	0.2
Xu *et al.*, 2023 [70]	MI	25–90	0.097 (10–90%RH)	1
Gao *et al.*, 2016 [69]	rGO HCF	60–90	5.2 (10–90%RH)	8.1
This work	RFMCD MMF	3–94	0.050 (5-83%RH)	0.065

For detailed comparative analysis, Table 7.2 presents response time, recovery time and the dynamic range of various sensors that employ different sensing schemes and having linear response over the observed dynamic range. As can be observed from the Table 7.2 and to the best of author's knowledge, in comparison to all other sensors employing various sensing schemes, proposed sensor brilliantly surpasses all, and stands out with its outstanding ultrafast response and recovery times over the maximum width of dynamic range (~80%RH) reported in the literature.

Stability, repeatability and reliability are other critical parameters for RH detection. Rigorous analysis was carried out to examine short-term and long-term performance of the

proposed sensor. For analysing short-term response, sensor was exposed for about 30 minutes at RH levels, once stabilized at three typical values: 15%RH (low), 40%RH (medium) and 87%RH (high). The standard deviations of normalized intensity are observed to be $\pm 4.84\times10^{-4}$, $\pm 4.14\times10^{-4}$ and $\pm 5.57\times10^{-4}$, respectively, at 15%RH, 40%RH and 87%RH levels. Hence, maximum resolution of the sensor for RH detection is observed to be ±0.049%RH, which validates the excellent stability and accuracy of RH detection. For analysing long-term response, experiments were repeated on four different days with an interval of 3, 5 and 4 days, thus spanning a total of 16 days. These experiments were performed at three different RH levels (18%, 55% and 80%RH). Peak intensities of fiber sensor output spectra are depicted in Fig.7.5. Compared to day one, maximum variation in normalized output of the proposed sensor is observed to be less than 0.8% at all the three RH levels. This shows the excellent repeatability and reliability of the developed optical fiber humidity sensor. Thus, the reported sensor employing intensity modulation through evanescent wave absorption facilitated by thin GO sensing film synthesized over a short length of centrally decladded

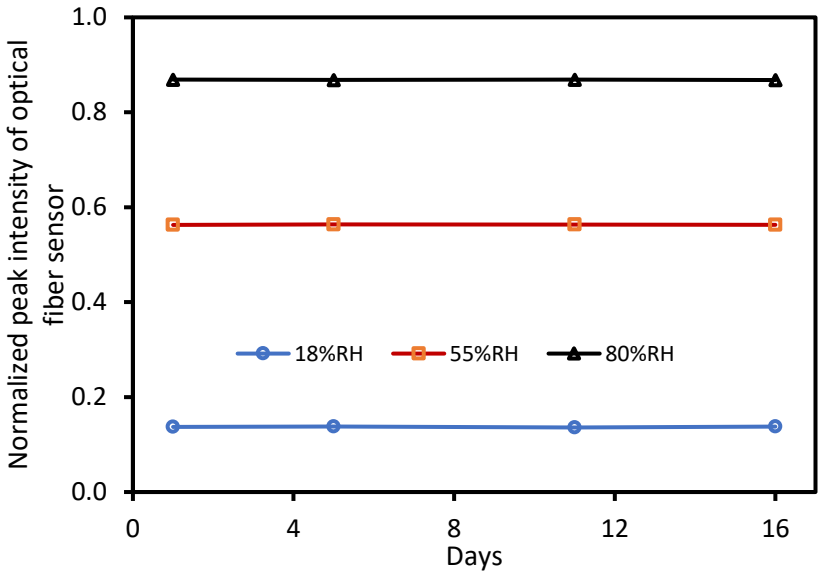

Fig 7.6 : *Repeatability and reliability test: Fiber sensor output on four different days at 18%, 55%, and 80% RH.*

reduced-to-few-micron straight and uniform core of multimode optical fiber and having an ultrafast, reliable, repeatable, and linear response achieved over almost the widest possible dynamic range with optimum sensitivity is of great importance for real-field applications where dynamic and rapid evolution of ambient humidity perturbations is required to be monitored in real-time basis.

7.4 Conclusion

In conclusion, a simple optical fiber humidity sensor employing evanescent-wave modulation through GO immobilized thin sensing film over a reduced-to-few-micron straight and uniform decladded core of PCS multimode optical fiber is presented for the first time to the best of author's knowledge in this work. Rigorous experimental investigations show that the proposed sensor has a throughout linear response over the dynamic range as wide as 3%–94%RH with a relatively high sensitivity of $0.0115RH^{-1}$ and linearity of 0.9949. Importantly, sensor is observed to be ultrafast, having response time as low as 50ms and recovery time as low as 65ms, which are observed for the first time to the best of author's knowledge. Additionally, an excellent accuracy of RH detection for the proposed sensor is established by the observed maximum resolution of ±0.049%RH. Further, the proposed sensor is observed to be highly reversible, stable, repeatable and reliable. This is also reflected from the long-term performance characteristics of the sensor that establishes a maximum variation of less than 0.8% in the peak intensity of output spectra over a duration of 16 days. Hence, the proposed sensor is of great importance in monitoring dynamic and rapid evolution of ambient humidity perturbations. Though this sensor is well suited for real-time breath monitoring and voice print recognition, however fixing it inside the testing wearable mask that covers nose and mouth both, required special and complex packaging of sensor. Hence, research is further extended to develop another optical fiber sensor as discussed in Chapter 8.

Chapter 8 : Highly sensitive biodegradable polymer-based novel optical fiber humidity sensor for human breath monitoring voiceprint recognition

8.1 Introduction

Humidity in exhaled breath can offer crucial insights into health conditions associated with the early stages of heart attacks, asphyxia, anxiety, and epilepsy. Furthermore, harnessing humidity data from exhaled air for human voice or speech recognition can be a valuable tool in enhancing security measures, especially in preventing security breaches involving the use of pre-recorded voices [2]. Most of the sensors used for breath monitoring and voice recognition are electronic, typically relying on resistive or capacitance-based mechanisms. However, these electronic sensors have their limitations, including instability and potential safety concerns when used in environments such as magnetic resonance imaging (MRI) procedures or oncological treatments involving radiation and powerful electric or magnetic fields [2]. Additionally, electronic humidity sensors often lack the capability for remote sensing, distributed sensing, and multiplexing. Optical fiber sensors offer a promising solution to address these limitations due to their unique properties, including high sensitivity, ease of miniaturization, immunity to electromagnetic interference, and the ability to perform multiplexing and remote sensing. The optical fiber RH sensor reported in Chapter 7 shows an ultrafast response over a wide dynamic range with high sensitivity and, hence, is highly advantageous for real time humidity detection in diverse applications. This sensor is well suited for real time breath monitoring and voice print recognition, however fixing it into the testing wearable mask, which covers both the nose and mouth, required a complex and specialized packaging of the sensor. Hence, one requires a simple sensor that carries the excellent features of the sensor, proposed in the previously chapter. This motivated to develop another novel optical fiber RH sensor in this part of the research.

Polyhydroxybutyrate (PHB) is a biodegradable polyester with properties like traditional plastics but with the added benefit of being environmentally friendly. It can be synthesized by numerous micro-organisms as a form of energy storage, making it a promising candidate for sustainable materials. PHB is composed of repeating units of 3-hydroxybutyrate (3HB)

monomers, linked by ester bonds. Its chemical structure grants it both biodegradability and biocompatibility, making it suitable for a variety of applications in industries ranging from packaging to sensing [114], [115]. Research described in this chapter aims to develop a simple optical fiber RH sensor, especially for breath monitoring and voice recognition that possibly retains excellent response characteristics as achieved in the previous chapter. The sensor developed in this part of the research, exploits polyhydroxybutarate-doped polyvinyl alcohol (PHB doped PVA) as a humidity sensing agent synthesized onto the centrally decladded fiber, a novel approach for the development of a humidity sensor. where biodegradable polymer polyhydroxy butyrate (PHB) immobilized PVA sensing cladding over centrally decladded fiber is employed to design and develop RH sensor. To the best of the author's knowledge, PHB is used for the first time to develop an optical fiber humidity sensor. Experimental results show that the proposed sensor exhibits very fast response over the linear humidity range of 58-98%RH with a very high sensitivity of 66 mV/%RH. This high sensitivity achieved in the higher dynamic range (58-98%RH) is highly advantageous for real-time humidity detection in diverse applications, including breath monitoring and non-contact humidity sensing. Furthermore, the experiment for breath monitoring and voice recognition is also conducted successfully. Results demonstrate that the proposed sensor not only effectively monitors respiration under various conditions but also detects variations in voice tone due to variations in exhaled humidity levels.

8.2 Experiment

8.2.1 Synthesis of polyhydrxybutarate (PHB)

Axenic culture of cyanobacteria *Chlorogloea fritschii* TISTR 8527 was obtained from the Thailand Institute of Scientific and Technological Research. The inoculum was prepared in a 250 mL shake flask with 150 mL of modified BG-11 medium with a pH of 7.5 [116]. The experiment was performed in a 500 mL flask containing 300 mL of a culture medium. The culture was mixed with sparging air using a silicone rubber sparger with pinholes. The culture was inoculated with 5% (v/v) of the inoculum. An illumination of a cool white LED of 100 $\mu M/m^2s$ was used with 12:12 h light and dark period at room temperature. Induction of the polyhydroxybutyrate (PHB) was done with 0.2% (w/v) acetate at dark conditions after the culture reached the stationary phase. The culture was harvested by centrifugation, and the pellet was lyophilized and stored for further use. The biomass was treated with hypochlorite at 37° C for 1 hour. Afterwards, the pellet was washed with water,

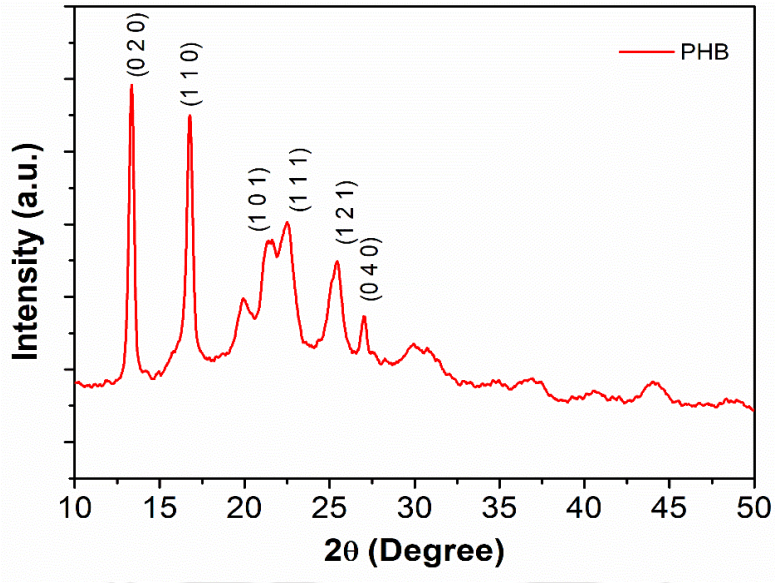

Fig 8.1 : *XRD of polyhydrxobutarate (PHB).*

Which was followed by washing with acetone and ethanol. The PHB is extracted from the pellet using boiling chloroform and is filtered to remove cell debris. The polymer was recovered by evaporation of chloroform and dried at room temperature [117].

8.2.2 Characterization of polyhydrxybutarate (PHB)

X-ray diffractometer (XRD, Rigaku TTRAX III) in Bragg– Brentano geometry, operating at 5 kW with Cu-Kα radiation (λ = 1.5406Å), is used for the structural characterization of PHB at room temperature. XRD spectra are measured in the range of 2θ from 10° to 50°. Fig 8.1 shows the XRD spectra of pressed PHB. Diffraction peaks appeared at 2θ = 13°, 16°, 21°, 22°, 25°, and 27°. These peaks correspond to (020), (110), (101), (111), (121) and (040) planes. The two most intense and significant scattering peaks observed at 13° and 16° indicate the presence of an orthorhombic unit cell. The two relatively minor peaks observed at 25° and 27° correspond to α-PHB crystal. The other two minor peaks observed at 25° and 27° indicate partial crystalline nature of PHB [118].

8.2.3 Sensing probe preparation

A piece of plastic cladding silica fiber (PCS) having a core diameter of 125µm and length of 50cm (125/380T, Ceramoptec) was used for sensing probe preparation. The fiber ends were prepared properly to ensure optimal power coupling. After that, 5 cm of cladding from the central region of a 50 cm long PCS fiber was removed. The decladded portion was cleaned and coated with polyhydroxybutyrate (PHB purchased from Sigma Aldrich) doped polyvinyl alcohol (PVA) solution using the dip coating method. The PHB-doped PVA solution was

prepared by mixing 10 mg of PHB powder in 20 ml of 0.25% (W/V) PVA solution. The prepared sensing probe was then dried at room temperature of 110°C for 2 hours. Surface morphology, microstructure, and the thickness of deposited film were examined by FESEM.

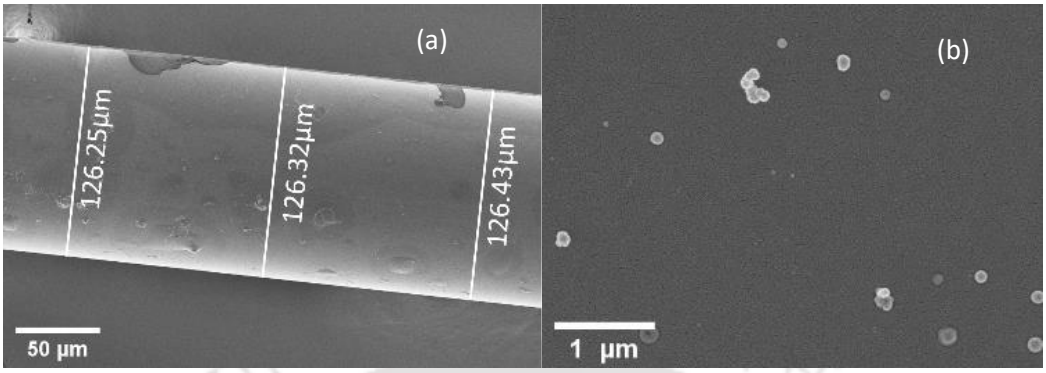

Fig 8.2 : *(a) FESEM pic of PHB doped PVA coated fiber (b) FESEM pattern of surface morphology of the sensing region*

Fig 8.2(a) depicts an image of the 6-dip coated region of the optical fiber. The average diameter in this region for 6-dip coating is observed to be 126.33µm. This establishes an average thickness of 0.67µm for the sensing film. The surface morphology of the deposited sensing film is depicted in Fig 8.2(b), which shows an interconnected high-quality porous structure with moderate roughness.

8.2.4 Charecterization of the sensor

Similar procedure as explained in chapter 2, was fallowed to characterized the sensor.

8.3 Result and discussion

8.3.1 Response of BHB based Sensor

The sensor operates on the principle of intensity modulation via evanescent wave (EW), where optical power in the cladding region interacts with the PVA-doped polyhydroxy butyrate (PHB) sensing thin film. Rigorous investigations were carried out by repeat set of experiments in order to establish the response characteristics of the proposed sensor. Data were recorded until the stabilization of humidity inside the humidity chamber. Fig 8.3 (a) illustrates the characteristic response of the optical fiber relative humidity (RH) sensor with

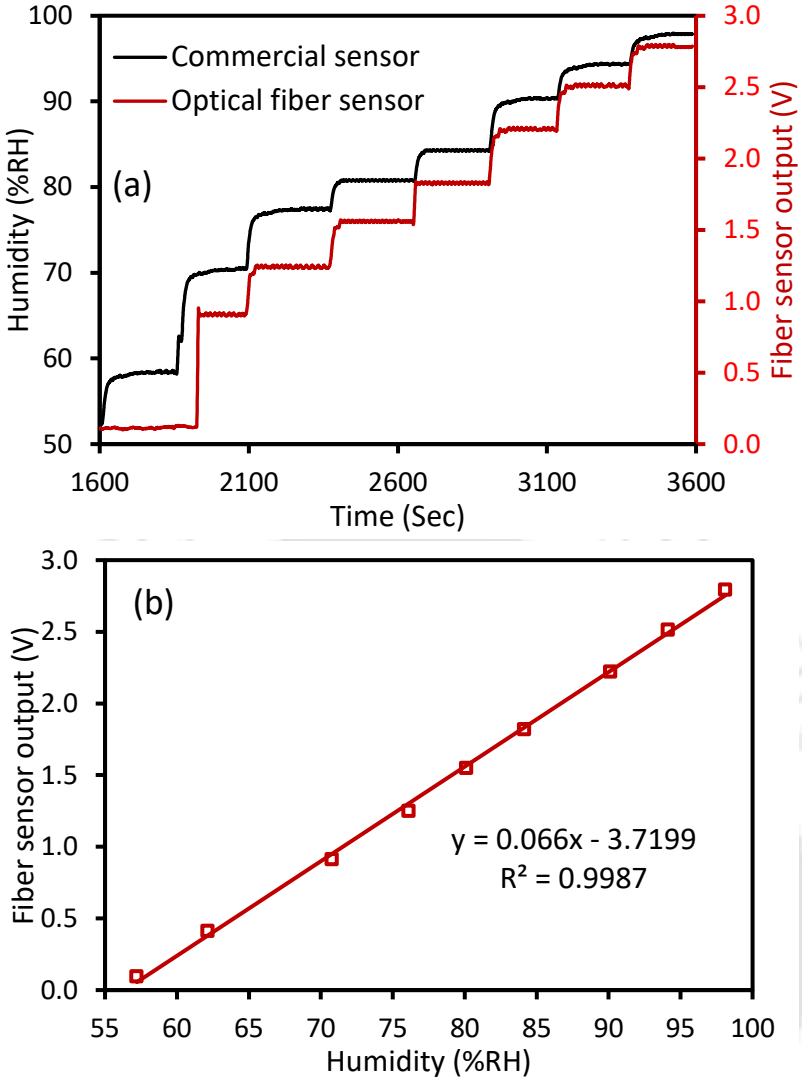

Fig 8.3 : *(a) Time response behaviour of humidity sensor against cyclic humidity. (b) Experimentally observed sensor response.*

6-dip film thickness. A similar qualitative response was observed while decreasing the humidity. The time response of the sensor reveals an increase in the fiber sensor output as the relative humidity (RH) increases inside the chamber. This is attributed to the optical and physical properties of immobilized PHB and PVA. From the perspective of fiber optics, power of the guided modes is tightly confined within the core when the sensor is exposed to high RH values. At low RH values, however, guided power leaks out through the leaky modes in the sensing region. Thus, at low RH values, less power reaches at the output end of the fiber; whereas, at high RH values more power reaches the output end of the fiber. In order to get deeper insight, the fiber sensor's output is plotted against %RH in Fig. 8.3(b). As can be observed, the proposed sensor responds linearly to the applied RH perturbations over the dynamic range of 58-98%RH with a sensitivity of 66mV/%RH.

Next, the dynamic performance of the fiber sensor was examined by subjecting it to repeated and rapid changes in relative humidity (RH) between 55% and 98%. To achieve this, the humidity chamber was initially dried to 55% RH and then quickly humidified to 98% RH by passing air from the mouth through the pipe into the chamber. The time response of the sensor is illustrated in Fig. 8.4. The optical fiber sensor output shows an instant and smooth change during forward (55% RH to 98% RH) and the reverse (98% RH to 55% RH) cycles of humidity change. Also, the fiber output is observed to be extraordinarily identical at extreme RH values during humidification and desiccation cycles. This shows a highly reversible and repeatable nature of the proposed sensor. An average response and recovery time of 0.0125s are observed for the developed sensor.

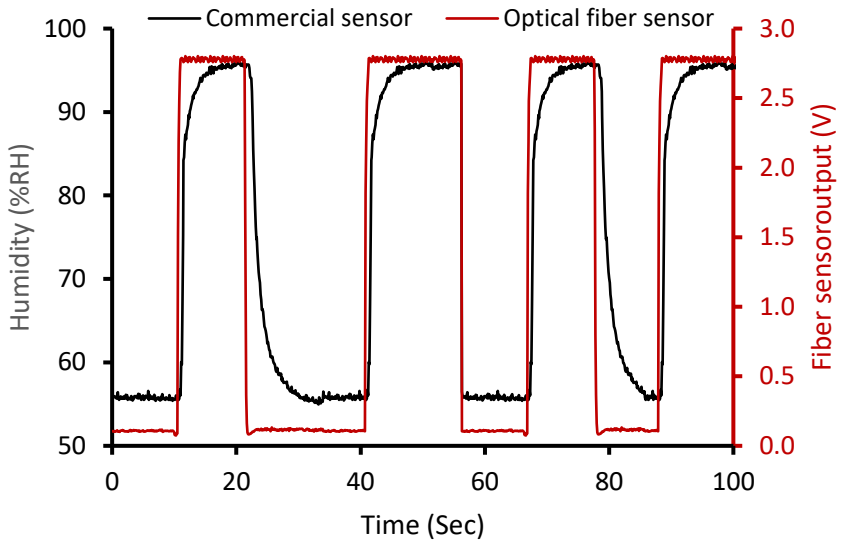

Fig 8.4 : *Time response behaviour of humidity sensor against cyclic humidity.*

Stability, repeatability and reliability are other critical parameters for RH detection. Rigorous analysis was carried out to examine short-term and long-term performance of the proposed sensor. For analyzing short-term response, the sensor was exposed to approximately 30 minutes at three typical RH values: 62%RH, 84%RH, and 94%RH. The results obtained from these tests are presented in Fig 8.5 (a). The standard deviations of intensity are observed to be ±3.44mV, ±5.47mV, and ±0.29mV, respectively, for the 62%RH, 84%RH, and 94%RH

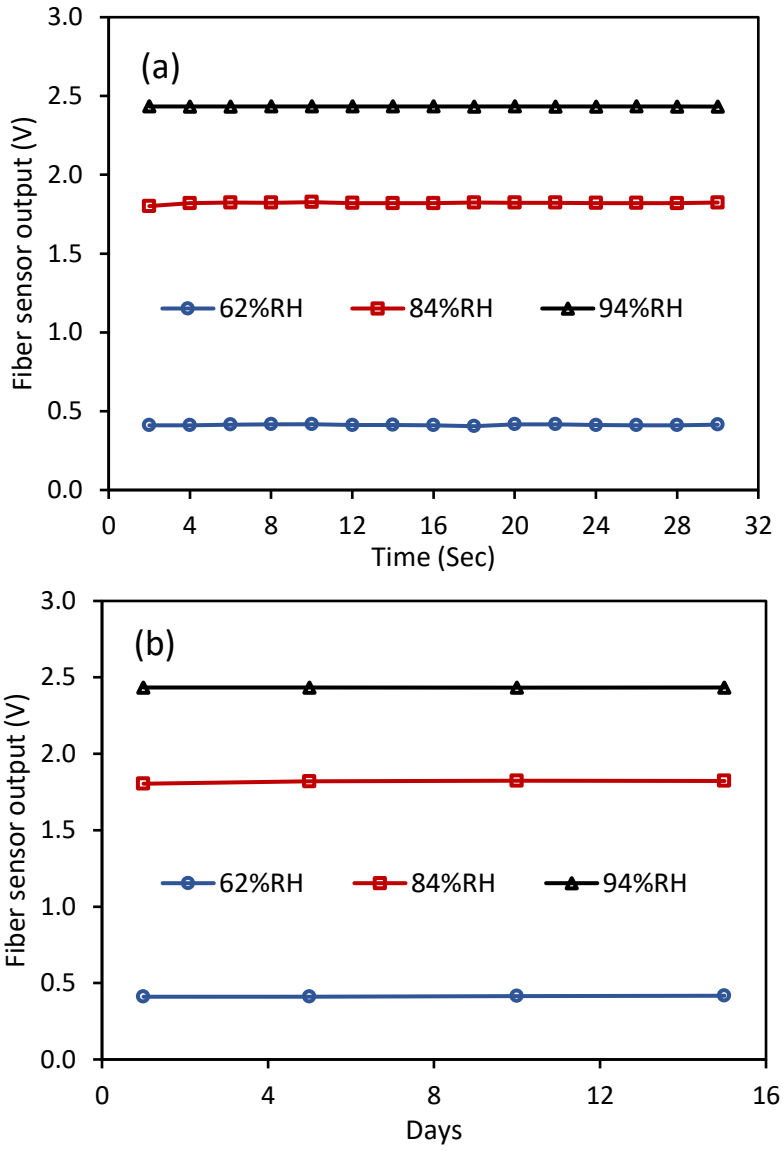

Fig 8.5 : *(a) Short-term stability (b) Long-term stability, repeatability, and reliability test: Fiber sensor output on the three different days, each at an interval of 4, 5, and 5 days for 62%, 84% and 94%RH.*

levels. Therefore, the sensor demonstrates a maximum resolution for RH detection of ±0.0818%RH, affirming its excellent stability and accuracy in RH detection. For analyzing long-term response, experiments were repeated on four different days with an interval of 4, 5 and 5 days, thus spanning a total of 15 days. The experiment was performed at three different relative humidity levels (62%RH, 84%RH and 94%RH). The results from these tests are depicted in Fig 8.5 (b). Remarkably, the maximum variation in the output of the optical fiber sensor, compared to the initial measurement on day one, is observed to be impressively low at ±0.5% for all three %RH levels. This shows the exceptional reliability and

repeatability demonstrated by the developed sensor. Consequently, the outstanding performance of the proposed sensor, which utilizes a straight and uniform optical fiber and is based on the PHB doped PVA film, hold significant importance for practical real-field applications.

8.3.2 Breath monitoring voiceprint recognition

Real-time respiratory monitoring of patients is a vital aspect of modern healthcare. This monitoring approach enhances patient safety, facilitates early diagnosis of respiratory conditions, and optimizes treatment plans. The PHB-based optical fiber sensor demonstrates remarkably fast response and recovery characteristics, along with excellent long-term stability when operating within a high humidity range of 58–98% RH. Consequently, the PHB-based optical fiber sensor proves highly advantageous for real-time humidity detection in diverse applications, including breath monitoring and non-contact humidity sensing. For breath monitoring, a new (but having identical film configuration) 2.5cm long sensing probe is developed and fixed in a nebulizer mask as shown in Fig 8.6 (a). The schematic diagram of the experiment

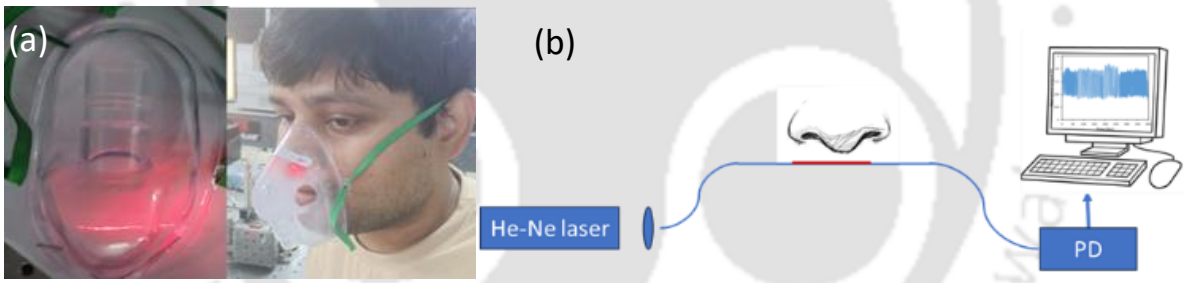

Fig 8.6 : *(a) Sensor in nebulizer mask (b) Experimental setup for breath monitoring.*

used for breath monitoring is shown in Fig 8.6 (b). The light from He-Ne laser is launched from one end of the sensor, and another end of the sensor is connected to the photodetector. The sensor's output intensity is continuously measured throughout the breath cycle at intervals of 10ms. During nose-breathing, the exhaled air typically contains nearly saturated humidity, while the inhaled air is relatively dry. This cyclic variation in humidity surrounding the sensor is detected through the output intensity variation. Fig 8.7 (a) depicts the intensity

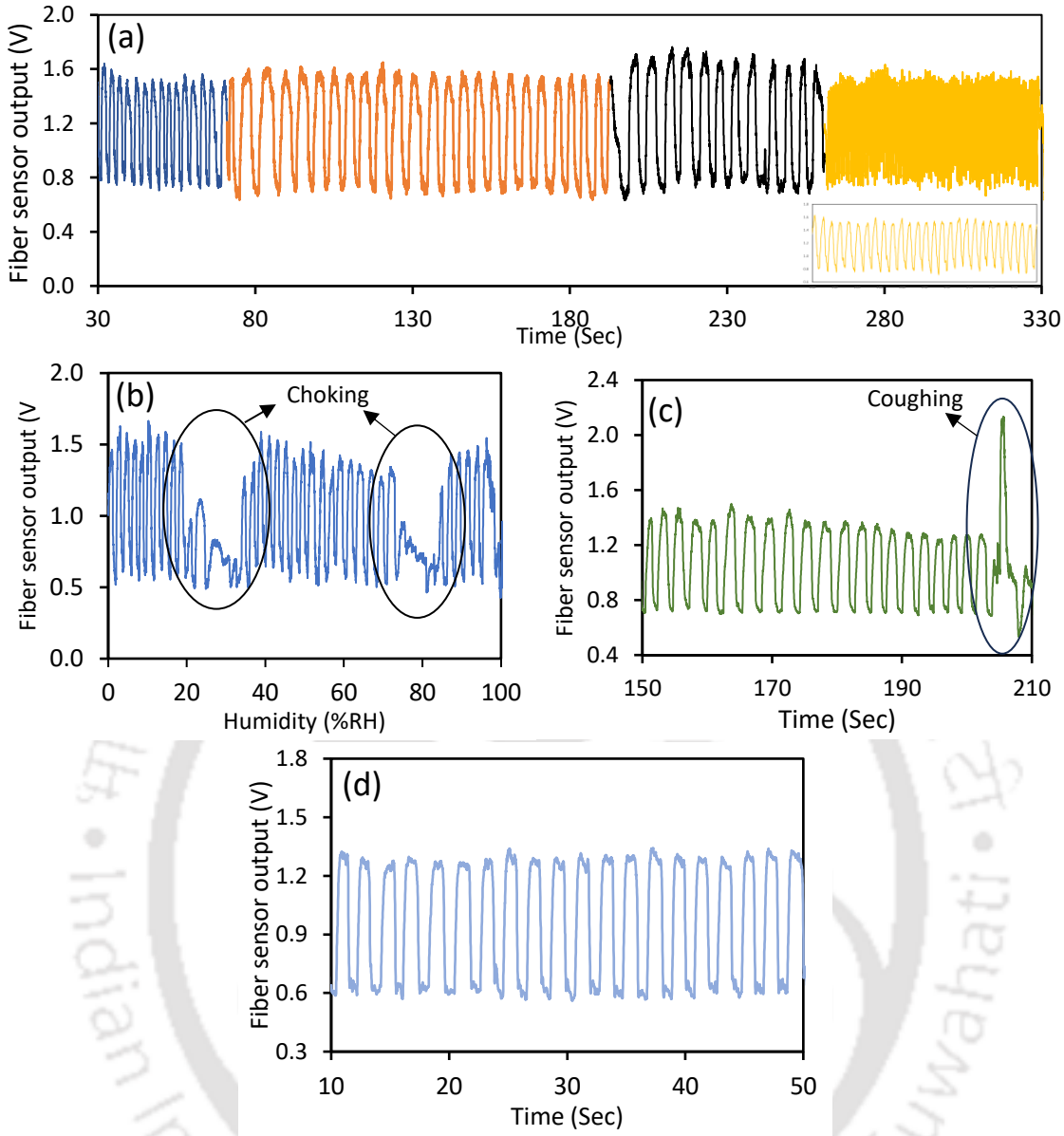

Fig 8.7 : *(a) Response of this sensor under various breaths for 30-year-old man (b) Sensor response during choking (c) Response of the sensor for 80-year-old man (d) Response of the sensor for 5-year-old kid under normal breath.*

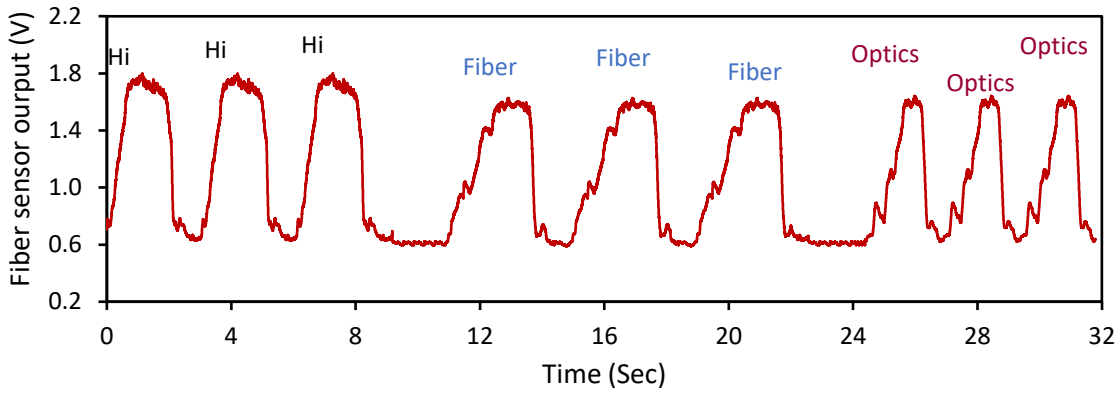

Fig 8.8 : *Response of the sensor for the words Hi, Fiber and Optics.*

variation of fiber sensor output for the 31-year-old male participant during various normal, deep, mouth, and fast breaths, respectively. In addition, response of the sensor was investigated during the instances of choking, and in capturing breath patterns of na 80-year-old man and a five-year-old child. Captured responses of the sensor during breath monitoring are depicted in Fig 8.7 (b), (c), and (d). These results highlight the sensor's ability to monitor various breath types accurately. When we engage in speaking, alterations in humidity occur around the mouth, aligning with the patterns of speech. Consequently, it becomes possible to identify the voiceprint of an individual by analysing the fluctuations in relative humidity during the speech. Owing to high sensitivity and fast response, the developed sensor possesses significant potential for detecting fluctuations in humidity during diverse speaking scenarios. Fig 8.8 illustrates the sensor response when a person speaks words such as hi, fiber, and optics. The sensor's remarkable capability to identify human speech is highlighted when speaking. Therefore, the integration of the proposed sensor with conventional breath monitoring and speech recognition systems offers a considerably enhanced method for secure voice authentication for personal identification.

8.4 Conclusion

An optical fiber humidity sensor based on EW intensity modulation employing PVA-doped polyhydroxy butyrate (PHB) is successfully developed. proposed sensor exhibits a linear response over the dynamic range of 58-98%RH, with a sensitivity of $0.0236RH^{-1}$. A very fast response and recovery time of 0.0125s is observed during humidification as well as desiccation. The proposed sensor is also tested for the real-time breath monitoring and speech recognition. From the result, it can be concluded that the proposed sensor not only measures various breath types accurately but also provides accurate information about respiratory rate, respiratory depth, and exhaled air humidity.

Chapter 9 : Biowaste (ash from menthol boiling plant) based highly sensitive novel optical fiber humidity sensor having large dynamic range

9.1 Introduction

The last chapter describes the development and experimental investigations of optical fiber RH sensors based on intensity modulation via evanescent wave absorption employing PHB biopolymer. A good linear sensitivity with a very fast response and recovery time are achieved. In order to investigate further optimization possibilities and to make a comparative study, an out-of-box and novel idea of using a bio west (Ash from menthol boiling plant) to develop optical fiber is executed and the related research work is reported in this chapter. Ash is used, for the first time to the best of author's knowledge, to develop RH sensor. From XRD analysis, it is established that the ash is a combination of hydroxylapatite (HAP) ($Ca_5(PO_4)_3OH$) and calcite ($CaCO_3$). The HAP is highly hydrophilic due to the abundance of ion such as Ca^{2+}, PO_4^{3-} and OH^- [119]. On the other hand, Calcite ($CaCO_3$) is also a hydrophilic material [120]. Hence, ash is expected to be more hydrophobic than hydroxylapatite and calcite spritely. To realize the sensor, ash is chemically coated over the 5cm centrally decladded PCS fiber. Experimental investigation establishes the breakthrough in using ash-immobilized cladding onto the decladded optical fiber as the RH sensing cladding. The proposed sensor exhibits linear response over 4%-90%RH with an optimum sensitivity of 9.8mV/%RH ($0.0076RH^{-1}$). For the dynamic performance (time-response), the optimized sensing probe is subjected to rapid cyclic relative humidity (RH) change from 3% RH to 80% RH. Average response and recovery time of 0.011s and 0.012s, respectively, are observed for the proposed sensor. Further, the sensor is tested for short-term and long-term stability performance. A maximum standard deviation of ±3.65 mV is observed during the short-term stability test, that gives rise to the maximum resolution of ±0.37%RH. Maximum variation of the sensor output is observed to be less than 0.27% during the long-term stability test. This shows the excellent reliability and repeatability of the developed sensor.

9.2 Experiment

9.2.1 Ash processing

For the development of the sensor, ash collected from a menthol-boiling plant was processed. For the processing of ash, big grain was removed by filtering it with a fine mesh. After that, ash was dissolved in a mixture of ethanol and DI water in a ratio of 1:1. Subsequently, the mixture was sonicated for 20h. Then the solution was filtered and dried at 100ºC for 6hrs in an oven to get the desired powder of ash.

9.2.2 Characterization of Ash

X-ray diffractometer (XRD, Rigaku TTRAX III) in Bragg– Brentano geometry, operating at 5 kW with Cu-K_α radiation (λ=1.5406Å), was used for the structural characterization of ash at room temperature. XRD spectra are measured in the range of 2θ from 5° to 60°. Figure 9.1(a) shows the XRD spectra of pressed ash. The room temperature XRD pattern shows reflection from the crystalline hydroxylapatite (HAP) phase ($Ca_5(PO_4)_3OH$) [121] along with a small amount of Calcite phase ($CaCO_3$). The strong presence of the most intense (211) peak at 2θ~31.84° along with the reflections (300),

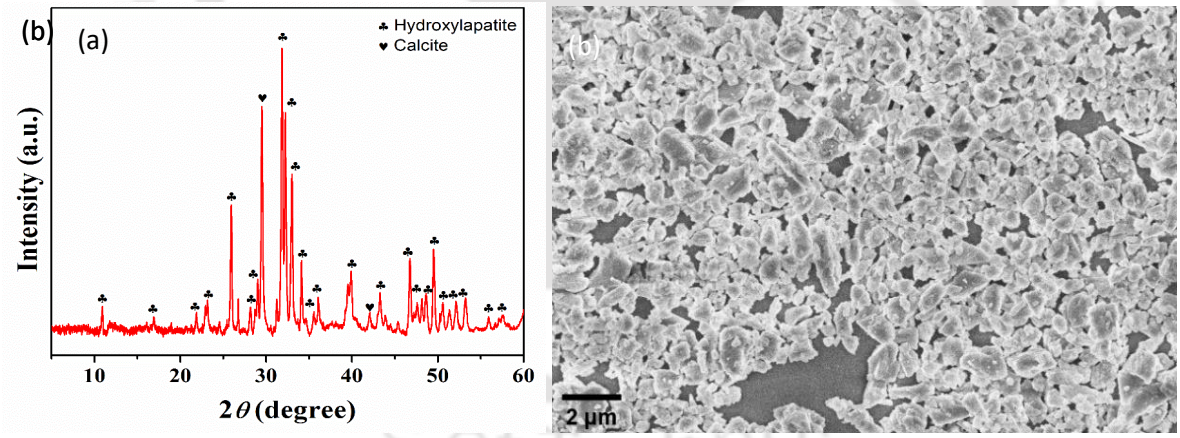

Fig 9.1 : *(a) XRD of processed Ash (b) FESEM picture of Ash.*

(202), and (002) peaks at 2θ~32.24°, 32.98°, and 25.94° confirm the presence of the HAP phase; whereas the presence of peaks at 2θ~32.24° and 42.06° support the presence of small amount of calcite phase [122] in the room temperature XRD pattern. The HAP phase is indexed to a hexagonal phase (s.g. No.- 176) with a lattice parameter $a = b = 9.39685$ Å, and $c = 6.86403$ Å. Whereas, the calcite phase is indexed to a trigonal phase (s.g. No.- 167) with lattice

parameters $a = b = 4.9830$ Å and $c = 17.0190$ Å. A picture of processed ash powder in FESEM is shown in Fig 9.1 (b).

9.2.3 Sensing probe preparation

The proposed sensor was developed by using PCS multimode fiber having a core diameter of 125µm. A total of 50 cm length of this fiber was taken to prepare the sensor. Both ends were polished to achieve optically flat end faces in the transverse section, which is critically important for achieving maximum power coupling efficiency from the source to the fiber and the fiber to the detector. The cladding was removed from a 5 cm section in the central region of the fiber. Ash was synthesized over the decladded portion of the fiber. For this, first, a suitable ash is dispersed in acetone and then, the decladded portion of fiber was dip coated in the mixed solution. Afterwards, the coated probe was dried in the oven at a temperature of 80°C for 1h. Drying at 80°C results in the evaporation of acetone, leaving a thick ash film over the decladded portion of the fiber. The prepared sensing probe was kept in a desiccator under a partial vacuum chamber for two days to remove the trace of acetone and water from the ash film. FESEM picture of ash-coated fiber is shown in Fig 9.2.

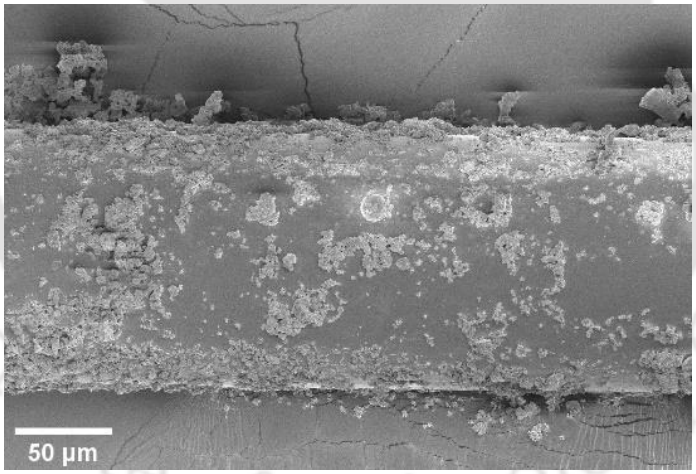

Fig 9.2 : *FESEM picture of ash-coated fiber.*

9.2.4 Characterization of sensor

Similar procedure as explained in chapter 2, was fallowed to characterized the sensor.

9.3 Result and discussion

9.3.1 Sensor response

The proposed sensor exploits the phenomenon of intensity modulation by utilizing evanescent wave interaction with ash-based sensing film positioned in the cladding of the fiber.

The sensor utilizes the easiest sensing configuration, where the sensing film is synthesized onto the centrally decladded region of a straight and uniform PCS optical fiber. For the proper experimental investigation, the developed sensing probe was characterized carefully. The

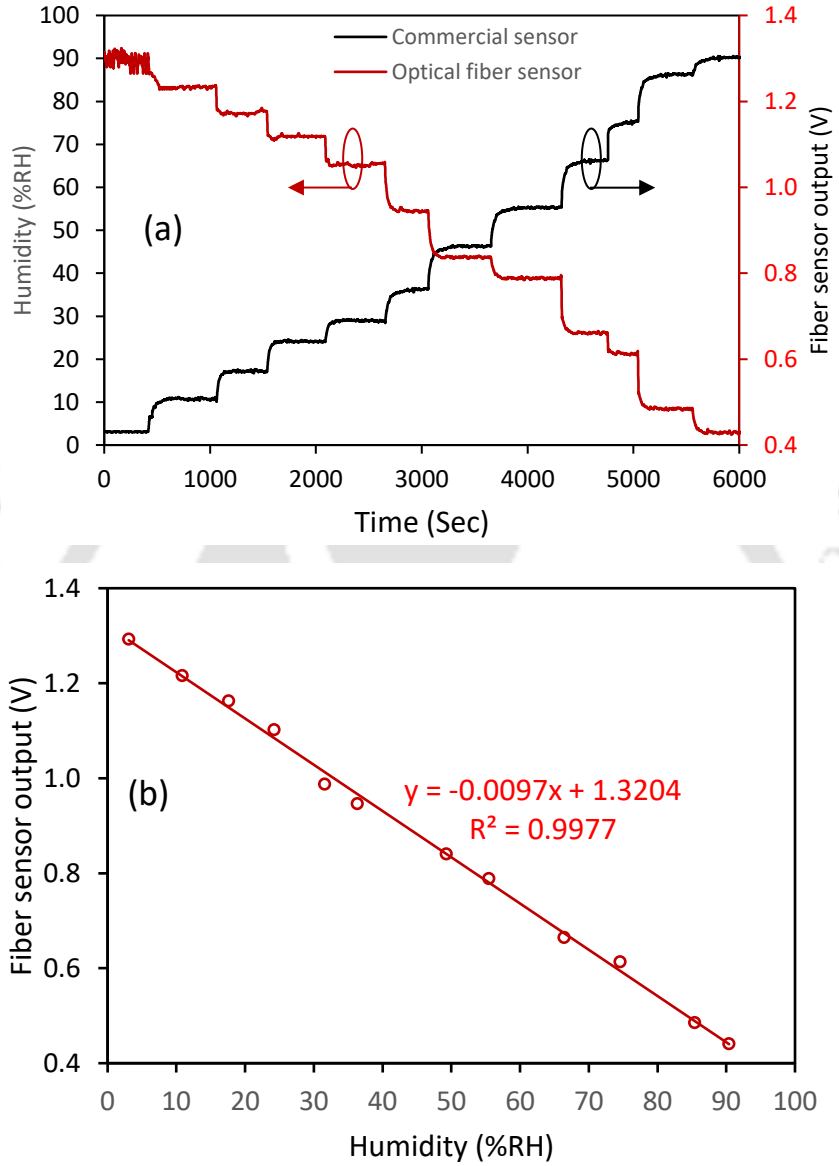

Fig 9.3 : *(a) Time variation of the commercial humidity sensor and the optical fiber RH sensor (b) Experientially observed sensor response.*

response of the optical fiber RH sensor is depicted in Fig 9.3 (a). The experiment was repeated multiple times in order to establish the sensor response. A similar qualitative response was observed when humidity decreased. The fiber sensor output decreases as the humidity increases within the chamber. The presence of water molecules in the chamber increases with humidity. Hence, with an increase in humidity, water molecules get adsorbed by ash film which increases the dielectric constant of the sensing film. This leads to a change in the refractive index in the

sensing region. Corresponding leakage of the guided power to the cladding modes results in an intensity modulation. In order to get a deeper understanding, the output of the fiber sensor is plotted against the RH in Fig. 9.3(b). It is evident from the plot that the proposed sensor demonstrates a linear response to the applied RH variations within the dynamic range of 4-90% RH. The sensitivity for humidification is observed to be 9.7 mV/%RH ($0.0075RH^{-1}$). A similar response was observed for dehumidification as well. According to XRD, ash is a combination of hydroxyapatite and calcite. Both hydroxyapatite and calcite are hydrophilic materials, and are already used for conventional humidity sensors [119], [120].

Apart from the sensitivity and the dynamic range, detection speed is also a highly critical parameter for assessing a sensor's performance. This parameter reflects the ability of the to monitor dynamic and rapid changes in ambient humidity. An RH sensor with the quickest response and recovery time, coupled with reversible response characteristics, holds significant importance. Therefore, the dynamic performance and repeatability features

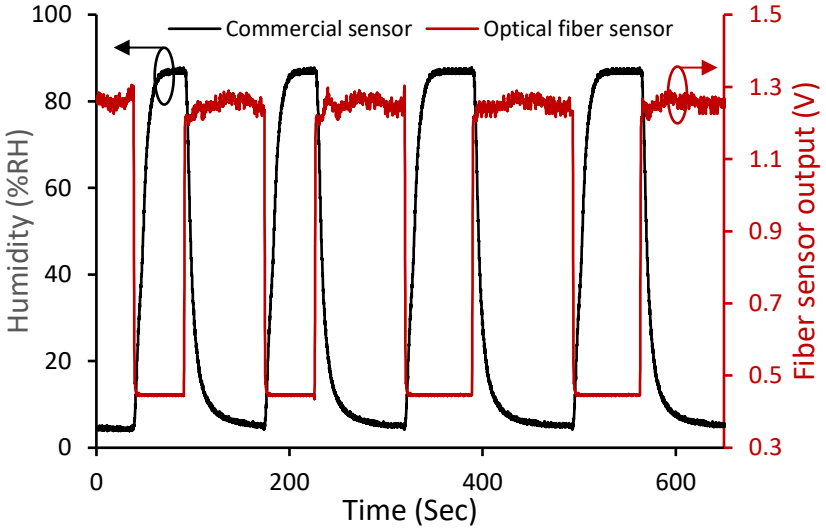

Fig 9.4 : *Response of the sensor during cyclic perturbation.*

of the proposed sensor were examined by subjecting it to rapid and cyclic RH step changes between minimum (6%RH) and maximum (86%RH) humidity values. The observed response is depicted in Fig 9.4. The output of the proposed sensor exhibits nearly instantaneous and smooth changes during both the forward (6%RH to 86%RH) and the reverse (86%RH to 6%RH) cycles of humidity fluctuations. The time response of the optical fiber sensor remains nearly identical during both humidification and dehumidification processes. This shows the highly repeatable and reversible nature of the proposed sensor. From Fig 9.4, it is observed that the average response time during humidification is 0.0132s, and the recovery time during

desiccation processes is 0.014s. These times are significantly lower than the response time of commercial sensors.

Finally, short-term and long-term stability tests were conducted to thoroughly analyze the sensor's performance. In order to analyze the short-term response, the sensor was exposed for 30 minutes at three different relative humidity (RH) levels: 42% RH, 65% RH, and 80% RH. The observed standard deviations of normalized intensity were approximately ±2.01 mV, ±3.6mV, and ±1.46mV, respectively, at the 42% RH, 56% RH, and 80% RH levels respectively. Therefore, the maximum resolution of the sensor for RH detection is observed to be

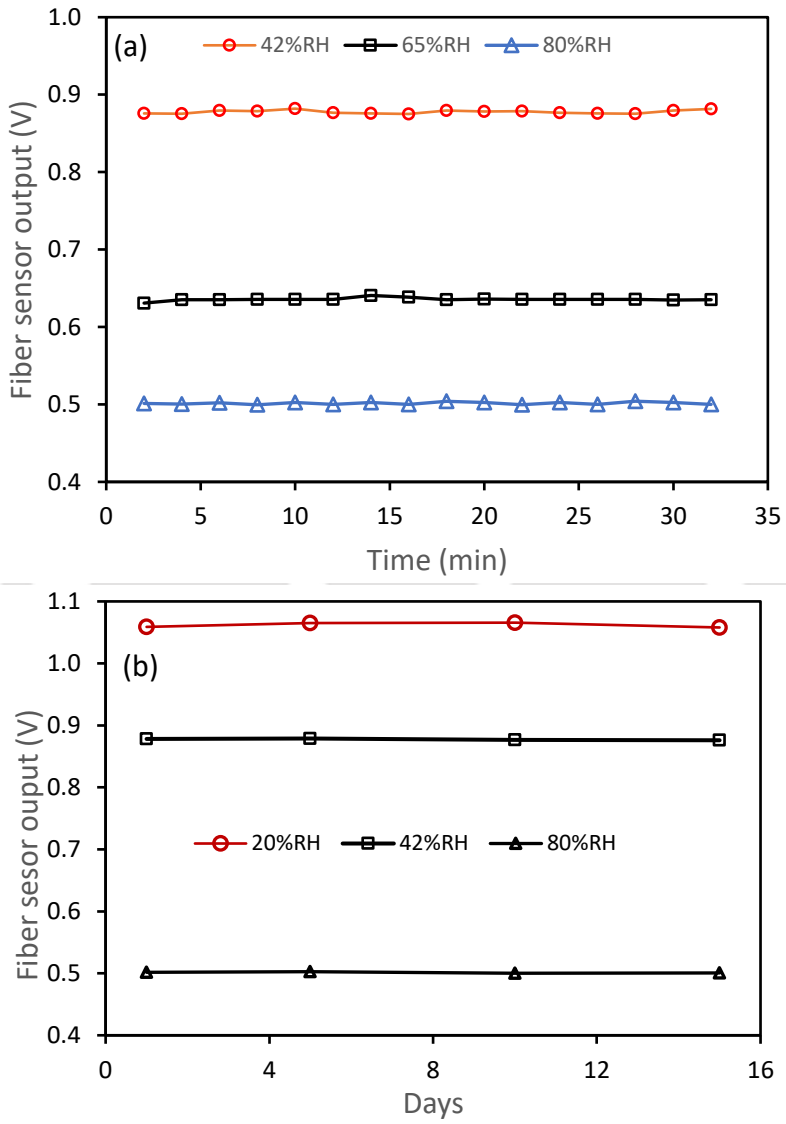

Fig 9.5 : *(a) Short term stability test (b) Long-term stability, repeatability, and reliability test: Fiber sensor output on the three different days, each at an interval of 4, 5, and 5 days for 20%, 42% and 80%RH.*

approximately ±0.37% RH. This validates the sensor's excellent stability and accuracy of RH detection. Experiments with the same sensing optical fiber probe were repeated for the long-term stability test at intervals of 4, 5, and 5 days. A total of four sets of repeated experiments were conducted on four different days over a span of 15 days. Fiber sensor outputs corresponding to the three different humidity values (25%, 55%, and 85% RH) is

shown in Fig. 9.5 (b), as an example. From the figure, it can be observed that the sensor output remains nearly constant over a period of 15 days. Maximum variation in the optical fiber sensor output, relative to day 1, at the three different humidity values is observed to be approximately ±0.27%. This demonstrates the exceptional reliability and repeatability of the reported sensor.

9.3.2 Breath monitoring and voice print recognition

Fiber RH sensors hold significant applications in human respiration monitoring. Human respiration, being one of the most critical physiological functions, offers valuable insights into heart [123] and lung conditions. The ash-based optical fiber sensor offers rapid response and long-term stability and operates effectively in humidity (2–90% RH), making it ideal for breath monitoring and humidity sensing. As discussed in the previous chapter, a new sensing probe with a length of 2.5 cm is developed and integrated into the nebulizer mask. The experimental setup used in Chapter 8 is also employed for respiratory and breath monitoring. Fig 9.6 depicts the intensity variation of fiber sensor for the 31-year-old male participant during various normal, fast, mouth, and deep breaths, respectively. The sensor demonstrates its ability to monitor and differentiate the breathing rate during slow, normal, and fast breathing. The variation of RH during exhales shows a sharp drop in output intensity value and return to the ambient level during inhales. The sensor demonstrates its ability to differentiate the breathing rate during slow, normal, and fast breathing. Notably, the sensor

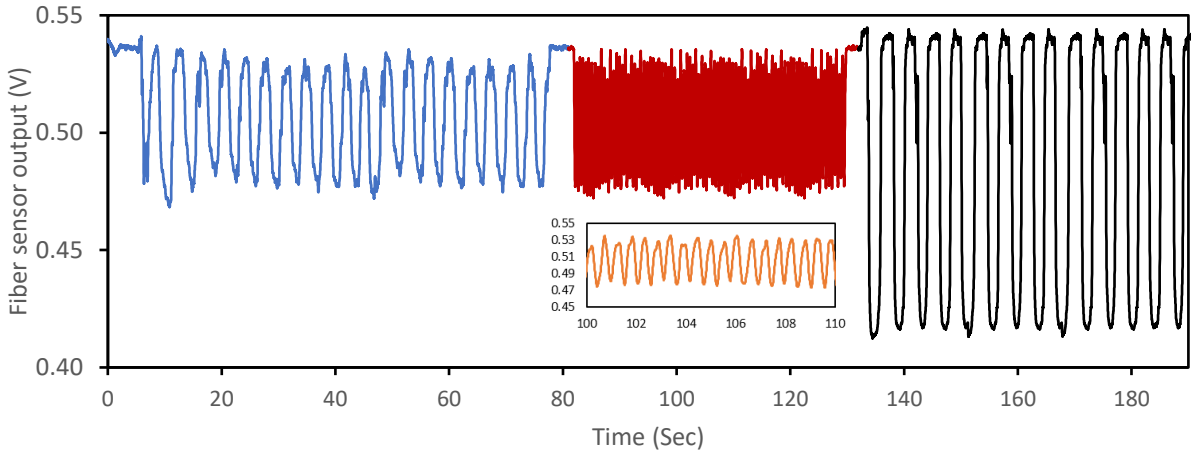

Fig 9.6 *Response of this sensor under various breaths for 30-year-old man.*

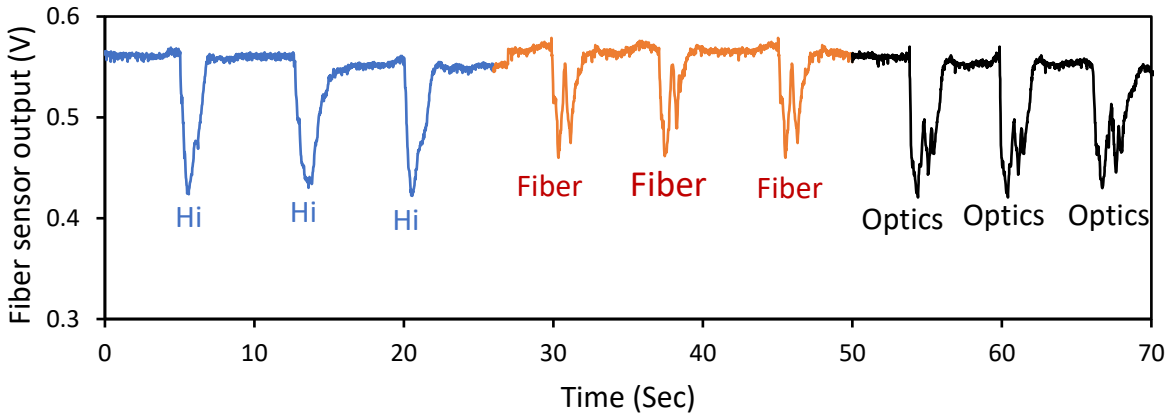

Fig 9.7 : *Detection of human voiceprints from variation in humidity during speaking.*

can also detect the depth of each kind of breath. This experimental result exhibits promising potential as a portable sensor for human respiratory monitoring systems during magnetic resonance imaging (MRI) procedures or oncological treatments. Furthermore, the developed optical fiber humidity sensor was employed to analyze variations in relative humidity (RH) during speech for the purpose of detecting human voiceprints. Fig 9.7 illustrates the sensor response when words such as hi, fiber, and optics has been spoken by 31-year-old men. From the above result, it can be concluded that the sensor demonstrates the capability to detect subtle fluctuations in humidity levels within exhaled air in real-time, particularly when speaking words, such as, "hi," "fiber," and "optics." Indeed, the uniqueness of individual voices begins deep within the lungs, where the exhaled air creates a distinct airstream. By incorporating this fundamental element, exhaled air, alongside conventional speech recognition systems, voice recognition for personal identification can significantly enhance safety in next-generation devices.

9.4 Conclusion

In conclusion, a simple and novel optical fiber humidity sensor employing biowaste (Ash) cladding over a centrally decladded region of the fiber is successfully developed. A thorough experimental study is carried out to examine the response characteristics of the proposed sensor. The fiber sensor exhibits a linear response across a wide dynamic range from 4% to 90%RH with a sensitivity of 9.7mV/%RH ($0.0075RH^{-1}$). The developed sensor demonstrates an extremely rapid response and recovery, with times recorded at 0.011s and 0.012s, respectively. This highlights the ultrafast nature of RH detection achieved by the sensor. Additionally, an excellent accuracy of RH detection for the proposed sensor is established by the observed maximum resolution of ±0.3699%RH. In addition, the sensor response is observed to be highly reversible, reliable, and repeatable. Furthermore, the developed sensor is also able to detect the humidity fluctuations in human exhaled air during various breaths and different voiceprints.

Chapter 10: Conclusion of Thesis

This thesis presents a comprehensive experimental study aimed at achieving a linear response across the widest possible dynamic range, ensuring optimal sensitivity, high resolution, ultrafast response time, and high repeatability and reliability by employing a simple optical fiber sensor configuration. The developed sensor has also been utilized for human breath monitoring and voice print recognition applications. Intensity modulation via evanescent wave (EW) is utilized to develop optical fiber relative humidity (RH) sensors, employing novel sensing configurations and designs within a very short sensing region. The responses of the developed sensors were optimized by varying chemical composition, reaction parameters, and thickness of sensing material. Further, the response characteristics such as dynamic range sensitivity, response, and recovery times were compared with the other optical fiber RH sensors reported in the literature. The first part of the research, a nanostructured GO-doped silica sol-gel film with appropriate thickness and composition is synthesized over the centrally decladded for the development of the sensor. The sensor demonstrates linear response across a wide dynamic range (15.0−95.3%RH), with optimal sensitivity (0.1036 dB/%RH). It exhibits high reversibility and stability, with average response and recovery times of 0.1436s and 0.1547s, respectively. Another optical fiber RH sensor is developed to further enhance sensitivity by incorporating reduced graphene oxide (rGO) within a sol-gel silica nanostructured film, utilizing the same fiber configuration. Optimizing the sensing cladding configuration results in an enhanced sensitivity of 56.3mV/%RH (0.1262dB/%RH) over the RH range 5-57%RH. The average response time of the sensors is 0.18s. Continuing efforts to enhance sensitivity and dynamic range led to the development of another optical fiber sensor using graphene oxide quantum dots (GQDs). The optimized GQD-based sensor enhances sensitivity, extends the linear operation range, and improves response/recovery times. It achieves a sensitivity of 0.2437 dB/%RH over a dynamic range of 4−70%RH, with average response/recovery times of 0.025s. Although sensitivity, dynamic range, and response/recovery times have improved, there is still ample opportunity to enhance the sensor's response further. Therefore, another sensor has been developed, utilizing a sensing cladding based on a GO-ZnO doped silica nanocomposite. A linear sensitivity of 33.6mV/%RH over the 17-91%RH range of linear response and response/recovery times of 0.33s and 0.45s are observed. In order to enhance

response characteristics, another optical fiber sensor is developed, incorporating a sensing cladding based on GO-ZnO-Fe nanocomposite. This sensor demonstrates a sensitivity of 60.6mV/%RH across a dynamic range of 17−80% RH, with response/recovery times of 0.031s. Therefore, the addition of Fe to the GO-ZnO nanocomposite not only enhances sensitivity but also improves response time. Further, another sensor employing an rGO-TiO_2 nanocomposite is also developed and experimentally investigated. A linear sensitivity as high as 103mV/%RH over a 3−70%RH dynamic range with recovery/response times of 0.025s are observed for this sensor. The quest to improve response/recovery times led to extending the research further. Another sensor is developed using GO-coated reduced-to-few-micron core-diameter (RFMCD) PCS multimode optical fiber. Experimental results demonstrate that the proposed sensor exhibits the widest linear dynamic range of 3−94%RH with a sensitivity of $0.0115\%RH^{-1}$. Importantly, an ultrafast response time of 50ms is achieved. To the best of the author's knowledge, such ultrafast response is achieved for the first time. While the sensor is ideal for real-time breath monitoring and voice print recognition, integrating it into a wearable mask covering both nose and mouth require careful and specialized sensor packaging. Therefore, the research extends to incorporate a biodegradable polymer, polyhydroxybutyrate (PHB), immobilized with PVA sensing cladding over the centrally decladded fiber. A sensitivity of 66mV/%RH (0.0236%RH-1) over 58−98% RH dynamic range and the response/recovery times of 0.0125s are observed for the sensor. This biodegradable polymer based optical fiber RH sensor is successfully employed for the real-time breath monitoring and voice print recognition. In the final phase of the research, biowaste (ash from a mentha oil boiling plant) is used for developing an optical fiber RH sensor. This sensor demonstrates a linear response over a broad dynamic range of 4−90%RH, boasting an optimal sensitivity of 9.7mV/%RH, with response/recovery times of 0.013s and 0.014s, respectively. It is worth mentioning that all the novel sensors developed in the research presented here exhibit high degree of reversibility, repeatability, stability.

References

[1] G. Korotcenkov, Handbook of Humidity Measurement, Volume 2: Electronic and Electrical Humidity Sensors. 2019.

[2] J. He, P. Xiao, J. Shi, Y. Liang, W. Lu, Y. Chen, W. Wang, P. Théato, S. W. Kuo, and T. Chen, High Performance Humidity Fluctuation Sensor for Wearable Devices via a Bioinspired Atomic-Precise Tunable Graphene-Polymer Heterogeneous Sensing Junction," *Chemistry of Materials*, vol. 30, no. 13, pp. 4343–4354, 2018, doi: 10.1021/acs.chemmater.8b01587.

[3] T. L. Yeo, T. Sun, and K. T. V. Grattan, "Fibre-optic sensor technologies for humidity and moisture measurement," *Sensors and Actuators A: Physical*, vol. 144, no. 2, pp. 280–295, Jun. 2008, doi: 10.1016/J.SNA.2008.01.017.

[4] Z. M. Rittersma, "Recent achievements in miniaturised humidity sensors-a review of transduction techniques," *Sensors and Actuators A: Physical*, Vol. 96, pp. 196-210, 2002.

[5] U. Kang and K. D. Wise, "A high-speed capacitive humidity sensor with on-chip thermal reset," *IEEE Transactions on Electron Devices*, vol. 47, no. 4, pp. 702–710, 2000, doi: 10.1109/16.830983.

[6] X. Xiao, L. Wang, M. Luo, X. Hu, D. Chen, H. Zhang, Y. Zhang, P. Feng, J. Tao, Y. Fu, D. Wang, Z. He, and S. Yu, High, "Baudrate Silicon Photonics for the Next-generation Optical Communication," *ECOC*, We4E.1, pp. 2022–2025, 2022.

[7] S. K. Khijwania, K. L. Srinivasan, and J. P. Shingh, "Performance optimized optical fiber sensor for humidity measurement," *Optical Engineering*, vol. 44, no. 3, p. 034401, 2005, doi: 10.1117/1.1870753.

[8] N. K. Sharma and B. D. Gupta, "Fabrication and characterization of pH sensor based on side polished single mode optical fiber," *Optics Communications*, vol. 216, no. 4–6, pp. 299–303, 2003, doi: 10.1016/S0030-4018(02)02343-X.

[9] H. S. Haddock, P. M. Shankar, and R. Mutharasan, "Fabrication of biconical tapered optical fibers using hydrofluoric acid," *Materials Science and Engineering: B*, vol. 97, no. 1, pp. 87–93, 2003, doi: 10.1016/S0921-5107(02)00434-8.

[10] H. Tai, T. Yoshino, and H. Tanaka, "Fiber-optic evanescent-wave methane-gas sensor using optical absorption for the 3392-μm line of a He–Ne laser," *Optics Letters*, vol. 12, no. 6, p. 437, 1987, doi: 10.1364/ol.12.000437.

[11] A. Prasanth, S. R. Meher, and Z. C. Alex, "Metal oxide thin films coated evanescent wave based fiber optic VOC sensor," *Sensors and Actuators A: Physical*, vol. 338, no. November 2021, p. 113459, 2022, doi: 10.1016/j.sna.2022.113459.

[12] B. Culshaw and A. Kersey, “Fiber-Optic Sensing : A Historical Perspective,” vol. 26, no. 9, pp. 1064–1078, 2008.

[13] K. O. Hill and G. Meltz, “Fiber Bragg grating technology fundamentals and overview,” *Journal of Lightwave Technology*, vol. 15, no. 8, pp. 1263–1276, 1997, doi: 10.1109/50.618320.

[14] A. D. Kersey, M. A. Davis, H. J. Patrick, M. LeBlanc, K. P. Koo, C. G. Askins, M. A. Putnam, and E. J. Friebele , “Fiber grating sensors,” Journal of Lightwave Technology, vol. 15, no. 8, pp. 1442–1462, 1997, doi: 10.1109/50.618377.

[15] B. H. Lee, Y. H. Kim, K. S. Park, J. B. Eom, M. J. Kim, B. S. Rho, and H. Y. Choi Interferometric fiber optic sensors,” Sensors, vol. 12, no. 3, pp. 2467–2486, 2012, doi: 10.3390/s120302467.

[16] A. Miliou, “In-fiber interferometric-based sensors: Overview and recent advances,” *Photonics*, vol. 8, no. 7, 2021, doi: 10.3390/photonics8070265.

[17] P. S. J. Russell, “Photonic Crystal Fibers,” *Optics InfoBase Conference Papers*, vol. 299, no. JANUARY, pp. 358–363, 2003.

[18] D. H. Kim and J. U. Kang, “Sagnac loop interferometer based on polarization maintaining photonic crystal fiber with reduced temperature sensitivity,” *Optics Express*, vol. 12, no. 19, p. 4490, 2004, doi: 10.1364/opex.12.004490.

[19] H. Y. Fu, H. Y. Tam, L. Y. Shao, X. Dong, P. K. A. Wai, C. Lu, and S. K. Khijwania, “Pressure sensor realized with polarization-maintaining photonic crystal fiber-based Sagnac interferometer,” *Applied Optics*, vol. 47, no. 15, pp. 2835–2839, 2008, doi: 10.1364/AO.47.002835.

[20] D. S. Ballantine and H. Wohltjen, “Optical Waveguide Humidity Detector,” *Analytical Chemistry*, vol. 58, no. 13, pp. 2883–2885, 1986, doi: 10.1021/ac00126a068.

[21] Q. Zhou, M. R. Shahriari, D. Kritz, and G. H. Sigel, “Porous Fiber-Optic Sensor for High-Sensitivity Humidity Measurements,” *Analytical Chemistry*, vol. 60, no. 20, pp. 2317–2320, 1988, doi: 10.1021/ac00171a035.

[22] D. C. Bownass, J. S. Barton, and J. D. C. Jones, “Detection of high humidity by optical fibre sensing at telecommunications wavelengths,” *Optics Communications*, vol. 146, no. 1–6, pp. 90–94, 1998, doi: 10.1016/S0030-4018(97)00525-7.

[23] C. Bariáin, I. R. Matías, F. J. Arregui, and M. López-Amo, “Optical fiber humidity sensor based on a tapered fiber coated with agarose gel,” *Sensors and Actuators, B: Chemical*, vol. 69, no. 1, pp. 127–131, 2000, doi: 10.1016/S0925-4005(00)00524-4.

[24] A. Gaston, I. Lozano, F. Perez, F. Auza, and J. Sevilla, “Evanescent wave optical-fiber sensing (temperature, relative humidity, and pH sensors),” *IEEE Sensors Journal*, vol. 3, no. 6, pp. 806–811, 2003, doi: 10.1109/JSEN.2003.820349.

[25] A. Alvarez-Herrero, H. Guerrero, and D. Levy, "High-Sensitivity Sensor of Low Relative Humidity Based on Overlay on Side-Polished Fibers," *IEEE Sensors Journal*, vol. 4, no. 1, pp. 52–56, 2004, doi: 10.1109/JSEN.2003.822214.

[26] S. K. Shukla, G. K. Parashar, A. P. Mishra, P. Misra, B. C. Yadav, R. K. Shukla, L. M. Bali, and G. C. Dubey, Nano-like magnesium oxide films and its significance in optical fiber humidity sensor," *Sensors and Actuators, B: Chemical*, vol. 98, no. 1, pp. 5–11, 2004, doi: 10.1016/j.snb.2003.05.001.

[27] J. M. Corres, F. J. Arregui, and I. R. Matías, "Sensitivity optimization of tapered optical fiber humidity sensors by means of tuning the thickness of nanostructured sensitive coatings," *Sensors and Actuators, B: Chemical*, vol. 122, no. 2, pp. 442–449, 2007, doi: 10.1016/j.snb.2006.06.008.

[28] I. R. Matias, F. J. Arregui, J. M. Corres, and J. Bravo, "Evanescent field fiber-optic sensors for humidity monitoring based on nanocoatings," *IEEE Sensors Journal*, vol. 7, no. 1, pp. 89–95, 2007, doi: 10.1109/JSEN.2006.886889.

[29] A. Vijayan, M. Fuke, R. Hawaldar, M. Kulkarni, D. Amalnerkar, and R. C. Aiyer, "Optical fibre based humidity sensor using Co-polyaniline clad," *Sensors and Actuators, B: Chemical*, vol. 129, no. 1, pp. 106–112, 2008, doi: 10.1016/j.snb.2007.07.113.

[30] R. Aneesh and S. K. Khijwania, "Zinc oxide nanoparticle based optical fiber humidity sensor having linear response throughout a large dynamic range," *Applied Optics*, vol. 50, no. 27, pp. 5310–5314, 2011, doi: 10.1364/AO.50.005310.

[31] R. Aneesh and S. K. Khijwania, "Titanium dioxide nanoparticle based optical fiber humidity sensor with linear response and enhanced sensitivity," *Applied Optics*, vol. 51, no. 12, pp. 2164–2171, 2012, doi: 10.1364/AO.51.002164.

[32] J. Mathew, Y. Semenova, and G. Farrell, "A fiber bend based humidity sensor with a wide linear range and fast measurement speed," *Sensors and Actuators, A: Physical*, vol. 174, no. 1, pp. 47–51, 2012, doi: 10.1016/j.sna.2011.11.029.

[33] Y. Xiao, J. Zhang, X. Cai, S. Tan, J. Yu, H. Lu, Y. Luo, G. Liao, S. Li, J. Tang, and Z. Chen, "Reduced graphene oxide for fiber-optic humidity sensing," *Optics Express*, vol. 22, no. 25, p. 31555, 2014, doi: 10.1364/oe.22.031555.

[34] B. Du, D. Yang, X. She, Y. Yuan, D. Mao, Y. Jiang, and F. Lu, "MoS2-based all-fiber humidity sensor for monitoring human breath with fast response and recovery," *Sensors and Actuators, B: Chemical*, vol. 251, pp. 180–184, 2017, doi: 10.1016/j.snb.2017.04.193.

[35] S. Azad, E. Sadeghi, R. Parvizi, A. Mazaheri, and M. Yousefi, "Sensitivity optimization of ZnO clad-modified optical fiber humidity sensor by means of tuning the optical fiber waist diameter," *Optics and Laser Technology*, vol. 90, no. December 2016, pp. 96–101, 2017, doi: 10.1016/j.optlastec.2016.11.005.

[36] D. Gomez, S. P. Morgan, B. R. Hayes-Gill, R. G. Correia, and S. Korposh, "Polymeric optical fibre sensor coated by SiO2 nanoparticles for humidity sensing in the skin microenvironment," *Sensors and Actuators, B: Chemical*, vol. 254, pp. 887–895, 2018, doi: 10.1016/j.snb.2017.07.191.

[37] B. Du, D. Yang, X. She, Y. Yuan, D. Mao, Y. Jiang, and F. Lu, , "High-sensitivity fiber-optic humidity sensor based on microfiber overlaid with niobium disulfide," *Journal of Materials Science*, vol. 55, no. 35, pp. 16576–16587, 2020, doi: 10.1007/s10853-020-05230-0.

[38] N. Zhong, X. Xin, H. Liu, X. Yu, H. Chang, B. Tang, D. Zhong, M. Zhao, H. Zhang, and J. Zhao, "Plastic optical fiber sensor for temperature-independent high-sensitivity detection of humidity," *Applied Optics*, vol. 59, no. 19, p. 5708, Jul. 2020, doi: 10.1364/ao.391090.

[39] Y. Huang, W. Zhu, Z. Li, G. Chen, L. Chen, J. Zhou, H. Lin, J. Guan, W. Fang, X. Liu, H. Dong, J. Tang, H. Guan, H. Lu, Y. Xiao, J. Zhang, H. Wang, Z. Chen, and J. Yu, " High-performance fibre-optic humidity sensor based on a side-polished fibre wavelength selectively coupled with graphene oxide film," *Sensors and Actuators, B: Chemical*, vol. 255, pp. 57–69, 2018, doi: 10.1016/j.snb.2017.08.042.

[40] Z. Harith, M. Batumalay, N. Irawati, S. W. Harun, H. Ahmad, and T. Hu, "ZnO nanorod-coated tapered plastic fiber sensors for relative humidity," *Optics Communications*, vol. 473, no. April, p. 125924, 2020, doi: 10.1016/j.optcom.2020.125924.

[41] E. Owji, H. Mokhtari, F. Ostovari, B. Darazereshki, and N. Shakiba, "2D materials coated on etched optical fibers as humidity sensor," *Scientific Reports*, vol. 11, no. 1, pp. 1–10, 2021, doi: 10.1038/s41598-020-79563-w.

[42] X. Huang, M. Lai, Z. Zhao, Y. Yang, J. Li, H. Song, J. He, Y. Ma, and B. Liu, " " Fiber optic evanescent wave humidity sensor based on SiO 2 /TiO 2 bilayer films ," *Applied Optics*, vol. 60, no. 8, p. 2158, 2021, doi: 10.1364/ao.416286.

[43] Y. Liu, P. Li, N. Zhang, X. Zhang, S. Chen, Z. Liu, J. Guang, and W. Peng, ", "Fiber-optic evanescent field humidity sensor based on a micro-capillary coated with graphene oxide," *Optical Materials Express*, vol. 9, no. 11, p. 4418, 2019, doi: 10.1364/ome.9.004418.

[44] J. Guo, M. Chang, Y. Xiao, Q. Song, D. Zhao, and B. Jia, "Simple high-sensitivity optical fiber humidity sensor," *Applied Optics*, vol. 60, no. 21, p. 5990, 2021, doi: 10.1364/ao.422732.

[45] H. S. Ziming Zhao, Min Lai, Yang Yang, Jinze Li and A. B. L. Jixiang He, Hengheng Zhang, Yaya Mao, Yan Ma, "PVA / Tween 20 thin-film-based fiber optic humidity sensor with enhanced sensing performance," *Applied Optics,* vol. 61, no. 7, pp. 1834–1840, 2022.

[46] E. Afsharipour, K. D. Malviya, M. Montazeri, E. Mortazy, R. Soltanzadeh, A. Hassani, F. Rosei, and M. Chaker, “Evanescent-Field Excited Surface Plasmon-Enhanced U-Bent Fiber Probes Coated with Au and ZnO Nanoparticles for Humidity Detection,” *Processes,* vol. 11, no. 2, 2023, doi: 10.3390/pr11020642.

[47] L. Alwis, T. Sun, and K. T. V. Grattan, “Analysis of Polyimide-Coated Optical Relative Humidity Sensor,” *IEEE Sensors Journal*, vol. 13, no. 2, pp. 767–771, 2013.

[48] Y. Wang, C. Shen, W. Lou, F. Shentu, C. Zhong, X. Dong, and L. Tong, " Fiber optic relative humidity sensor based on the tilted fiber Bragg grating coated with graphene oxide,” *Applied Physics Letters*, vol. 109, no. 3, pp. 1–6, 2016, doi: 10.1063/1.4959092.

[49] W. Wang, T. Sun, J. Peng, J. Dai, and M. Yang, “Humidity Sensor Based on Fiber Bragg Grating Coated with Different Pore-Foaming Agent Doped Polyimides,” *IEEE Photonics Technology Letters*, vol. 29, no. 22, pp. 1963–1966, 2017, doi: 10.1109/LPT.2017.2757946.

[50] J. Zhang, X. Shen, M. Qian, Z. Xiang, and X. Hu, “An optical fiber sensor based on polyimide coated fiber Bragg grating for measurement of relative humidity,” *Optical Fiber Technology*, vol. 61, no. November 2020, p. 102406, 2021, doi: 10.1016/j.yofte.2020.102406.

[51] Z. Li, B. Dong, E. Chen, Y. Li, W. Zhao, Y. Wang, and C. Gao, “High sensitivity FBG humidity sensor coated with graphene and polyimide films,” *Optical Fiber Technology*, vol. 66, no. July, p. 102635, 2021, doi: 10.1016/j.yofte.2021.102635.

[52] A. J. Swanson, S. G. Raymond, S. Janssens, R. D. Breukers, M. D. H. Bhuiyan, J. W. Lovell-Smith, and M. R. Waterlan, “Development of novel polymer coating for FBG based relative humidity sensing,” *Sensors and Actuators, A*: Physical, vol. 249, pp. 217–224, 2016, doi: 10.1016/j.sna.2016.08.034.

[53] M. Tian, Y. Huang, C. Li, and M. Lv, “High-performance humidity sensor based on a micro-nano fiber Bragg grating coated with graphene oxide,” *Optics Express*, vol. 28, no. 18, p. 26395, 2020, doi: 10.1364/oe.402648.

[54] M. A. Riza, Y. I. Go, S. W. Harun, and S. B. Ahmad Anas, “Optimal etching process and cladding dimension for improved coating of porous hemispherical ZnO nanostructure on FBG humidity sensor,” *Laser Physics*, vol. 33, no. 7, 2023, doi: 10.1088/1555-6611/acd7d7.

[55] K. P. W. Dissanayake, W. Wu, H. Nguyen, T. Sun, and K. T. V. Grattan, “Graphene-Oxide-Coated Long-Period Grating-Based Fiber Optic Sensor for Relative Humidity and External Refractive Index,” *Journal of Lightwave Technology*, vol. 36, no. 4, pp. 1145–1151, 2018, doi: 10.1109/JLT.2017.2756097.

[56] J. Hou, J. Dai, F. Zhang, and M. Yang, “Advanced Fiber-Optic Relative Humidity Sensor Based on Graphene Quantum Dots Doped Polyimide Coating,” *IEEE Photonics Technology Letters*, vol. 34, no. 14, pp. 725–728, 2022, doi:

10.1109/LPT.2022.3181756.

[57] Y. Wang, C. Shen, W. Lou, and F. Shentu, “Fiber optic humidity sensor based on the graphene oxide/PVA composite film,” *Optics Communications*, vol. 372, pp. 229–234, 2016, doi: 10.1016/j.optcom.2016.04.030.

[58] S. Liu, H. Meng, S. Deng, Z. Wei, F. Wang, and C. Tan, “Fiber Humidity Sensor Based on a Graphene-Coated Core-Offset Mach–Zehnder Interferometer,” *IEEE Sensors Letters*, vol. 2, no. 3, pp. 1–4, 2018, doi: 10.1109/lsens.2018.2849750.

[59] C. Bian, J. Wang, X. Bai, M. Hu, and T. Gang, “Optical fi ber based on humidity sensor with improved sensitivity for monitoring applications,” *Optics and Laser Technology*, vol. 130, no. May, p. 106342, 2020, doi: 10.1016/j.optlastec.2020.106342.

[60] X. Fan, Q. Wang, M. Zhou, F. Liu, H. Shen, Z. Wei, F. Wang, C. Tan, and H. Meng, " Humidity sensor based on a graphene oxide-coated few-mode fiber Mach-Zehnder interferometer,” Optics Express, vol. 28, no. 17, p. 24682, 2020, doi: 10.1364/oe.390207.

[61] J. Peng, Y. Qu, W. Wang, T. Sun, and M. Yang, “Thin-film-based optical fiber Fabry–Perot interferometer used for humidity sensing,” *Applied Optics*, vol. 57, no. 12, p. 2967, 2018, doi: 10.1364/ao.57.002967.

[62] Z. Zhang, H. Gong, C. Yu, K. Ni, and C. Zhao, “Fiber optic Fabry–Perot interferometer based on HA/PVA composite film for humidity sensing,” *Optical Fiber Technology*, vol. 68, no. June 2021, p. 102816, 2022, doi: 10.1016/j.yofte.2021.102816.

[63] L. Liang, H. Sun, N. Liu, H. Luo, T. Gang, Q. Rong, X. Qiao, and M. Hu, " High-sensitivity optical fiber relative humidity probe with temperature calibration ability,” *Applied Optics*, vol. 57, no. 4, p. 872, 2018, doi: 10.1364/ao.57.000872.

[64] S. Liu, Y. Ji, J. Yang, W. Sun, and H. Li, “Physical Nafion film temperature / humidity sensing based on optical fiber Fabry-Perot interference,” *Sensors & Actuators: A. Physical*, vol. 269, pp. 313–321, 2018, doi: 10.1016/j.sna.2017.11.034.

[65] C. Li, X. Yu, W. Zhou, Y. Cui, J. Liu, and S. Fan, “Ultrafast miniature fiber-tip Fabry–Perot humidity sensor with thin graphene oxide diaphragm,” *Optics Letters*, vol. 43, no. 19, p. 4719, 2018, doi: 10.1364/ol.43.004719.

[66] S. Liu, X. Zhang, Q. Wang, S. Chen, F. Wang, J. Wang, G. Wang, W. Yang, and M. Huang, “Integrated and Robust Fabry-Perot Humidity Sensor Based on Metal-Organic Framework onto Fiber-Optic Facet,” IEEE Sensors Journal, vol. 23, no. 12, pp. 12906–12914, 2023, doi: 10.1109/JSEN.2023.3273905.

[67] M. Shao, B. Liu, Y. Wang, Y. Liu, and X. Qiao, “Optical Fiber Fabry-Perot Humidity Sensor Based on BPQDs-PVA Sandwiched in SMF,” *IEEE Photonics Technology Letters*, vol. 35, no. 24, pp. 1379–1382, 2023, doi: 10.1109/LPT.2023.3323475.

[68] Y. Zhao, R. jie Tong, M. qing Chen, and Y. Peng, “Relative humidity sensor based on Vernier effect with GQDs-PVA un-fully filled in hollow core fiber,” *Sensors and Actuators, A: Physical*, vol. 285, pp. 329–337, 2019, doi: 10.1016/j.sna.2018.11.042.

[69] R. Gao, D. F. Lu, J. Cheng, Y. Jiang, L. Jiang, and Z. M. Qi, “Humidity sensor based on power leakage at resonance wavelengths of a hollow core fiber coated with reduced graphene oxide,” *Sensors and Actuators, B: Chemical*, vol. 222, pp. 618–624, 2016, doi: 10.1016/j.snb.2015.08.108.

[70] B. Xu, Y. Guo, X. Ma, Y. Zhang, C. L. Zhao, and D. N. Wang, “Highly Sensitive Fiber Relative Humidity Sensor Based on Tip Michelson Interferometer With Agarose Gel Coating,” *IEEE Sensors Journal*, vol. 23, no. 2, pp. 1139–1145, 2023, doi: 10.1109/JSEN.2022.3224238.

[71] M. Shao, H. Sun, J. Liang, L. Han, and D. Feng, “In-Fiber Michelson Interferometer in Photonic Crystal Fiber for Humidity Measurement,” *IEEE Sensors Journal*, vol. 21, no. 2, pp. 1561–1567, 2021, doi: 10.1109/JSEN.2020.3019717.

[72] L. Li, Z. Wang, Q. Ma, M. Wang, Q. Wu, H. Chen, and B. Peng, " Sagnac Ring Humidity Sensor with a Melting Cone Based on Graphene Properties,” IEEE Sensors Journal, vol. 21, no. 14, pp. 16061–16065, 2021, doi: 10.1109/JSEN.2021.3075443.

[73] Z. Wang, L. Li, Q. Ma, M. Wang, W. Wei, P. Yang, S. Jiang, W. Tao, and B. Peng, “Loop-Fiber coated with graphene oxide incorporating a FBG to sense humidity and temperature simultaneously,” *Optics Communications*, vol. 508, no. December 2021, p. 127819, 2022, doi: 10.1016/j.optcom.2021.127819.

[74] V. V. Perera, N. L. Fernando, B. Nissanka, and D. R. Jayasundara, “In situ real time monitoring of hygroscopic properties of graphene oxide and reduced graphene oxide,” *Adsorption*, vol. 25, no. 8, pp. 1543–1552, 2019, doi: 10.1007/s10450-019-00131-4.

[75] S. Sahoo, M. Bhuyan, and D. Sahoo, “Tuning of dielectric and magnetic performance of graphene oxide via defect regulation by metal oxide nanoparticle for high temperature device,” *Journal of Alloys and Compounds*, vol. 935, p. 168097, 2023, doi: 10.1016/j.jallcom.2022.168097.

[76] B. Tao, J. Yin, F. Miao, and Y. Zang, “High-performance humidity sensor based on GO/ZnO/plant cellulose film for respiratory monitoring,” *Ionics*, vol. 28, no. 5, pp. 2413–2421, May 2022, doi: 10.1007/S11581-022-04478-7/TABLES/1.

[77] W. S. Hummers and R. E. Offeman, “Preparation of Graphitic Oxide,” *Journal of the American Chemical Society*, vol. 80, no. 6, p. 1339, 1958, doi: 10.1021/ja01539a017.

[78] S. K. Mishra, S. N. Tripathi, V. Choudhary, and B. D. Gupta, “SPR based fibre optic ammonia gas sensor utilizing nanocomposite film of PMMA/reduced graphene oxide prepared by in situ polymerization,” *Sensors and Actuators, B: Chemical*, vol. 199, pp. 190–200, 2014, doi: 10.1016/j.snb.2014.03.109.

[79] S. Alam, T. K. Sahu, D. Gogoi, N. R. Peela, and M. Qureshi, “Bio-template assisted hierarchical ZnO superstructures coupled with graphene quantum dots for enhanced water oxidation kinetics,” *Solar Energy*, vol. 199, no. January, pp. 39–46, 2020, doi: 10.1016/j.solener.2020.02.015.

[80] S. Yu, H. Zhang, J. Zhang, and Z. Hu, “High-sensitivity RGO-TiO2 humidity sensor driven by triboelectric nanogenerators for non-contact monitoring of human respiration,” *Journal of Alloys and Compounds*, vol. 935, p. 168006, 2023, doi: 10.1016/j.jallcom.2022.168006.

[81] L. Jia-xin, T. Zheng-rong, J. Lei, Z. Wei-hua, Q. Juan, and L. Jing-wei, “Fiber temperature and humidity sensor based on photonic crystal fiber coated with graphene oxide,” *Optics Communications*, vol. 467, no. March, p. 125707, 2020, doi: 10.1016/j.optcom.2020.125707.

[82] Y. Zhao, A. W. Li, Q. Guo, X. Y. Ming, Y. Q. Zhu, X. C. Sun, P. Li, and Y. Sen Yu, , “Relative humidity sensor of S fiber taper based on graphene oxide film,” *Optics Communications*, vol. 450, no. April, pp. 147–154, 2019, doi: 10.1016/j.optcom.2019.05.072.

[83] J. Lin and C. W. Brown, “Sol-gel glass as a matrix for chemical and biochemical sensing,” *TrAC - Trends in Analytical Chemistry*, vol. 16, no. 4, pp. 200–211, 1997, doi: 10.1016/S0165-9936(97)00021-6.

[84] L. Xu, J. C. Fanguy, K. Soni, and S. Tao, “Optical fiber humidity sensor based on evanescent-wave scattering,” *Optics Letters*, vol. 29, no. 11, p. 1191, 2004, doi: 10.1364/ol.29.001191.

[85] A. K. Mcevoy, C. Mcdonagh, and B. D. Maccraith, “Optimisation of Sol-Gel-Derived Silica Films for Optical Oxygen Sensing,” *Journal of Sol-Gel Science and Technology*, vol. 8, no. 1–3, pp. 1121–1125, 1997, doi: 10.1007/BF02436994.

[86] S. A. Grant and R. S. Glass, “A sol-gel based fiber optic sensor for local blood pH measurements,” *Sensors and Actuators, B: Chemical*, vol. 45, no. 1, pp. 35–42, 1997, doi: 10.1016/S0925-4005(97)00263-3.

[87] N. I. Zaaba, K. L. Foo, U. Hashim, S. J. Tan, W. W. Liu, and C. H. Voon, “Synthesis of Graphene Oxide using Modified Hummers Method: Solvent Influence,” *Procedia Engineering*, vol. 184, pp. 469–477, 2017, doi: 10.1016/j.proeng.2017.04.118.

[88] V. Ruddy, “An effective attenuation coefficient for evanescent wave spectroscopy using multimode fiber,” *Fiber and Integrated Optics*, vol. 9, no. 2, pp. 143–151, 1990, doi: 10.1080/01468039008202901.

[89] D. Gloge, “Weakly Guiding Fibers,” *Applied Optics*, vol. 10, no. 10, p. 2252, 1971, doi: 10.1364/ao.10.002252.

[90] S. K. Khijwania and B. D. Gupta, “Fiber optic evanescent field absorption sensor with high sensitivity and linear dynamic range,” *Optics Communications*, vol. 152, no. 4–

6, pp. 259–262, 1998, doi: 10.1016/S0030-4018(98)00168-0.

[91] M. Goumri, B. Lucas, B. Ratier, and M. Baitoul, “Electrical and optical properties of reduced graphene oxide and multi-walled carbon nanotubes based nanocomposites: A comparative study,” *Optical Materials*, vol. 60, pp. 105–113, 2016, doi: 10.1016/j.optmat.2016.07.010.

[92] V. V. Perera, N. L. Fernando, B. Nissanka, and D. R. Jayasundara, “In situ real time monitoring of hygroscopic properties of graphene oxide and reduced graphene oxide,” *Adsorption*, vol. 25, no. 8, pp. 1543–1552, 2019, doi: 10.1007/s10450-019-00131-4.

[93] D. Zhang, H. Chang, P. Li, R. Liu, and Q. Xue, “Fabrication and characterization of an ultrasensitive humidity sensor based on metal oxide/graphene hybrid nanocomposite,” *Sensors and Actuators, B: Chemical*, vol. 225, pp. 233–240, 2016, doi: 10.1016/j.snb.2015.11.024.

[94] A. D. D. L, J. Hwang, M. Yusuf, K. H. Park, S. Park, and J. Kim, “Simultaneous Measurement of Humidity and Temperature with Cytop-reduced Graphene Oxide-overlaid Two-mode Optical Fiber Sensor,” *Sensors and Actuators, B: Chemical*, vol. 298, no. July, p. 126841, 2019, doi: 10.1016/j.snb.2019.126841.

[95] H. Ahmad, M. T. Rahman, S. N. A. Sakeh, M. Z. A. Razak, and M. Z. Zulkifli, “Humidity sensor based on microfiber resonator with reduced graphene oxide,” *Optik*, vol. 127, no. 5, pp. 3158–3161, 2016, doi: 10.1016/j.ijleo.2015.11.184.

[96] Y. Sun, J. Guo, Y. Xiao, J. Fan, J. Chen, D. Zhao, and B. Jia, " Twisted weakly coupled relative humidity sensor coated with a graphene oxide/polyvinyl alcohol composite,” *Applied Optics*, vol. 61, no. 22, p. 6658, 2022, doi: 10.1364/ao.463248.

[97] A. Ghaffarkhah, E. Hosseini, M. Kamkar, A. A. Sehat, S. Dordanihaghighi, A. Allahbakhsh, C. van der Kuur, and M. Arjmand, " Synthesis, Applications, and Prospects of Graphene Quantum Dots: A Comprehensive Review,” *Small*, vol. 18, no. 2, pp. 1–48, 2022, doi: 10.1002/smll.202102683.

[98] N. Agrawal, D. Bhagel, P. Mishra, D. Prasad, and E. Kohli, “Post-synthetic modification of graphene quantum dots bestows enhanced biosensing and antibiofilm ability: efficiency facet,” *RSC Advances*, vol. 12, no. 20, pp. 12310–12320, 2022, doi: 10.1039/d2ra00494a.

[99] Y. Zhao, R. jie Tong, M. Q. Chen, and F. Xia, “Relative humidity sensor based on hollow core fiber filled with GQDs-PVA,” *Sensors and Actuators, B: Chemical*, vol. 284, no. December 2018, pp. 96–102, 2019, doi: 10.1016/j.snb.2018.12.130.

[100] N. Wang, W. Tian, H. Zhang, X. Yu, X. Yin, Y. Du, and D. Li, “An easily fabricated high performance fabry-perot optical fiber humidity sensor filled with graphene quantum dots,” *Sensors (Switzerland)*, vol. 21, no. 3, pp. 1–11, 2021, doi: 10.3390/s21030806.

[101] Y. Liu, Y. Zhang, H. Lei, J. Song, H. Chen, and B. Li, “Growth of well-arrayed ZnO

nanorods on thinned silica fiber and application for humidity sensing," *Optics Express*, vol. 20, no. 17, p. 19404, 2012, doi: 10.1364/oe.20.019404.

[102] B. Li, T. Liu, Y. Wang, and Z. Wang, "Journal of Colloid and Interface Science ZnO / graphene-oxide nanocomposite with remarkably enhanced visible-light-driven photocatalytic performance," *Journal of Colloid And Interface Science*, vol. 377, no. 1, pp. 114–121, 2012, doi: 10.1016/j.jcis.2012.03.060.

[103] B. Li, T. Liu, Y. Wang, and Z. Wang, "ZnO/graphene-oxide nanocomposite with remarkably enhanced visible-light-driven photocatalytic performance," *Journal of Colloid and Interface Science*, vol. 377, no. 1, pp. 114–121, 2012, doi: 10.1016/j.jcis.2012.03.060.

[104] M. Batumalay, S. W. Harun, N. Irawati, H. Ahmad, and H. Arof, "A study of relative humidity fiber-optic sensors," *IEEE Sensors Journal*, vol. 15, no. 3, pp. 1945–1950, 2015, doi: 10.1109/JSEN.2014.2368979.

[105] I. Heng, F. W. Low, C. W. Lai, J. C. Juan, N. Amin, and S. K. Tiong, "High performance supercapattery with rGO/TiO2 nanocomposites anode and activated carbon cathode," *Journal of Alloys and Compounds*, vol. 796, pp. 13–24, 2019, doi: 10.1016/j.jallcom.2019.04.347.

[106] D. Li, H. Lu, W. Qiu, J. Dong, H. Guan, W. Zhu, J. Yu, Y. Luo, J. Zhang, and Z. Chen, "Molybdenum disulfide nanosheets deposited on polished optical fiber for humidity sensing and human breath monitoring," *Optics Express*, vol. 25, no. 23, p. 28407, 2017, doi: 10.1364/oe.25.028407.

[107] A. Syuhada, M. S. Shamsudin, S. Daud, G. Krishnan, S. W. Harun, and M. S. A. Aziz, "Single-Mode Modified Tapered Fiber Structure Functionalized With GO-PVA Composite Layer for Relative Humidity Sensing," *Photonic Sensors*, vol. 11, no. 3, pp. 314–324, 2021, doi: 10.1007/s13320-020-0595-0.

[108] S. K. Khijwania and B. D. Gupta, "Fiber optic evanescent field absorption sensor based on a tapered probe: effect of fiber parameters on the response curve," *International Conference on Fiber Optics and Photonics: Selected Papers from Photonics India '98*, vol. 3666, no. May, pp. 578–584, 1999, doi: 10.1117/12.347980.

[109] H. J. Kbashi, "Fabrication of Submicron-Diameter and Taper Fibers Using Chemical Etching," *Journal of Materials Science and Technology*, vol. 28, no. 4, pp. 308–312, 2012, doi: 10.1016/S1005-0302(12)60059-0.

[110] H. Bi, K. Yin, X. Xie, J. Ji, S. Wan, L. Sun, M. Terrones, and M. S. Dresselhaus, " Ultrahigh humidity sensitivity of graphene oxide," *Scientific Reports*, vol. 3, no. 5 V, pp. 1–7, 2013, doi: 10.1038/srep02714.

[111] Z. Q. Li, E. A. Henriksen, Z. Jiang, Z. Hao, M. C. Martin, P. Kim, H. L. Stormer, and D. N. Basov, "Dirac charge dynamics in graphene by infrared spectroscopy," *Nature Physics*, vol. 4, no. 7, pp. 532–535, 2008, doi: 10.1038/nphys989.

[112] X. Wang, Y. Deng, X. Chen, P. Jiang, Y. K. Cheung, and H. Yu, “An ultrafast-response and flexible humidity sensor for human respiration monitoring and noncontact safety warning,” *Microsystems and Nanoengineering*, vol. 7, no. 1, 2021, doi: 10.1038/s41378-021-00324-4.

[113] H. Wu, T. Sun, J. Peng, J. Dai, and M. Yang, “Polar-groups-modified polyimide based on a fiber Bragg grating for relative humidity sensors,” *Applied Optics*, vol. 59, no. 8, p. 2468, 2020, doi: 10.1364/ao.381376.

[114] M. Winnacker, “Polyhydroxyalkanoates: Recent Advances in Their Synthesis and Applications,” *European Journal of Lipid Science and Technology*, vol. 121, no. 11, pp. 1–9, 2019, doi: 10.1002/ejlt.201900101.

[115] P. Poltronieri, V. Mezzolla, and O. F. D’Urso, “PHB Production in Biofermentors Assisted through Biosensor Applications,” p. 4, 2017, doi: 10.3390/ecsa-3-e014.

[116] T. Monshupanee, P. Nimdach, and A. Incharoensakdi, “Two-stage (photoautotrophy and heterotrophy) cultivation enables efficient production of bioplastic poly-3-hydroxybutyrate in auto- sedimenting cyanobacterium,” *Nature Publishing Group*, no. November, pp. 1–9, 2016, doi: 10.1038/srep37121.

[117] J. H. LAW and R. A. SLEPECKY, “Assay of poly-beta-hydroxybutyric acid.,” *Journal of bacteriology*, vol. 82, no. 1958, pp. 33–36, 1961, doi: 10.1128/jb.82.1.33-36.1961.

[118] S. Pradhan, “Production , ultrasonic extraction , and characterization of poly (3 - hydroxybutyrate) (PHB) using Bacillus megaterium and Cupriavidus necator,” no. July 2018, 2020, doi: 10.1002/pat.4351.

[119] L. Khtaoui, M. Laghrouche, F. Fernane, and A. Chaouchi, “High-sensitivity humidity sensor based on natural hydroxyapatite,” *Journal of Materials Science: Materials in Electronics*, vol. 32, no. 7, pp. 8668–8686, 2021, doi: 10.1007/s10854-021-05538-w.

[120] N. A. Wojas, A. Swerin, V. Wallqvist, M. Järn, J. Schoelkopf, P. A. C. Gane, and P. M. Claesson, “Iceland spar calcite: Humidity and time effects on surface properties and their reversibility,” *Journal of Colloid and Interface Science*, vol. 541, pp. 42–55, 2019, doi: 10.1016/j.jcis.2019.01.047.

[121] A. A. Shaltout, M. A. Allam, and M. A. Moharram, “FTIR spectroscopic, thermal and XRD characterization of hydroxyapatite from new natural sources,” Spectrochimica Acta - Part A: Molecular and Biomolecular Spectroscopy, vol. 83, no. 1, pp. 56–60, 2011, doi: 10.1016/j.saa.2011.07.036.

[122] S. S. Al-Jaroudi, A. Ul-Hamid, A. R. I. Mohammed, and S. Saner, “Use of X-ray powder diffraction for quantitative analysis of carbonate rock reservoir samples,” *Powder Technology*, vol. 175, no. 3, pp. 115–121, 2007, doi: 10.1016/j.powtec.2007.01.013.

[123] S. Mondal, S. J. Kim, and C. G. Choi, “Honeycomb-like MoS2 Nanotube Array-

Based Wearable Sensors for Noninvasive Detection of Human Skin Moisture," *ACS Applied Materials and Interfaces*, vol. 12, no. 14, pp. 17029–17038, 2020, doi: 10.1021/acsami.9b22915.